RESEARCH AND DEVELOPMENT ON METHODS FOR THE ENGINEERING
EVALUATION AND CONTROL OF TOXIC AIRBORNE EFFLUENTS

Contract No. A4-159-32

Volume II

R.L. Bell
Department of Chemical Engineering
University of California, Davis

Prepared for the California
Air Resources Board

June 1987

RESEARCH AND DEVELOPMENT OF METHODS FOR THE ENGINEERING
EVALUATION AND CONTROL OF TOXIC AIRBORNE EFFLUENTS

by

Richard L. Bell
Cynthia L. Castronovo
Christine Laban
Gloria Lindner
David Shonnard
Kimiye Tanaka

June 1987

CONTENTS

FIGURES

TABLES

ACKNOWLEDGMENTS

DISCLAIMER

The statements and conclusions in this report are those of the contractor and not necessarily those of the California Air Resources Board. The mention of commercial products, their source or their use in connection with material reported herein is not to be construed as either an actual or implied endorsement of such products.

SUMMARY

The work presented in this report is a summary of the study of VOC transport from crude oil impoundments (sumps) and the initiation of work concerned with emissions from the landfarming of hydrocarbon wastes.

The data for the study of VOC transport from sumps has been taken from 3 sumps operated by Chevron USA in the Bakersfield, California, area. Two sumps referred to as 31X and 36W are located in the Cymric Oil Field approximately 30 miles to the west of Bakersfield. The third sump called Monte Cristo is in the Kern River Field located in the eastern outskirts of Bakersfield. The oil fields in this area are now being produced by steam flood or secondary recovery, and on a volumetric basis about 8 times more water than oil is produced. The oil/water mixture is separated by gravity in large open impoundments referred to as sumps. Accurate methods for measuring and predicting the loss to the atmosphere of volatile organic compounds (VOC) from these sumps has been a focus of study both for the California Air Resources Board (CARB) and the Department of Chemical Engineering at the University of California Davis (UCD).

UCD has developed a comprehensive program for studying VOC emissions which includes field tests, laboratory experiments and mathematical modeling. It was apparent from the outset that unlike aqueous (low viscosity) impoundments, a high viscosity layer of crude oil formed on the surface of the water in the crude oil sumps. It was hypothesized that the highly viscous layer could be assumed to be vertically unmixed. A mathematical model of single component isothermal transport from the oil was developed based on this assumption. The effect of heat transfer to and from the sump will be added to the model. The

single component model is currently being extended to the multicomponent case and the effect of residence time in the sump is being added to the model. The model will be applicable not only to crude oil impoundments but to any impoundments in which the liquid can be considered vertically unmixed.

Based on the theoretical study it was found that the important variables were the single component partial pressure and molecular diffusivity in the crude oil. An exhaustive literature survey failed to produce experimental values or specific methods for estimating these values in crude oil. One problem is that all methods for predicting equilibrium partial pressure depend on the liquid phase mole fraction which is unknown for crude oil. A second problem is that correlations for diffusivity are based on low viscosity solvents and the few data points which exist for high viscosity solvents do not provide a sound basis for the estimation of diffusivity in crude oil. By extrapolating methods applicable to more well defined mixtures, order of magnitude estimates of molecular weight, vapor pressure and diffusivity were obtained. These estimates were used in the theoretical study to obtain order of magnitude results for single component fluxes. It was found that the effect of temperature depends very strongly on the partial pressure of the components present. For high vapor pressure compounds which have high partial pressures such as pentane there is virtually no temperature effect, but for low vapor pressure compounds such as decane temperature effects can be quite large.

Plans were developed for measuring diffusivities of single components in the crude oil. During this contract year the equipment for making these measurements has been constructed and initial calibration experiments have been completed. The results have been very promising and in particular, the measurements of molecular diffusivity have confirmed the order of magnitude of our ori-

ginal estimates. These studies are of central importance to the theoretical effort and will be continuing.

Since the theoretical approach we adopted was based on component-by-component predictions, it was essential that we determined which components or classes of components were present in the volatile fraction of the crude oil. A procedure was developed in the laboratory for quantitative distillation of the fraction of crude oil which contained the VOC. During the initial contract period (A2-157-32) we had a contract with Hewlett Packard which included the loan of a gas chromatograph with a mass spectrometer detector (GCMS). This instrument was used to determine the peak areas present in the sump inlet and outlet samples. By comparing the VOC peak areas, a very clear picture of the relative loss of each component (peak) was obtained. The peaks were identified by first comparing the mass spectra of the peak with the National Bureau of Standards reference library stored in the GCMS computer library. This gave the 10 most probable compounds. These compounds were then screened using boiling point criteria and finally the compound spectra were compared visually with the published NBS mass spectra. Although the GCMS was returned to Hewlett Packard in August 1985, the analysis of the data has been a significant effort during the present contract year. We now have certain identification of 67 different molecular species or isomers.

Based on the analyses of inlet and outlet samples the relative loss of the individual VOC components has been estimated and from this an estimate of the total loss of VOC has been obtained. These estimates compare very favorably with those obtained by CARB using the "flux box" method.

The conditions in the sump (temperature, composition, residence time) and in the atmosphere (temperature, solar radiation, wind) which determine the rate of

loss of VOC are continually changing daily and seasonally. The data which were obtained early in the study represented a "snapshot" of this dynamic system. The theoretical model is viewed as a tool for extrapolating these snapshots to a more global basis. Consequently, a major field effort during this contract period was to conduct a 5 day continuous monitoring and sampling test of sump 36W. This was coordinated with a scheduled CARB test of the same sump. Inlet and outlet samples were obtained every 4 hours and continuous sump temperatures and meterological data were obtained. These data were collected to determine the magnitude of diurnal variations and the effect they have on emissions. An extremely important result of this test was to confirm the assumption that the oil layer is vertically unmixed and the boundary condition that the temperature at the oil/water interface is virtually constant. The chemical analyses are not yet available.

During this contract year we initiated a study of emissions resulting from the application of hydrocarbon wastes to the soil. This is generally referred to as "landfarming." There are two major areas of interest. The first derives from the fact that a large amount of gasoline saturated soil must be disposed of in the next few years as a result of leaking gasoline storage tanks. The rate of volatilization of gasoline from soil and the effect of biodegradation on emissions is a subject of considerable current interest. The second area is concerned primarily with heavy refinery wastes applied to the soil. The soil is then tilled by "discing" and the wastes presumably oxidized by biological action. As opposed to the gasoline case in which the hydrocarbon is all VOC, the heavy wastes have low VOC content. The primary effort during this contract year has been to conduct a literature review and explore the various theoretical and experimental approaches to these problems. From the literature study it was

concluded that neither the theoretical nor experimental methods for either case are well developed. We have adopted an approach which begins with a systematic study of volatilization and degradation of hydrocarbons in the gasoline range. This will provide some immediate answers to questions about gasoline-saturated soils and provide a sound basis for the studies of heavier hydrocarbon wastes. By use of a combination of carbon-14 radio isotope tracing and conventional gas chromatographic analysis, the rate of volatilization and the fate of specific molecular species can be examined.

RESEARCH AND DEVELOPMENT OF METHODS FOR THE ENGINEERING
EVALUATION AND CONTROL OF TOXIC AIRBORNE EFFLUENTS
Contract No. A4-159-32

REPORT TO AIR RESOURCES BOARD

R.L. Bell
Department of Chemical Engineering

INTRODUCTION

During the 1985-86 contract period the Department of Chemical Engineering at UC Davis had 2 joint projects with the California Air Resources Board (CARB). The first of these was a continuation of the study of the transport of volatile organic compounds (VOC) from crude oil sumps to the atmosphere. This project was subdivided into four parts: Identification of the VOC, mathematical modeling of the transport processes, measurement of diffusion coefficients of the VOC in crude oil and measurement of vapor pressure of the VOC in crude oil. The second project was the initiation of a study of land farming of oily wastes.

The primary results from each of these projects will be presented below and the details of each will be included in the Addenda.

I. TRANSPORT OF VOLATILE ORGANIC COMPOUNDS

1.0 Identification of the VOC

As part of a grant from Hewlett Packard we were given a one year loan of a Model 5890/5970 gas chromatograph/mass spectrometer (GCMS) system. This machine allowed us to begin identifying those compounds present in the VOC. During the summer of 1985 we were able to retain possession of the machines and substantial additional progress was made. However, in August, 1985, Hewlett Packard suddenly recalled the machine in accordance with the terms of the grant. We have been seeking other resources to replace it since that time.

The analysis of the VOC was done using a distillate from the curde oil samples. The capillary column in the GCMS system increased separation and resolution of peaks in the lower-boiling range, which allowed for increased ability to make positive identifications of specific peaks. The need to identify specific components of the volatile fraction was two-fold. First, it gave us a handle on photochemical reactivity of the mixture. Photochemical reactivity depends on the hydrocarbon family (olefinic > alkyl benzene > benzene > paraffinic hydrocarbons), the number of carbon atoms present, and the presence of oxygen, sulfur, cholorine, or nitrogen groups. From the analysis, we were able to neglect the influence of oxygenated, sulfonated, chlorinated, and nitrogenated compounds. The paraffinic alkanes (normal, branched, and cyclic alkanes) were the most abundant constituents of the mixture, with aromatics and olefins playing only minor roles. Second, with knowledge of specific constituents of the volatile fraction, it will be possible to select representative chemicals for which we wish to determine diffusion coefficient in the oil and the single component vapor pressure over oil.

Table 1:   Compounds Identified in the VOC

NAME OF COMPOUND IDENTIFIED	BOIL T (C)	GC RETENTION TIME (MIN)			INLET PEAK AREAS		
		N CRIST	31X	36W	N CRIST	31X	36W
2-METHYLBUTANE (ISOPENTANE)	27.8	5.199	-----	-----			
2,2-DIMETHYLBUTANE	49.7	6.484	-----	-----	98029		
2,3-DIMETHYLBUTANE	58.0	7.403	----	-----	680554		
2-METHYLPENTANE	60.3	-----	-----	7.539			
3-METHYLPENTANE	63.3	8.101	-----	8.121	35651		
HEXANE	68.7	8.860	-----	8.866			32584
2,2-DIMETHYLPENTANE	79.2	10.222	-----	-----	115780		
METHYLCYCLOPENTANE	71.8	10.390	10.325	10.382		17023	36030
2,4-DIMETHYLPENTANE	80.5	10.585	-----	-----	252107		
2,2,3-TRIMETHYLBUTANE	80.9	10.966	-----	10.956	201184		19580
BENZENE	80.1	-----	-----	11.919			76614
3,3-DIMETHYLPENTANE	86.1	12.326	-----	-----	141020		
CYCLOHEXANE	80.7	12.617	12.561	12.637	16065	38512	21459
2-METHYLHEXANE	90.0	13.268	-----	13.262			57303
2,3-DIMETHYLPENTANE	89.8	13.441	13.353	13.420	870324	26255	58325
1,1-DIMETHYLCYCLOPENTANE	87.5	-----	13.594	-----			
3-METHYL-1-HEXENE	83.9	13.669	-----	-----	71516		
3-METHYLHEXANE	91.9	13.975	13.900	13.981	33709	17790	92965
1-CIS-3-DIMETHYLCYCLOPENTANE	90.8	14.777	14.460	14.543	352184	63657	40748
1-TRANS-3-DIMETHYLCYCLOPENTANE	91.7	14.536	14.701	14.77	203641	78782	47674
1-TRANS-2-DIMETHYLCYCLOPENTANE	91.9	-----	14.939	15.021		197401	66597
2,2,3-TRIMETHYLPENTANE	109.8	15.141	-----	-----	35323		
HEPTANE	98.4	-----	-----	16.129			256045
METHYLCYCLOHEXANE	100.9	18.042	17.994	18.062	44279	436576	129427
1,1,3-TRIMETHYLCYCLOPENTANE	104.9	-----	18.279	18.346		86082	37034
ETHYLCYCLOPENTANE	103.5	-----	19.144	19.233		86594	
2,5-DIMETHYLHEXANE	109.1	19.329	-----	-----			
2,4-DIMETHYLHEXANE	109.4	19.539	19.447	-----	488299	27717	
1-TRANS-2-CIS-4-TRIMETHYLCYCLOPENTANE	109.3	20.202	20.064	20.126	1969937	204532	61558
1-TRANS-2-CIS-3-TRIMETHYLCYCLOPENTANE	110.4	20.909	20.840	-----	438728	374831	
3-METHYL-2,4-HEXADIENE	110.4	-----	-----	21.25			78415
TOLUENE	110.6	-----	21.522	21.615		103165	338676
2,3,4-TRIMETHYLPENTANE	113.5	21.679	21.133	-----			
2,3-DIMETHYLHEXANE	115.6	-----	-----	22.405			20697
1,1,2-TRIMETHYLCYCLOPENTANE	113.7	-----	22.408	-----		120501	
2-METHYL-3-ETHYLPENTANE	115.7	22.552	-----	-----	440134		
1,1,3,3-TETRAMETHYLCYCLOPENTANE	118	22.831	22.728	22.84	68374	26568	213569
2-METHYLHEPTANE	117.7	-----	22.998	23.008			356721
4-METHYLHEPTANE	117.7	23.273	23.142	23.242	53563		
3-METHYLHEPTANE	118.9	23.427	23.356	23.925	195651		
1-TRANS-4-DIMETHYLCYCLOHEXANE	119.4	24.365	24.047	24.342	310563	549732	
3-METHYLENEHEPTANE	120.0	23.762	-----	-----	221824		
1,1-CIS-3-TRANS-4-TETRAMETHYLCYCLOPENTANE	121.6	24.148	-----	-----	2020449		
1,1-DIMETHYLCYCLOHEXANE	119.6	24.977	24.881	24.981	221278	63504	

Table 1 (cont'd)

NAME OF COMPOUND IDENTIFIED	BOIL T (C)	GC RETENTION TIME (MIN)			INLET PEAK AREAS		
		M CRIST	31X	36W	M CRIST	31X	36W
1-METHYL-TRANS-3-ETHYLCYCLOPENTANE	121.2	25.379	25.532	25.362		80897	123555
1-METHYL-TRANS-2-ETHYLCYCLOPENTANE	121.2	-----	25.702	-----		317327	
1-ETHYL-1-METHYLCYCLOPENTANE	121.5	-----	25.911	-----			
1-METHYL-CIS-3-ETHYLCYCLOPENTANE	121.1	25.63	25.29	25.618	150073	87938	
4-TRANS-OCTENE	122.3	-----	-----	25.744			
1-TRANS-2-DIMETHYLCYCLOHEXANE	123.4	-----	26.273	26.328		268216	
OCTANE	125.7	-----	-----	27.035			241464
1,1-CIS-3-CIS-4-TETRAMETHYLCYCLOPENTANE	130.2	28.504	27.964	28.052		140477	122330
2,3,5-TRIMETHYLHEXANE	131.3	28.987	28.903	-----	127714		
2,4-DIMETHYLHEPTANE	132.9	30.302	-----	29.874	239725		34708
N-PROPYLCYCLOPENTANE	131.0	-----	29.131	-----		62829	
1,1,4-TRIMETHYLCYCLOHEXANE	135.0	30.598	30.886	-----	566489	87524	
2,6-DIMETHYLHEPTANE	135.2	-----	-----	30.652			162541
1,1,3-TRIMETHYLCYCLOHEXANE	136.6	31.564	-----	31.211	988792		77720
M-XYLENE	139.1	-----	33.675	33.769			111464
2,3-DIMETHYLHEPTANE	140.5	33.973	33.882	33.929	304145	185722	138507
3,4-DIMETHYLHEPTANE	140.6	34.213	34.120	-----	179034	86751	
1-METHYL-3-ISOPROPYLCYCLOPENTANE	142.0	34.642	34.400	-----	582834	160880	
1-TRANS-2-CIS-3-TRIMETHYLCYCLOHEXANE	144.0	35.827	35.742	-----	306173		
1-TRANS-2-CIS-4-TRIMETHYLCYCLOHEXANE	144.6	36.052	-----	-----			
1,2,4-TRIMETHYLCYCLOHEXANE	144.0	-----	36.155	-----			
O-XYLENE	144.4	-----	36.414	-----			
1-METHYL-CIS-3-ETHYLCYCLOHEXANE	148.5	-----	37.230	-----		1372746	
1-METHYL-TRANS-3-ETHYLCYCLOHEXANE	151.1	-----	37.364	-----			
					13025145	5370529	3054312

Figure 1: BOILING POINT VS. RETENTION TIME
50 METER X LINKED METHYL SILICONE

BOILING POINT DEG C

COLUMN RETENTION TIME MIN

□ ALKANES   + CYCLOALKANES   ◇ AROMATICS
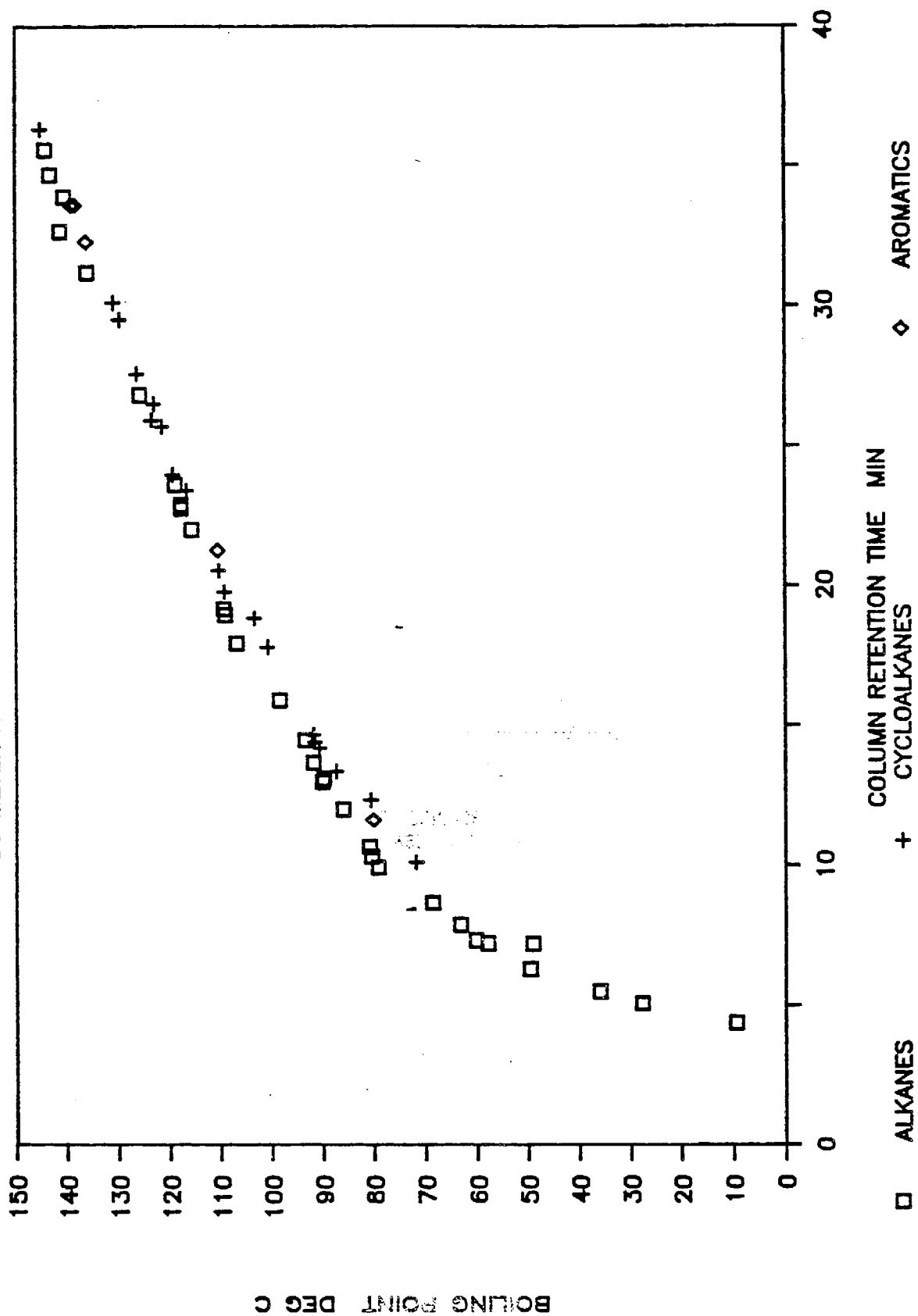
TIC AREA RATIOS FOR THREE SUMPS

HEWLETT PACKARD GCMS
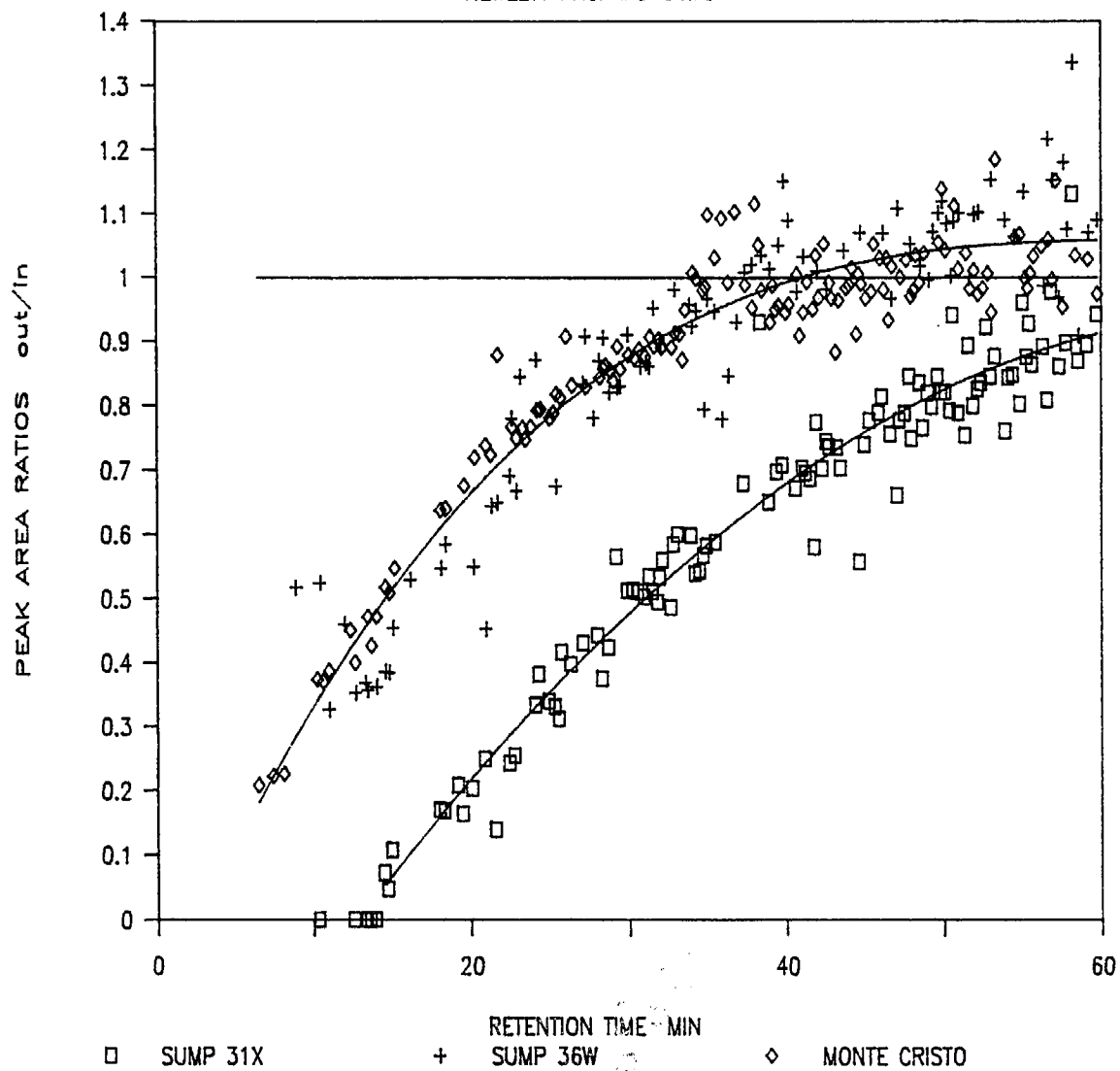
FIGURE 2

We now have reasonably certain identification of 68 different molecular spe-
cies from sumps 31X, 36W and Monte Cristo. A list of these compounds is given
in Table 1. The identification of a given peak was conducted by first comparing
the mass spectra from the GCMS with the library of mass spectra stored in the
GCMS computer library. This gave a list of the 10 most probable compounds which
matched the mass spectra of the peak. The boiling points of these 10 were then
compared to the expected boiling point based on their retention times in the
chromatographic column. The expected residence time was read from the correla-
tion shown in Figure 1. This correlation was obtained from analysis of the
Hewlett Packard PONA calibration standard which contains 103 known components.
Frequently the boiling point gave adequate discrimination for positive iden-
tification. However, final identification was made by manually comparing the
mass spectra of those components in the correct boiling range with the complete
spectra in the National Bureau of Standards (NBS) mass spectra library.

Beyond a retention time of about 37 minutes the peak resolution was so poor
that even with a 50 meter capillary column, speciation was impossible. Up to
about 60 minutes, however, individual peaks were sufficiently well defined, even
though overlapping, that reasonable area calculations could be made. Beyond 60
minutes all resolution was lost.

The ratio of the areas of the peaks from the inlet sample at the pond to the
same peaks in the outlet sample yields a measure of the fractional loss of the
correspond-ing compound. Figure 2 shows the area ratios for all peaks out to a
60 minute retention time. The data for Monte Cristo and 36W fell virtually on
the same curve while that for 31X formed a distinctly separate curve. The lines
through the points are the best polynomial fits of the data obtained by least
squares regression. In both cases the data appear to be approaching an asymp-

totic limit. At a given residence time in the sump, for components with a sufficiently high boiling point, there would be negligible volatilization to the atmosphere. It would therefore be expected that the peak area ratios approach some constant value. If the chromatograph was accurately calibrated the constant would be unity. The loss of the lighter components in the outlet sample results in a higher volumetric concentration of the remaining components. Therefore since the volumes of the samples injected into the chromotograph were the same for inlet and outlet samples, the areas of the outlet peaks will be somewhat greater even for peaks which had no loss. For this reason as seen in Figure 2, the asymptote appears to be about 1.06 instead of unity. The noise on the data is a result of the algorithm used to calculate peak areas. As a retention time of 60 minutes is approached the increasing noise is a result of poor resolution as discussed above. There is, however, a clear relationship between retention time (boiling point) and loss, regardless of the noise.

The data in Figure 2 show that 31X was losing substantially more VOC than either Monte Cristo or 36W. The temperatures of the sumps at the time of sampling were 85-90°C at the inlet and 62-70°C at the outlet as shown in Table 2. Since the three sumps had virtually identical temperatures the increased loss from 31X was probably due to residence time. However, there are no data to support this suggestion. Because the intersection of a curve and its asymptote occurs at infinity, we have arbitrarily defined the environmentally active VOC as those components which have lost 5% or more of peak area. Using an equation obtained by least-squares regression of the boiling point data in Figure 1, and the best fit lines in Figure 2, it was possible to develop a relationship for

TABLE 2

Oil Sump Temperature Data

Sump	Location	Temperature (C)
31X	INLET	85
	OUTLET	70
36W	INLET(S)	85-95
	OUTLET	69
	BRIDGE (1cm)	70
	BRIDGE (30cm)	69
	BRIDGE (70cm)	68
MC	INLET	90
	OUTLET	62

DEPTH = 5cm UNLESS OTHERWISE NOTED
  MC = Monte Cristo

the area ratio as a function of boiling point. The curves were then normalized
to an asymptote of unity and subtracted from one. As shown in Figure 3 the VOC
from Monte Cristo and 36W contained compounds to a boiling point of about 163°C
and in 31X to a boiling point of about 200°C. The amount lost is a function of
sump temperature, viscosity and residence time. These factors are under active
investigation.

A catalog of all mass spectra and physical properties of the compounds iden-
tified has been prepared for future reference and is included as part of this
report. In addition the presence of a large number of cycloaliphatic compounds
was investigated and a draft of a review paper by Ms. Tanaka is included with
this report.

Figure 3

FRACTIONAL LOSS OF VOC

A plot of FRACTIONAL LOSS (y-axis, 0 to 1.2) versus NORMAL BOILING POINT DEG C (x-axis, 0 to 240). Two curves are shown: "Monte Christo and 36W" and "31X".
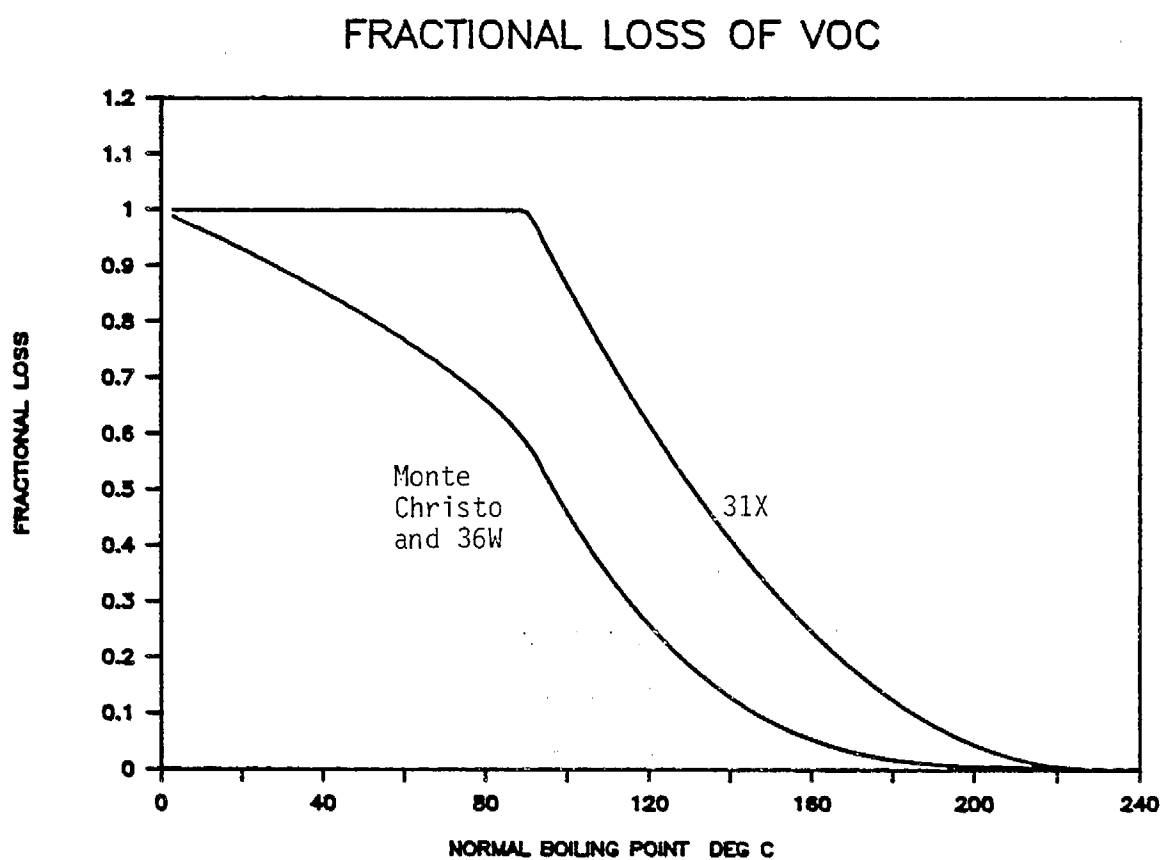
2.0 MATHEMATICAL MODELING OF THE TRANSPORT PROCESSES

The crude oil sumps are large basins (approximately 60 ft x 290 ft) in which water and oil are separated. The oil forms a layer of variable thickness (7 to 21 in.) on the water surface. The viscosity of the oil at the sump temperature (60 to 70°C) is on the order of 300 to 700 cp as shown in Table 3. These data were obtained with a Rheogoniometer at the Davis Chemical Engineering Rheology Laboratory. At this viscosity level there is very little vertical mixing in the oil layer as demonstrated by recent temperature measurements taken over a 5 day period at sump 36W in the Cymric oil field. The temperature measurements were taken every minute and averaged over 15 minutes. These averaged data are plotted in Figure 4 for depths of 1, 7 and 19 inches. These data clearly show that between the 7 and 19 inch depths the temperature does not change. However, at the 1 inch depth there are large temperature excursions which are not reflected 6 inches below. This is definitive evidence that there is insignificant vertical mixing, which supports the primary simplifying assumption of our model. The fact that the temperatures at 7 and 19 inches are the same also supports the constant temperature boundary conditions we have used in the heat transfer model. We recognize that for thin oil layers these assumptions will have to be relaxed. However, the focus of this study has been on primary sumps on which the oil pad is of substantial thickness.

Our initial effort was to develop an isothermal mass transfer model and the early results were reported in the May 1985 report. The vapor pressure of the transferring solute at the air/liquid interface is determined by the temperature at the surface. In the isothermal model we did not include heat of vaporization effects which will cool the surface, the transport of heat to or from the air by convective transport, or the effect of long and shortwave radiation. During

FIGURE 4

TEMPERATURE AS A FUNCTION OF TIME

SUMP 36W   MARCH 26 TO 31 1986
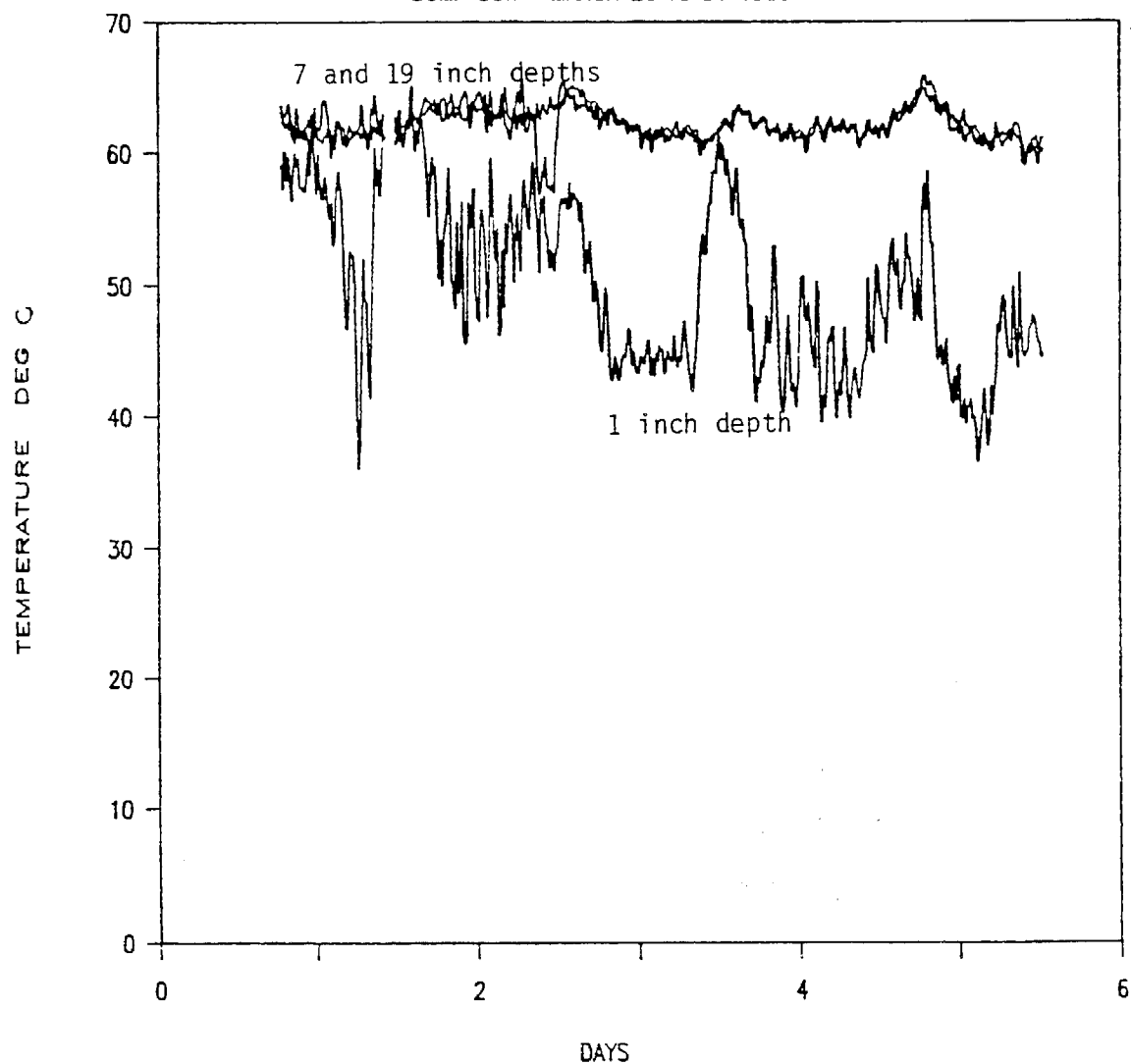
the contract year we have developed an approximate heat transfer model which includes the above effects. The mass and heat transfer models were not solved simultaneously. Instead, in order to explore the temperature effects and to determine if a full simultaneous solution was necessary, we predicted the surface temperature from the approximate model and used that temperature in the mass transfer calculations holding diffusivity constant. For thick oil pads our temperature data shown in Figure 4 suggest that this approach used as a first approximation is not unreasonable.

The full development of all model equations and the estimation of the model coefficients are discussed in detail in Addendum B.

Because of the complex interaction of time, the equilibrium constant, the heat transfer coefficient and the molecular diffusivity, it is difficult to generalize our results in terms of dimensionless groups. One of the most important questions, however, is the consequence of the thermal effects on mass transfer. To explore this question we chose to consider extreme cases which would bracket virtually all environmental conditions. The temperatures chosen were 273°K (0°C) and 373°K (100°C). We chose a series of known compounds from Table I which were relatively abundant and whose boiling points covered a representative range. These compounds were n-heptane (BP 99°C), 1,1,2-trimethyl cyclopentane (BP 114°C) n-octane (BP 126°C). N-pentane (BP 36°C) and n-decane (BP 174°C) were not found in the samples but were included to provide a wide boiling point range.

We first examined the case of low mass transfer resistance in the liquid phase to emphasize the effects of temperature on gas phase transport. This condition was imposed by setting the liquid phase diffusivity at 10^{-8} m^2/sec which

is 2 orders of magnitude greater than that which is expected. Under this assumption 3 cases were considered. In two of these cases the liquid was considered to be isothermal with temperatures of 273°K (0°C) and 373°K (100°C). The third case was for an oil layer initially at 373°K in contact with the atmosphere at 273°K. The surface temperature was calculated using average values of long and short wave length radiation and ambient air temperature for the Bakersfield area. The predicted surface temperature decreased with time and was used to calculate the component vapor pressure at the surface of the oil layer using Antoine's Equation (1).

N-pentane represents the extreme case of a low boiling compound with a high vapor pressure. The fluxes for the 273°K and 373°K case are identical as a function of time. The liquid phase diffusivities were specifically not corrected for temperature so these calculations explore only the effect on gas phase mass transfer. The reason, therefore, that the fluxes were the same is that for the low boiling compounds all of the resistance to mass transport lies in the liquid phase. This is in spite of the fact the liquid phase resistance is 2 orders of magnitude less than expected because the diffusivity was set at 10^{-8} m^2/sec.

We now contrast this with the cases for Trimethylcyclopentane (BP = 114°C, Figure 5) n-octane (BP = 126, Figure 6) and n-Decane (BP = 174°C, Figure 7). By reference to Figure 3 the contribution to the total loss of compounds in this boiling range is approximately 20% of the total for sumps 36W which we will focus on.

In Figures 5 thru 7 it is shown that the effect of temperature on the gas phase resistance increases substantially with increasing boiling point (i.e. decreased vapor pressure). However, it is the region between 1000 to 10,000

seconds during which most of the mass transfer occurs. Except for the highest boiling compounds the effect of a change of temperature of 100°C is on the order of 2 or less.

The conclusion which can be drawn from these calculations is that even for very high liquid diffusivities (i.e. low liquid phase resistance) the effect of temperature on the gas phase resistance for compounds in the boiling point range up to about 114°C is very small. Above this boiling temperature the effect on the gas phase resistance can be substantial but the compounds involved contribute very little to the VOC entering the atmosphere.

As the liquid phase resistance increases the net effect of the gas phase resistance will be reduced. Therefore, we now turn to the case which more realistically reflects the transport processes in sumps with thick oil layers. We know that both temperature and viscosity affect the liquid phase diffusivity. Further we have confirmed that the diffusivities we are measuring for high viscosity solvents are close to those reported by Hiss and and Cussler (2) and at 20°C are on the order of 10^{-12} m^2/sec.

The actual diffusivities of compounds at sump temperatures are in the order of magnitude of 10^{-10} m^2/sec rather than the 10^{-8} m^2/sec used in the previous calculation. The effect of lower diffusivities will be to reduce the influence of gas phase resistance. The next set of calculations are designed to explore that difference.

In this case however we must include the temperature effect on diffusivity. There are no data nor estimation procedures for solutes in crude oil. Consequently, until our own results are available (see section C) we have adapted the best methods available to estimate these diffusivities. The method starts with the Stokes-Einstien approach to liquid phase diffusion (3). This

theory predicts that the diffusion coefficient will be directly proportional to temperature and inversely proportional to viscosity to the first power. Wilke and Chang extended the theory and observed a direct proportionality on the square root of the molecular weight of the solvent and inversely proportional to the solute molar volume to the 0.6 power. This relationship is shown below.

$$D_{AS} \alpha \frac{M_s^{1/2} T}{\eta V_A^{0.6}}$$

This relationship seems to work quite well for dilute solutions and low viscosity.

Hiss and Cussler investigated diffusion of hydrocarbons in solvents of high viscosity. Without a molecular weight correction they determined that at constant temperature the diffusion coefficient was inversely proportional to the viscosity to the 2/3 power. We have examined their data and have included the molecular weight effect. However, to date we have not improved on their correlation. Therefore we have adopted the same dependence on temperature and solute molar volume as Wilke-Chang but have used the Hiss-Cussler viscosity dependence as shown below

$$D_A \alpha \frac{T}{\eta^{2/3} V_A^{0.6}}$$

Table 3 shows the data for the viscosity of crude oil as a function of temperature measured in the University of California, Davis Rheology Laboratory in the Department of Chemical Engineering. These are the data available at the end of the contract period covered by this report. These data together with a

TABLE 3
CRUDE OIL VISCOSITY (CENTIPOISE)

TEMP °C	MONTE CRISTO	36W	31W
22.5	3150	7100	163000
40.0	780	1500	3500
57.0	270	540	720

Viscosity of H_2O = 1 cp
Data obtained with a Rheogoniometer.

significant amount of subsequent data on crude viscosity have provided a correlation which allows us to predict the viscosity for use in the above equation. This work together with additional data in progress will be the subject of a special progress report. It is important to note that the only difference in the diffusion coefficients between solutes will be the molar volume. The molar volume for n-pentane is 115 cm^3/gmole and for n-decane is 195 cm^3/gmol. Therefore the ratio of diffusivities will be.

$$\frac{D_{c5}}{D_{c10}} = (\frac{115}{195})^{0.6} = 0.73$$

As a result the flux in the liquid phase has a small dependence on molecular species.

We have chosen Trimethylcyclopentane as the characteristic solute. The complete multicomponent analysis is the focus of our effort in the 86-87 contract year. Using Hiss and Cussler's data for n-hexane we have predicted the diffusivity of Trimethylcyclopentane (TMCP) in crude oil. The diffusion coeffiencent as a function of temperature is shown in Figure 8.

Using the predicted diffusion coefficient we have calculated the average flux of TMCP as a function of time for several temperatures as shown in Figure 9. This set of calculations is based on one mole of VOC in the inlet.

The combined direct temperature and temperature on viscosity effects result in a substantial temperature dependence of the flux. The temperature of 36W is 333°K and the average flux for this temperature has been included in Figure 9.

From Figure 4 we see that the maximum oil surface temperature excursions are on the order of 20°C. Subsequent data indicate excursions as high as 40°C occur. Therefore, we investigated the effect on the flux of holding the bulk liquid temperature constant but setting the surface temperature at several values in the range of 273°K to 333°K. As seen previously the surface temperature has an effect on the gas phase resistance. However, with the liquid phase diffusion coefficient set on the order of 10^{-10} m^2/sec the gas phase resistance was such a small contribution to the overall mass transfer resistance that there was no change in flux. We recognize that there must exist some temperature profile which will affect the diffusivity as a function of position. However, this will reduce the flux at the surface and consequently the present calculations represent an upper limit on the flux. The complete numerical solution including the temperature profile is now being conducted.

The remaining piece of information required for the calculation of loss from the sump is the initial concentration of VOC. Refering to Figure 3 it can be seen that in Sump 36W which we have chosen as the example because we have more data on it than other sumps, compounds with boiling points beyond 180°C do not contribute to the VOC. We therefore estimated the potential VOC in the inlet as follows.

The chromatographic analyses from which Figure 3 was obtained was from a distillate cut to 220°C. We have obtained the full boiling point curve for 36W crude and the specific gravity data from each boiling range. From these data we calculate that in the 220°C cut that 73 mass percent of the cut lies below 180°C. The 220°C cut was 3.85% of the crude by mass (the distillation mass balance closed at 100.09%). If 73% of this is potential VOC then the potential VOC is 2.81% of the crude. Using the specific gravity data we calculated the volume average specific gravity to be 0.837. Therefore, there exists 2.35×10^4 grams of potential VOC per cubic meter of oil. If we take the average molecular weight of VOC to be 112 which is that of TMCP then there are 209 gmol/m^3 of potential VOC in the inlet oil.

Using all of the Hiss and Cussler data to estimate the diffusivity of TMCP in crude oil we calculated an average flux of 2.61×10^{-7} gmol/m^2 sec per gmol of potential VOC per cubic meter of crude oil. This value corresponds to a time of 10,000 seconds (2.8 hours) which is the approximate residence time we have measured using tracer blocks. The average flux is therefore 2.61×10^{-7} multiplied by the potential VOC of 209 $\frac{gmol}{m^3}$ which gives an average flux of 5.64×10^{-5} $\frac{gmol}{m^2 sec}$.

The 36W sump is 88 meters long by 18 meters wide. The inlet is 16 meters from the inlet end of the sump which is shallow, rounded and essentially inactive. Therefore, we take the active area of the sump to be that extending from the primary inlet. The active area is therefore 72 meters long by 18 meters wide yielding an area of 1,296 meters. Using the average flux of 5.46×10^{-5} gmol/m^{2}sec, 8.64×10^4 sec/day and the above area, the loss is 5,986 gmols/day. Again using an average molecular weight of 112 (note that this can-

cels in the calculation) and 454 gms/pound the resultant loss is 1,477 pounds per day. This number can be compared to the ARB results reported in Report C-86-105 December 1986, page 25, table 5; 1000, 1300 and 1100 pounds/day for tests in 1982, 1983 and 1986 respectively.

The preliminary conclusion, pending further field test results of this method, is that the theoretical prediction being explored in this study yields emission rates which are in substantial agreement with ARB measurements. The full details of the background material will be in a special progress report to be issued during the 1986-1987 contract year.

REFERENCES

1. Reid, R.C., J.M. Pravsnitz, and T.K. Sherwood: "The Properties of Gases and Liquids," 3rd ed., p. 184, McGraw-Hill, New York, 1977.

2. Hiss, T.G., Cussler, E.L. (1973). Diffusion in High Viscosity Liquids, AIChE Journal, 19 (4): 698-703.

3. Wilke, C.R., Chang, P. (1955). Correlation of Diffusion Coefficients in Dilute Solutions, AIChE Journal, Vol. I, 264-270.

Trimethylcyclopentane   (MW = 112 , BP = 114 C, P_{vap}(BP) = 763 mmHg)
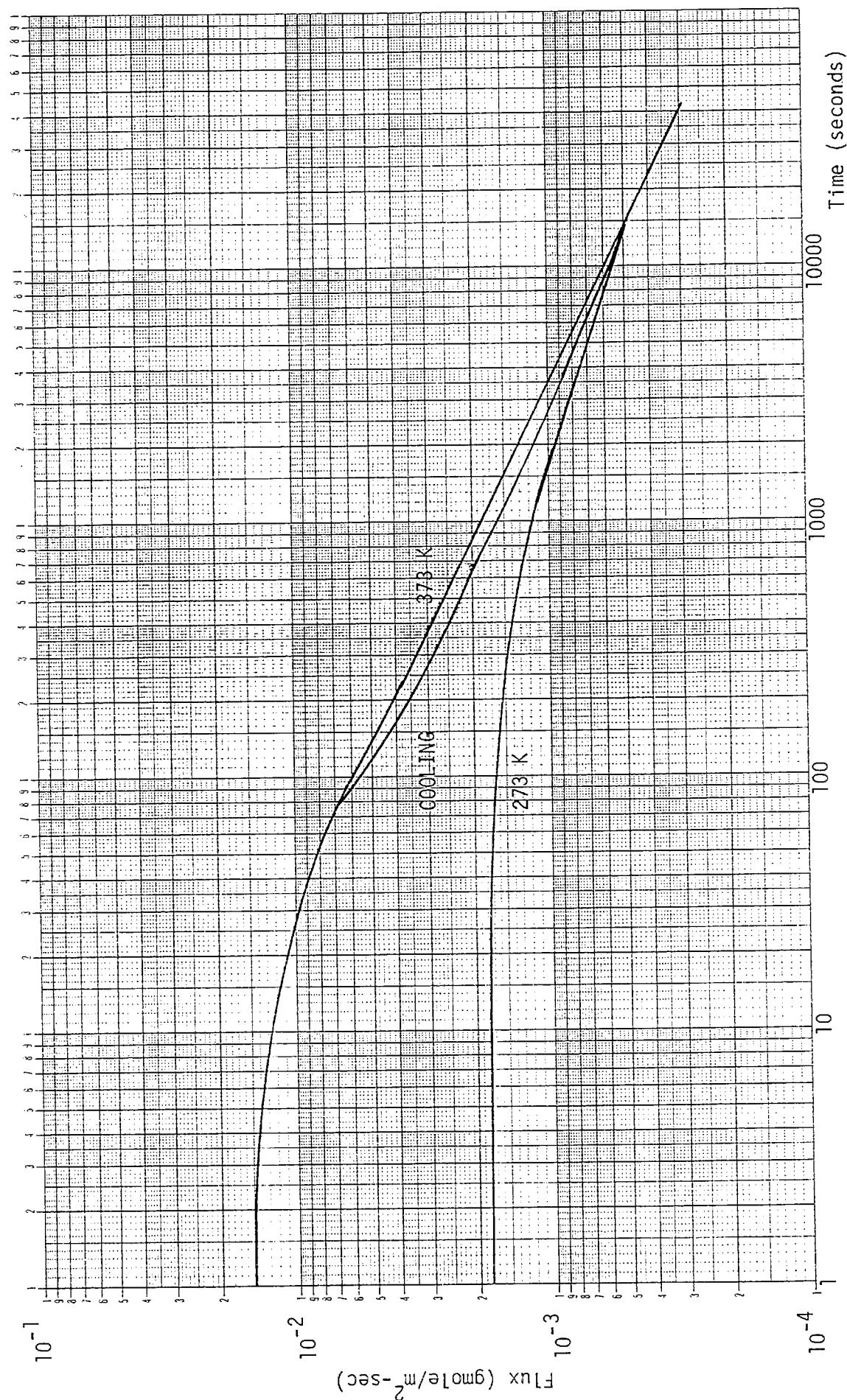
Figure 5

Basis: 15 gmole VOC/ m^3

n-Octane (MW = 114, BP = 126 C, P_{vap}(BP) = 764 mmHg)
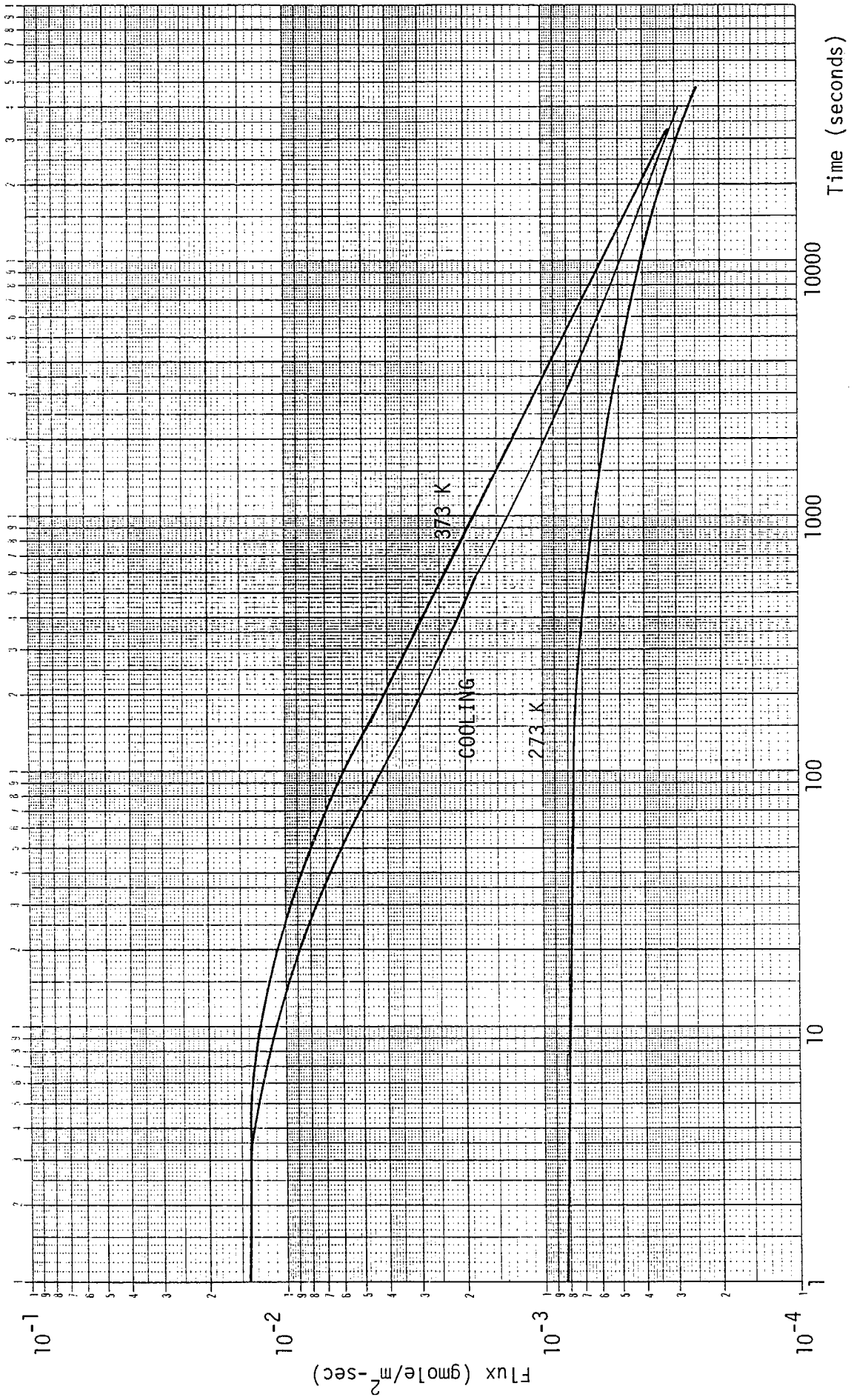
Figure 6

Basis: 15 gmole VOC/m^3

n-Decane (MW = 142, BP = 174 C, P_{vap}(BP) = 755 mmHg)
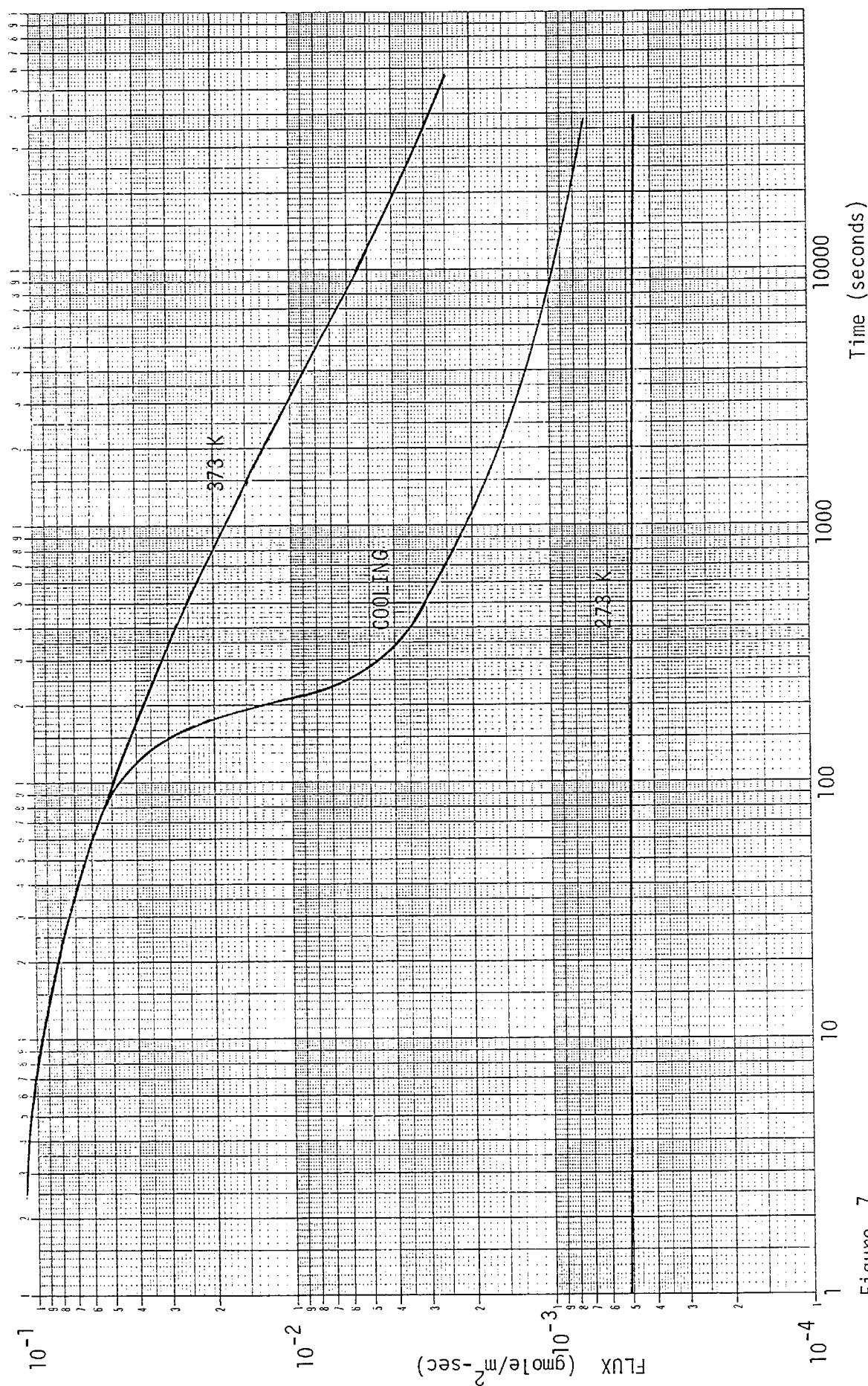
Figure 7

Basis: 15 gmole Voc/m^3

Figure 8

DIFFUSION COEFFICIENT VS TEMPERATURE

PREDICTED VALUES FOR TMCP IN CRUDE OIL
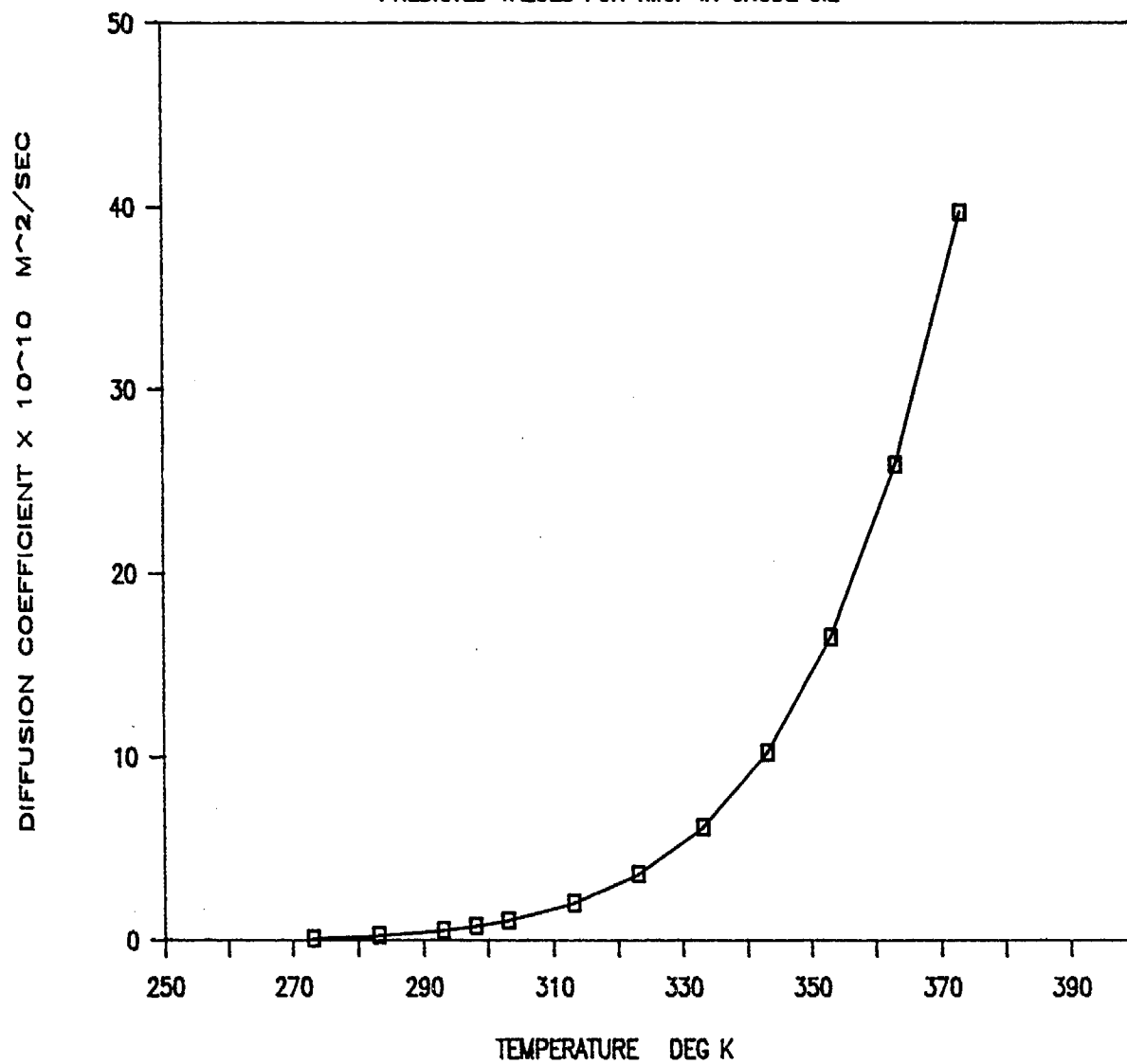
Figure 9

Trimethylcyclopentane   (BP = 114 C, MW = 112.21)
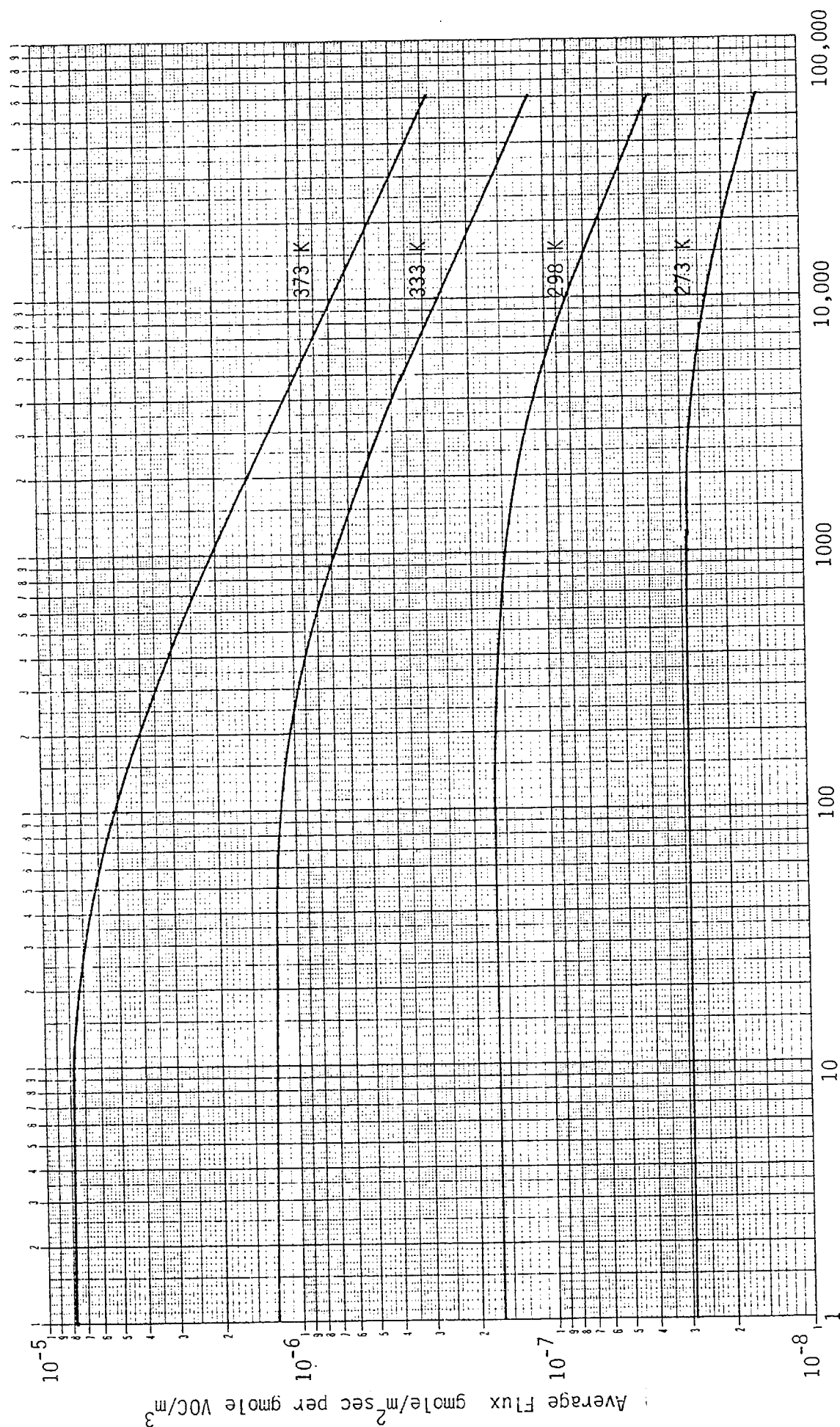
3.0 DIFFUSIVITY IN HIGH VISCOSITY SOLVENTS

In the mathematical model the molecular diffusivity of the VOC's is one of the most important parameters. To accurately model the transport to the atmosphere we must know the effect of solvent viscosity, solute molecular weight or volume, and temperature on the diffusivity. There are few references in the literature on diffusion in high viscosity solvents and none that we have found which are concerned with diffusivity in crude oil. Consequently we initiated an experimental program to measure the diffusivity.

The methods usually used for measurement of molecular diffusivity require that the liquid be transparent. This allows optical methods to be used to measure the changes in concentration of the solute from which diffusivity can be calculated. Our interest in crude oil which is entirely opaque precludes the use of any of these methods. The possibility of using radioactive tracers was considered but rejected based on the difficulty of obtaining the radioactive form of the compounds of interest, the expense of instrumentation and the problems of licensure.

The method of choice was to obtain a crude oil residue, by distillation, which was free of VOC. A selected compound would then be mixed with the residue in known quantities and the mixture placed in a thermostated cell where the surface of the oil would be swept by a pure gas stream. The concentrations of the solute in the effluent gas would then be measured by an FID detector. From the concentration-time data the diffusivity could be calculated. A complete description of the theoretical basis for the experiment, the equipment design and a set of preliminary data are included in Addendum C.

A series of pilot experiments have been completed to test the method and apparatus. Two high viscosity oils which were used by Hiss and Cussler

for diffusion studies were selected for the pilot study. N-heptane was used as as a representative VOC in order to compare the results from our apparatus to those reported by Hiss and Cussler.

The theory for this method predicts that the square of the flux from the cell is linearly proportional to reciprocal time. As shown in the following equation the slope of a plot of $(flux)^2$ vs $1/t$ is defined by the diffusivity D .

$$(Flux)^2 = (C_{A_0}^2 D/\pi)(1/t)$$

where C_{A_0} is defined as the initial concentration of the VOC A in the crude oil. Figure 11 shows a typical plot illustrating the linearity of our experimental data. The values for the diffusivities are in the range of 4×10^{-13} to 119×10^{-13} m^2/sec, which corresponds very closely to the data of Hiss and Cussler.

The pilot study has shown that the method will work. We have also verified the estimates of the magnitude for the diffusion coefficients we have been using in the mathematical modeling effort. The method is still under development but we anticipate excellent results from the crude oil work.

CELLO23: (FLUX)2 vs. 1/TIME
Heptane In S30000 at 60 deg C
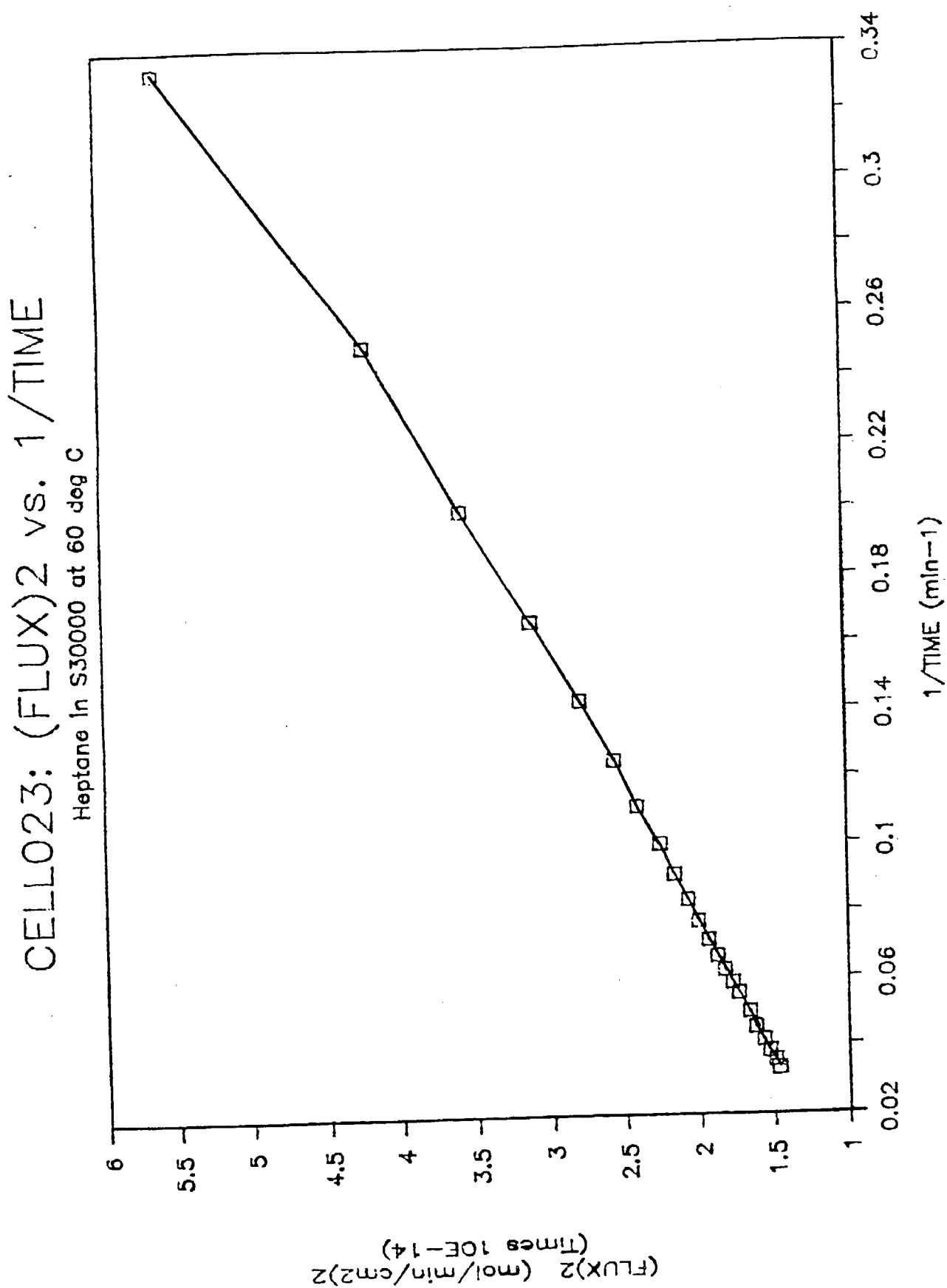
Figure 10

4.0 VAPOR-LIQUID EQUILIBRIUM OF PURE COMPONENTS IN CRUDE OIL

The vapor-liquid equilibrium constant is an essential parameter in the theoretical model. The typical measure of volatility in the petroleum industry is the Reid Vapor Pressure (RVP) as defined in ASTM D323-72, but this index does not provide the precise information we need for accurate modeling or predictive work. Consequently we initiated a program to measure the pure component vapor pressure in crude oil.

After a careful review of the available methods for measuring vapor pressure we elected to use an isoteniscope. This instrument was relatively inexpensive to build and has been proven over years of use to yield accurate data. A full description of the theory on which the method is based and a description of the apparatus is contained in Addendum D. The method is based on first removing all low boiling VOC from a sample of residuum by distillation. Inert gas is then removed from the sample by repeated heating and freezing cycles under a vacuum of about 10^{-4} Torr. An aliquot of previously degassed solute is then added to the residuum and mixed, then the vapor pressure is measured by mercury manometers in the isoteniscope.

We have completed construction of the isoteniscope and have run pure methylcyclopentane, methylcyclohexane and heptane over a temperature range of 30°C to 60°C. The average percent of difference between the measured and reported values is 4.5%. This includes two runs which obviously had trouble and gave percent differences of 13.95 and 19.50 with literature values. Using the remaining 9 runs gives an average percent difference of 0.998 which for purposes of this study is completely acceptable. The results are presented and discussed in Addendum D. We are now preparing to start the experiments with crude oil.

II. VOLATILE ORGANIC COMPOUND EMISSIONS FROM SOIL

1.0 Introduction

One of the most pressing environmental problems of our world today is the question of disposal of industrial wastes in an acceptable manner. As a specific example, large quantities of petroleum wastes are generated each year by the hydrocarbon processing industry and a significant fraction of this waste is disposed of in landfarming facilities. In this process, the versatility of certain soil microorganisms to degrade a wide range of hydrocarbon compounds is utilized such that the waste is transformed into CO_2 and water with a fraction of the waste incorporated into microbial biomass. The environmental impact of this treatment is generally considered to be favorable, however, volatilization and leaching of the hydrocarbon wastes do occur, as does accumulation of heavy metal ions and recalcitrant hydrocarbons. As a result of potential air pollution due to volatilization from soil of the lower boiling fraction in the waste, the California Air Resources Board has determined a need to study and model this treatment process. The purpose of this report is to summarize a review of the literature involving the soil processes of volatilization and degradation of organic compounds and to evaluate current mathematical models.

2.0 Volatilization of Soil Applied Organic Compounds

In order for volatilization from soil to occur, organic compounds must move through a complex structure of solid particles and void spaces to the soil surface. At the surface, the pollutant must then traverse a relatively stagnant atmospheric film of air to escape into the atmosphere. An understanding of the mechanisms of transport of the pollutant through the soil is very important for predicting volatilization from soils. Several of the important mechanisms of

pollutant transport are diffusion through the vapor and aqueous phases, the flow of water soluble pollutants to the surface due to capillary action, and evaporation of water from the soil surface. The physical processes in the soil which affect these mechanisms will be discussed in this section. These include the vapor pressure of the pollutant in the void space of the soil, the soil temperature, and the adsorption characteristics of the soil and pollutant. However, a summary of soil processes would not be complete without an understanding of microbial degradation of the pollutant in the soil and its effect on volatilization. In Section 3, the influence of microbial degradation will be discussed.

2.1 Vapor Pressure Of Organic Compounds In The Soil

The transport of volatile organics through the soil by vapor phase diffusion is an important mechanism in studying potential volatilization of any compound. The vapor pressure of a compound in the soil air space is a controlling parameter. As an example, the vapor pressure of the pesticide Dieldrin (Spencer et. al., 1969, 1973) in the soil was shown to be controlled by the concentration of pesticide in the soil and depended upon soil water content (see Figures 1, 2, and 3). In Figure 1, the vapor pressure of pesticide in the soil increases from zero to an equilibrium value which corresponds to pure pesticide vapor pressure. This behavior is a result of increasing pesticide concentrations in the soil until saturation of adsoption sites on the soil mineral and soil organic fraction surfaces occur. Figures 2 and 3 demonstrate the ability of water to displace adsorbed pesticide molecules from the soil surface due to preferential adsorption of water. This behavior demonstrates that the volatilization of soil incorporated organics can be greatly modified by adsorption processes. For example, Igue et. al. (1972) measured a decrease in an organochloride volatili-

Vapor Phase Desorption Isotherms

For Dieldrin in Soil
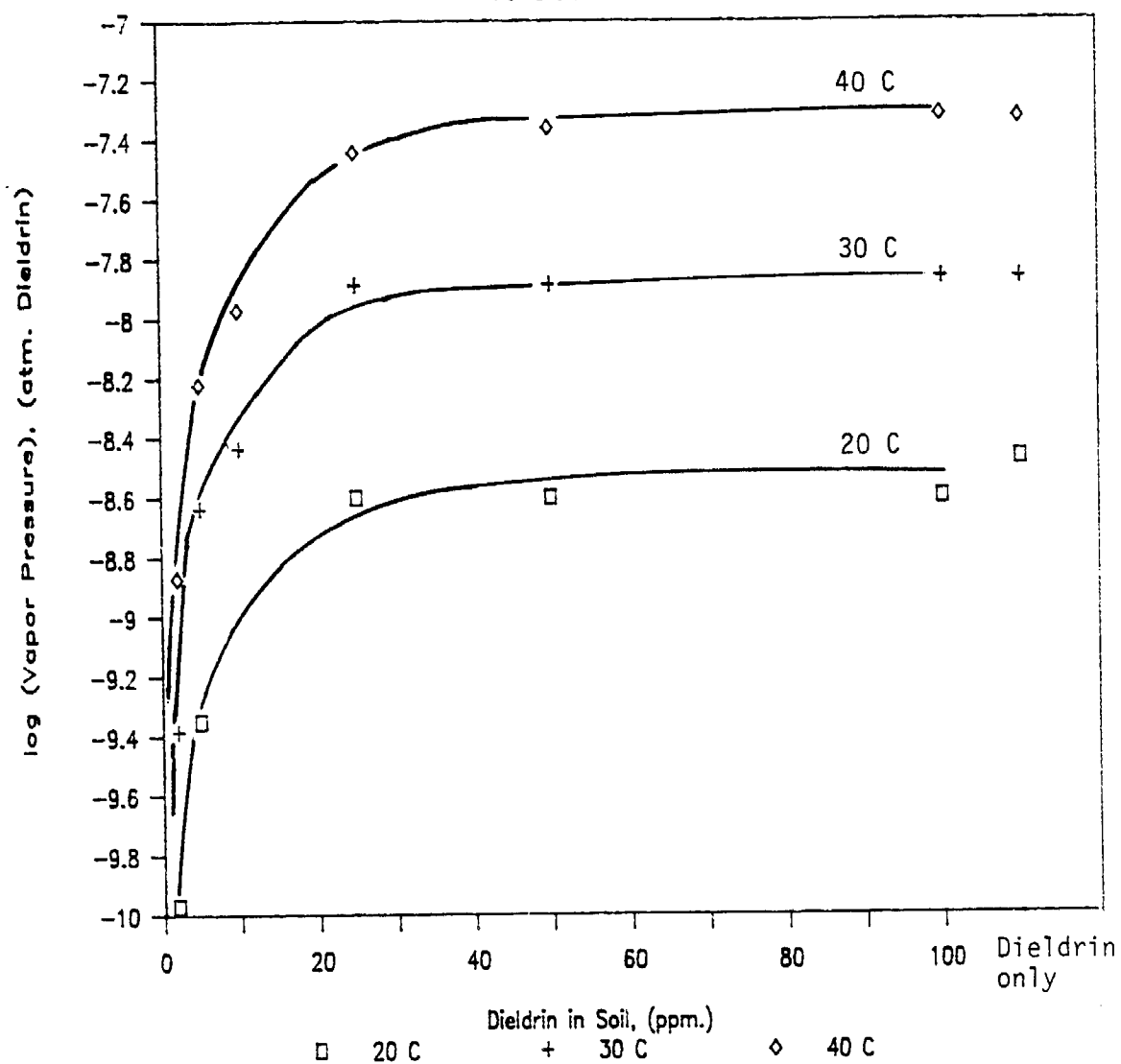
FIGURE 1. Vapor pressure of Dieldrin in soil as a function of
soil concentration. Water contents of 10% or
greater.
Dieldrin only refers to the vapor pressure of pure
pesticide at each temperature.

Effect of Soil Water Content on Vapor

Pressure of Dieldrin (Spencer 1969)
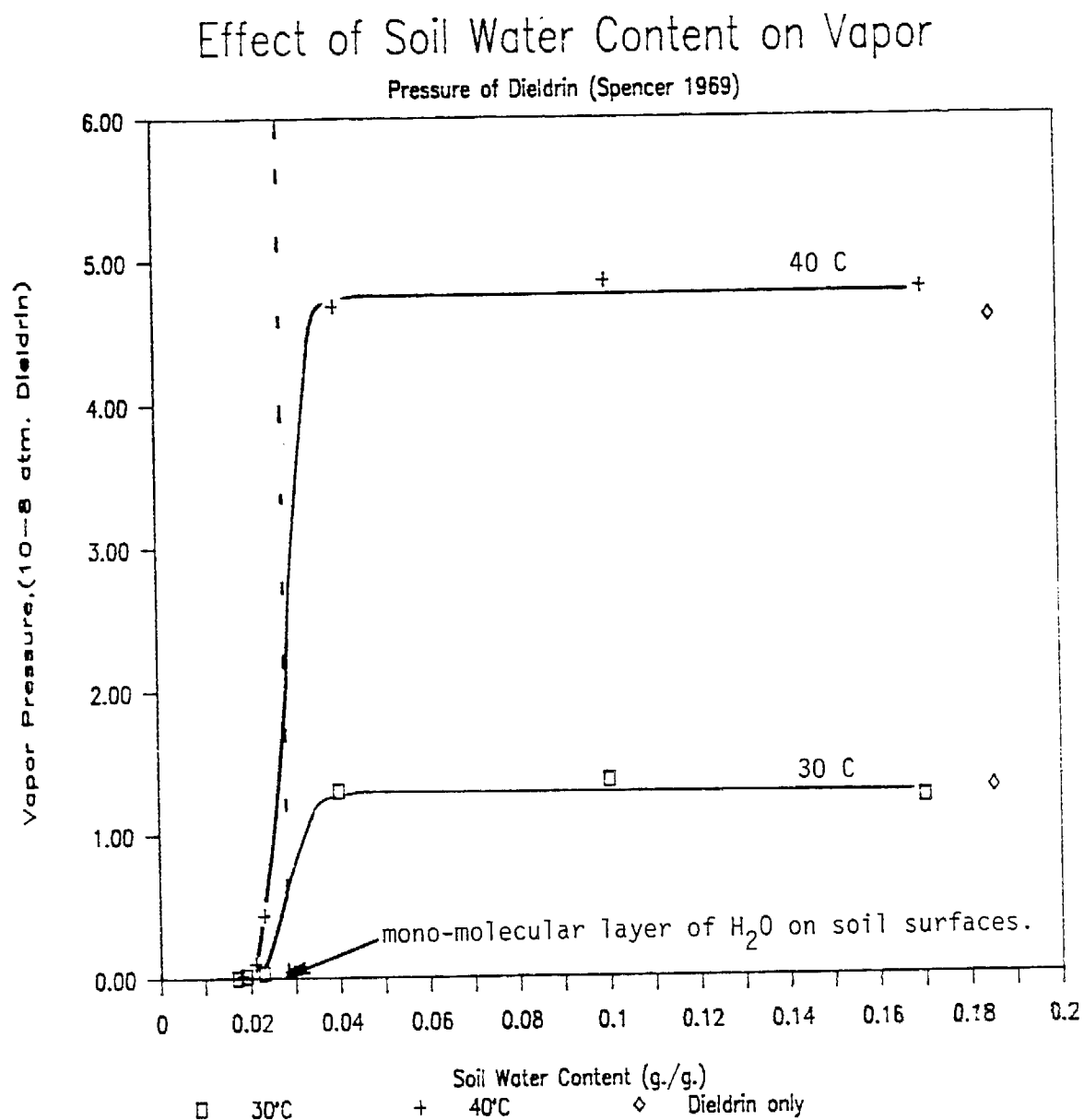
FIGURE 2. Vapor pressure of Dieldrin in soil as a function of
soil water content.
100 ppm Dieldrin in soil.

Effect of Soil Water Content on Vapor

Pressure of Dieldrin (Spencer 1969)
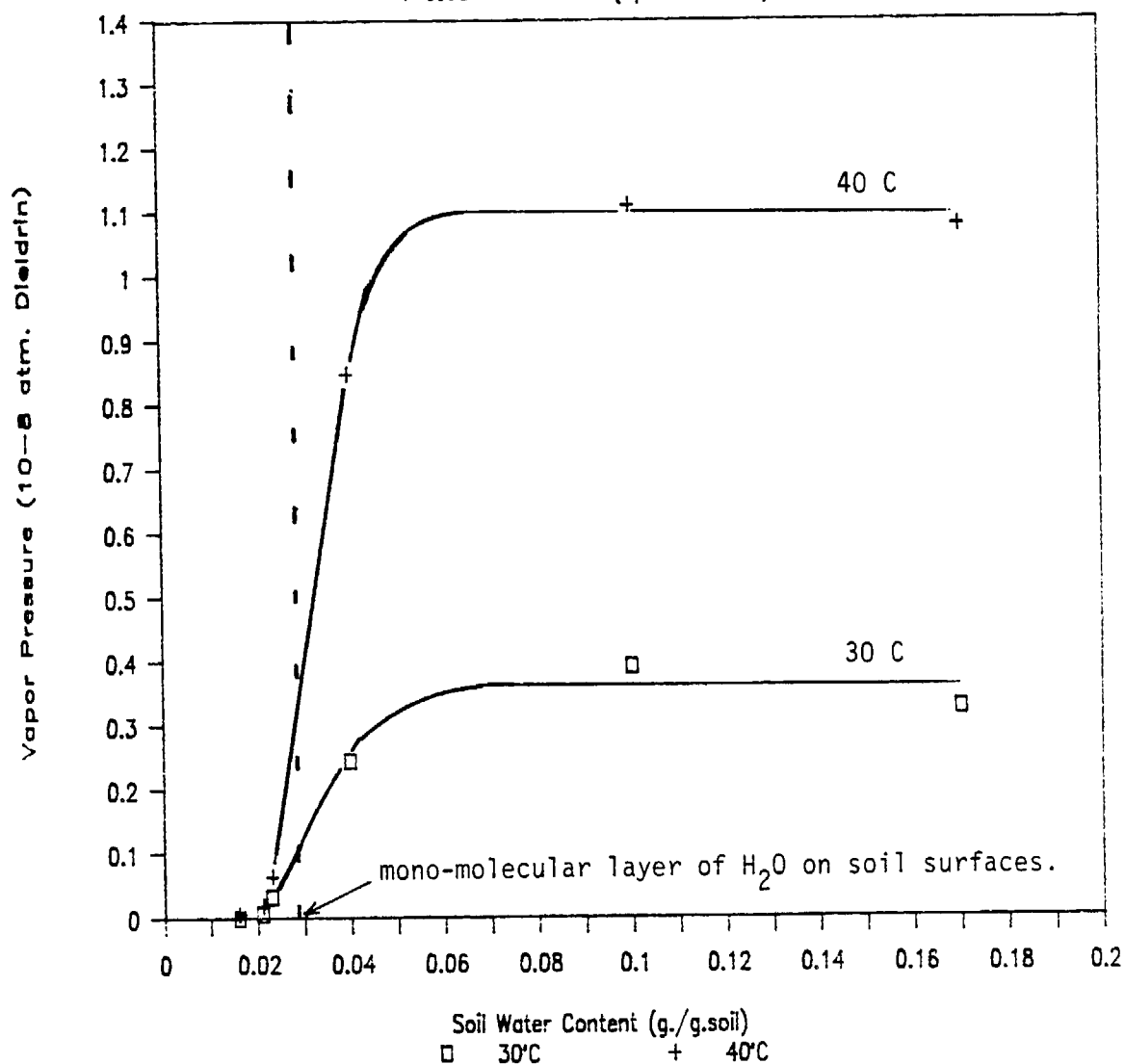
FIGURE 3. Vapor pressure of Dieldrin in soil as a function of
soil water content.
10 ppm Dieldrin in the soil.

zation upon drying of the soil. As the water content of the soil became low enough (< 2.8% w/w H_2O), water no longer preferentially adsorbed on the soil surface. The increased organochloride adsorption caused a large decrease in the vapor pressure and as a consequence, a decrease in the volatilization flux. Guenzi and Beard (1970) observed the same behavior for the volatilization of the pesticides Lindane and DDT from soils. In general, adsorption of pesticides or other organic compounds will be the greatest when soil water content is below that which equals a monolayer of water molecules on the soil particle surfaces. Competitive adsorption of soil organic compounds and water is still a factor, though a minor one, at high water contents and will tend to reduce volatilization. This phenomenon is described more completely in Section 2.5.

2.2 Adsorption of Organic Compounds on Soil

Vapor pressure behavior can be conveniently described by a linear desorption isotherm, as shown in Figure 4, for the pesticide Lindane (Spencer, 1970). The partitioning of an organic compound among the vapor, liquid, and solid phases is given by linear equilibrium relationships for each phase,

$$C_s = K_D \, C_\ell \tag{1}$$

where C_s is the concentration of the organic on the solid surface (g/g soil), C_ℓ is the concentration in the aqueous phase (g/cm^3), and K_D(cm^3/kg) is a distribution coefficient and is the slope of the adsorption isotherm. Due to the variation in soil organic fractions from different soil samples (0.1 - 5.0% in most cases), K_D is normalized by dividing it by the organic fraction:

$$K_{oc} = K_D/f_{oc} \tag{2}$$

where Koc is the normalized distributuion coefficient and foc is the organic

Desorption Isotherms for Lindane
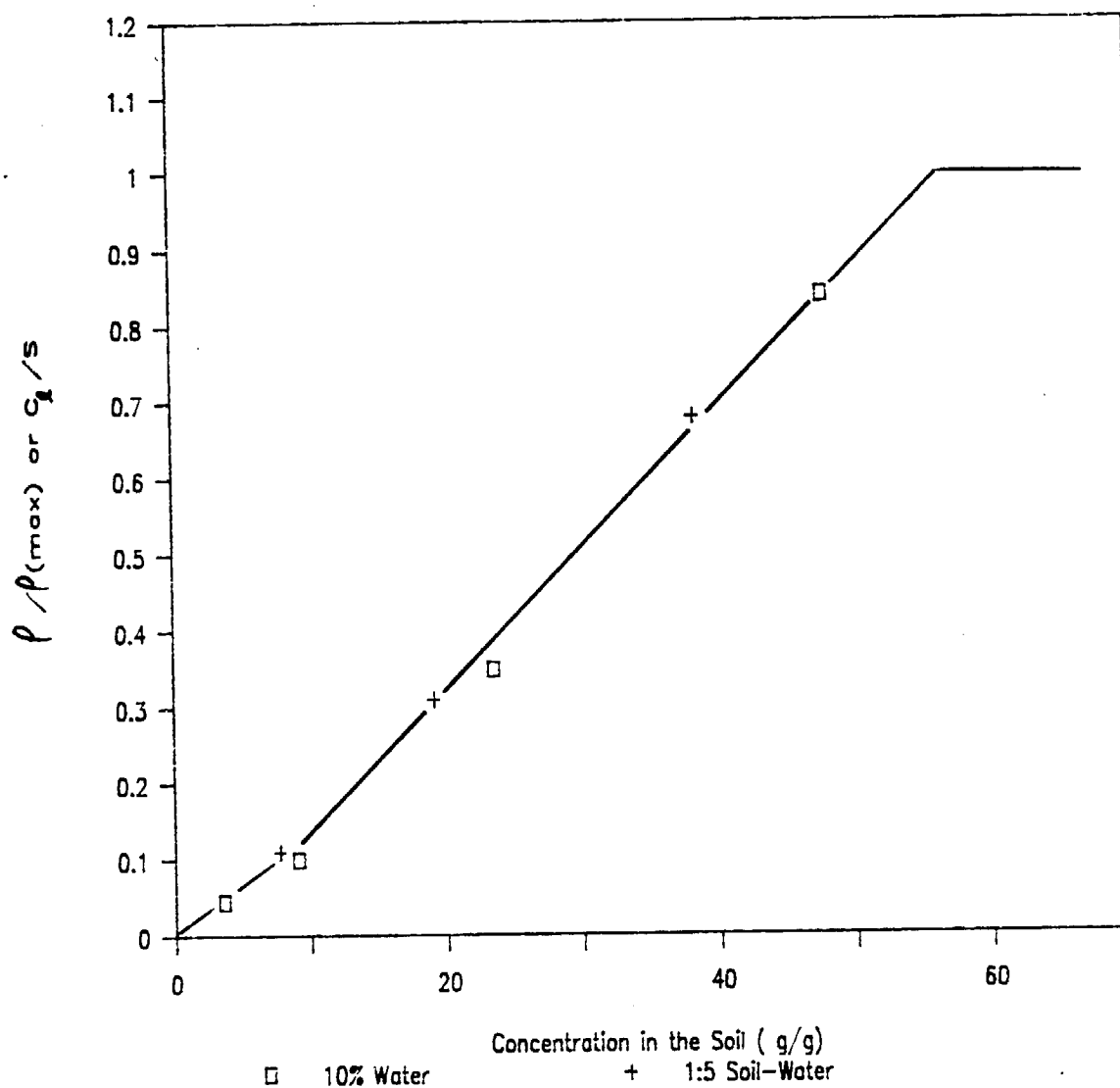
FIGURE 4. Desorption isotherms for Lindane at 30 C.

P = the vapor pressure of Lindane in the soil.

P_{max} = the saturation vapor press. of Lindane at 30 C.

C_{ℓ} = the aqueous phase concentration of Lindane.

S = the saturation aqueous phase concentration of Lindane at 30 C.

fraction. In a similar fashion, the vapor and aqueous phase concentrations of organic are in equilibrium and can be described by a linear relation,

$$C_g = K_H C_\ell \qquad (3)$$

where C_g is the gas phase concentration (g/cm^3) and K_H is Henry's Law constant. By combining the partition equations above, the vapor and adsorbed solid phase concentrations are described by

$$C_g = \frac{K_H}{K_{oc} f_{oc}} C_s \qquad (4)$$

In many instances in the landfarming of oily wastes, the soils are loaded with a relatively large amount of organic compounds. Dibble and Bartha (1979) reported up to 5% wt. oil/wt. soil. This is vastly in excess of the ability of the soil to adsorb it (0.001% to 0.01%). In such a case, the vapor pressures and aqueous solubilities of the organic compound will be at saturation values during much of the time that volatilization occurs.

2.3 Temperature Effects

The effect of temperature upon the vapor pressure of pesticides in soil was measured by Farmer et. al. (1972) and by Spencer et. al. (1969). Both studies showed a 3 to 4-fold increase in soil vapor pressure for every 10°C increase in temperature. The same increase occured for the volatilization flux of pesticide measured over time (Farmer et. al., 1972).

2.4 The Aqueous Phase

In the soil, partitioning of organic compounds occurs between the soil solid phase and aqueous phase and is similar to the aqueous vapor phase behavior

of the compound. The aqueous phase concentration of the organic compound has been found to follow a linear desorption isotherm at low concentrations of soil organic (Spencer, 1970). See Figure 4. At higher soil concentrations of organic compounds, aqueous phase saturation is reached. Aqueous phase concentrations of organic compounds become important when considering movement of the compound through the soil by diffusion in the water phase and also by mass transport of the organic due to capillary action. Mass transport refers to the movement of solubilized organic through the soil column by evaporation at the soil-air interface and the "wicking up" of subsurface water (Spencer et. al., 1973).

2.5 Soil Type

The soil composition, in terms of mineral particle size and the fraction of organic matter can affect the vapor pressure of a soil applied organic compound or pesticide (Spencer 1970). Table 1 demonstrates the effect of soil organic matter upon the vapor pressure of a pesticide applied at 10 ppm concentration. When considering soils with increasing soil organic matter contents (Table 1), a decrease in vapor pressure from the saturation value to 16% of the saturation value occurred. Clearly, organic compounds applied to the soil have a high affinity for the soil organic matter and preferentially adsorb at these sites even under wet soil conditions.

TABLE 1: Effect of Soil Organic Matter and Clay Content on Vapor Pressure of Dieldrin at 30°C in Wet and Dry Soils Containing 10 ppm of pesticide (Spencer 1970).

SOIL TYPE	SOIL ORGANIC MATTER(%)	CLAY(%)	Vapor Pressure WET p/p_{max}	DRY p/p_{max}
Very Fine Sandy Loam	0.19	16.3	0.87	0.008
Imperial Clay	0.20	67.3	1.00	0.014
Silt Loam	0.58	18.4	0.26	0.004
Sandy Loam	1.62	10.0	0.16	0.002
Clay Loam	2.41	33.4	0.16	0.003

p = vapor pressure of pesticide in the soil

p_{max} = the maximum vapor pressure of pesticide in the soil at 30°C (corresponds to pure pesticide vapor pressure at 30°C)

It should be noted that the concentrations of Dieldrin in the soils listed in Table 1 are very small (10 ppm) and that the same adsorption behavior will not occur in soils having much larger Dieldrin concentrations. At a large enough concentration of Dieldrin (or any other organic compound), the capacity of the soil for adsorption will be filled and no changes in vapor pressure will occur as a result of adsorption processes. In this instance, the soil vapor pressure will essentially be that of the pure compound and not modified by adsorption. As can be seen in Figures 1 and 4, the vapor pressure in soil is the saturation value (corresponding to the vapor pressure of the organic compound in the absence of adsorption processes) when the soil concentration of the organic compound is greater than about 50 ppm. In summary, adsorption processes in soil are only important for dilute concentrations of organic compounds in the soil.

2.6 Mechanisms of Transport Through Soil

Measurements of vapor loss from soils which have additions of organic compounds or pesticides have shown that the transport to the soil surface is controlled by diffusion and by mass flow of organic compounds during evaporation of water (Lyman et. al., 1982). Evaporation of water has been shown to increase volatilization from soils through the movement of water soluble compounds to the soil surface by capillary action. Accumulation and volatilization of the organic compound can then occur at the soil surface. Volatilization rates have been measured by Spencer et. al. (1973) from soils in which evaporation of water was controlled. Figure 5 demonstrates the importance of water evaporation upon the flux of Lindane from soil containing 10 ppm of the pesticide. Movement of pesticides through soils by water flow is a dominant transport mechanism for long time volatilization processes as demonstrated in Figure 5.

Initially, the volatilization process is controlled by the diffusion of the organic compound through the soil vapor and liquid phases, and only after long times, does water evaporation become dominant as a transport mechanism (Jury et. al., 1980; Spencer et. al., 1973). This behavior is modified -- either amplified or suppressed -- by the solubility of the organic compound in the aqueous phase. Transport of organic compounds by capillary action makes a greater contribution to the rate of volatilization for highly water soluble compounds. Similarly, the rate of water evaporation is important.

According to Lyman et. al., diffusion of soil organic compounds occurs by four pathways: vapor phase diffusion, aqueous phase diffusion, vapor-aqueous phase interfacial diffusion, and diffusion on the adsorption surfaces. Shearer et. al. (1973) and Ehlers et. al. (1969) have measured and calculated the contribution to the overall diffusion process of both vapor and aqueous phase

Lindane Volatilization Rate, 30'C,

Effect of Diffusion and water flow.
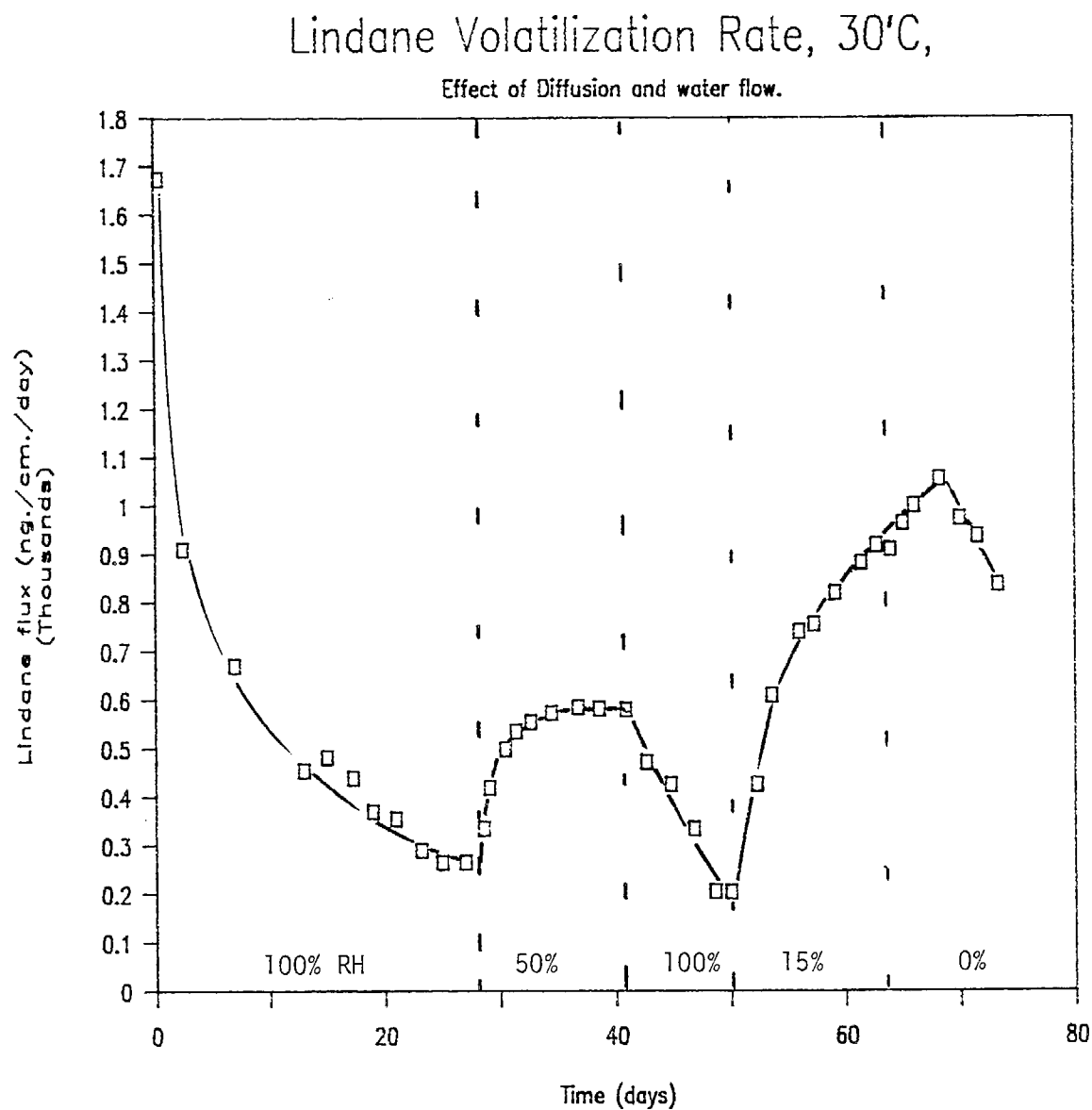
FIGURE 5. The effect of water evaporation on the flux of
Lindane from the soil.

ng. = nanograms (10^{-9}) grams.

RH = relative humidity of air.

diffusion. In a series of two journal articles, Ehlers et. al. (1969) have considered the theoretical aspects and mechanisms of movement by diffusion, and have observed the effects of bulk density, temperature, and soil water content on the overall diffusion coefficient in soil. They concluded that the vapor pressure of the soil organic compound was the most important factor at low water contents (presumably due to the vapor phase diffusion), while at higher values of water content, aqueous phase diffusion becomes most important.

3.0 Microbial Utilization of Organic Compounds

It is apparent that microorganisms in the soil occupy a very important position in returning fixed forms of carbon, such as hydrocarbons and cellulose, to free carbon as in the form of CO_2. Biochemical transformations of organic matter by aerobic and anaerobic microorganisms are favored based on thermodynamic considerations, but for many compounds found in the environment, these bioconversions occur at a negligible rate (Dagley, 1984). The rate of biodegradation of organic compounds of environmental concern is a function of the degree of similarity between the compound in question and naturally occuring compounds in the soil which degrade more quickly.

Soil microorganisms utilize the energy released upon oxidation of organic compounds to grow and maintain metabolic functions. Organic compounds can be degraded aerobically to CO_2, the most oxidized form of carbon, or anaerobically to form CH_4, the most reduced form of carbon. In both cases, energy is derived from the transport of electrons to the ultimate electron acceptors; aerobically to O_2 to form H_2O, and anaerobically to carbon to form CH_4 (Dagley, 1984). Biodegrading enzymes, which are synthesized by microorganisms, are the biological catalysts which mediate and accelerate these bioconversions.

3.1 Microbial Types

Microorganisms in the soil -- bacteria, actinomycetes, yeast and fungi -- are versatile decomposers of organic matter, and a search of the microbial world will reveal a few strains which can utilize virtually every one of the compounds biosynthesized by living matter (Dagley, 1978). For example, a great number of soil bacteria and yeast genera have been found to be able to utilize aliphatic hydrocarbon compounds as their sole carbon source (Britton, 1984). Though this ability to degrade aliphatic hydrocarbons is common, microorganisms demonstrate a substrate specificity that can be summarized in Table 2 (Britton, 1984).

TABLE 2: Microbial Specificity Toward Hydrocarbons

CLASSIFICATION	RANK
Degradability	aliphatics > cycloalkanes > aromatics
Chain Length	long chain > short chain n-alkanes
Chain Branching	straight chain > branched chain
Degree of Unsaturation	saturated > unsaturated aliphatics

3.2 Microbial Morphology Changes

When soil microorganisms are exposed to a hydrocarbon substrate, several morphological changes occur compared to the same species grown on water soluble growth substrates. For the genera Acintobacter, adaptation to the water insoluble hydrocarbons hexadecane, heptadecane, and 1-hexadecene, resulted in structural changes in the micro-organisms (Singer & Finnerty , 1984; Kennedy et. al., 1975; Scott et. al., 1976; Scott & Finnerty, 1976; Kennedy & Finnerty, 1975; Scott & Finnerty, 1976). These features of the ultrastructure of the micro-organism include: 1) intracytoplasmic membranes which have a high concentration

of hydrocarbon degrading enzymes, 2) hydrocarbon inclusions which are pools of hydrocarbon storage, and 3) cell walls and cell membranes which are enriched in hydrocarbon substrate. These features, which demonstrate the ability of the microorganism to concentrate the insoluble hydrocarbon inside the cell wall, enable a higher rate of degradation.

3.3 Mechanisms In Hydrocarbon Degradation

In the process of aerobic degradation of hydrocarbon substrates, bacteria demonstrate a feature which belongs almost exclusively to this type of microorganism, namely the ability to incorporate molecular oxygen directly into the compound being degraded (Dagley, 1984). This unique ability to oxidize hydrocarbons allows bacteria to convert these normally nondegradable compounds into substances found in more common biochemical pathways. Two important enzyme systems which begin the degradation process are monooxygenases and dioxygenases. Monooxygenases catalyze reactions such as

$$RH + O_2 + 2 H \rightarrow R\text{-}OH + H_2O \tag{1}$$
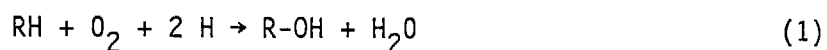
in which one atom of the O_2 molecule is incorporated into the hydrocarbon and the other combines with two hydrogens to form water. The two hydrogen atoms are made available by a hydrogen carrying biomolecule in the cell. Dioxygenases incorporate both atoms of O_2 into the benzene ring structure to form a dihydroxyl intermediate which then undergoes ring fission (Dagley, 1978).

3.4 Landfarming Studies of Oily Wastes

In a laboratory study for the degradation of an oily waste, the optimum environmental conditions were determined by Dibble and Bartha (1979). Oil degradation was monitored by CO_2 evolution and analysis of residual hydrocarbon. The optimum application rate of oily waste was determined to be 10ℓ.oily waste/m^2 loaded twice over a growing season, and resulted in the highest overall degradation for all hydrocarbon classes (aliphatics, aromatics, and asphaltics). For this application rate, the overall reduction of hydrocarbon was approximately 50% over a 285 day period. The optimum soil-water content was determined to be 30%-90%, a soil pH of 7.5-7.8, a carbon to nitrogen ratio of 60:1, a carbon to phosphorus ratio, of 800:1, and a temperature of 20°C. The study did not include a measure of the effect on volatilization of biodegradation of the oily fraction nor of post degradative by-products. In another study of biodegradation of oils in the soil, the effects of additions of deficient nutrients and bacteria innoculum were measured (Jobson et. al., 1974). The results showed a reduction in the n-saturate content of the crude and a persistance of the isoprenoids, phytane and pristane. An increase in polarity of the residual soil crude oil was found to be due to the introduction of oxygen into various compounds. This last finding indicates potential leaching of the more water-soluble by-products.

3.5 The Kinetics of Microbial Utilization of Hydrocarbons

From a search of the literature involving the biodegradation and utilization of hydrocarbon substrates, a promising kinetic model was found (Erickson, 1969). Assumptions were made that the hydrocarbon was the only limiting component (i.e. that all other nutrients were present in great excess) in a batch

reactor system, that Michaelis-Menten-Monod kinetics applied, and that growth of the microorganism only occured at the surface of a hydrocarbon drop. By assuming further that the growth-limiting hydrocarbon was dissolved in an inert oil drop and that the reduction in the drop size was negligible, a solution was obtained which predicted the variation of substrate and increase in cell population with time. The model results were in good agreement with batch fermentation data for growth of yeast on a mixture of n-alkanes in gas-oil. This kinetic model is particularly well suited for degradation of waste oil in landfarming studies due to the similar nature of the substrates.

4.0 Volatilization Models for Soil Hydrocarbons

Several models have been proposed to estimate the volatilization rates from soils in which small amounts of organic compounds have been incorporated. A review of current models for vapor transport from both soil surface and soil incorporated organics is available (Lyman et. al., 1984). The models differ in the degree of simplicity and specialization which is inherent in their derivation. The Hartley equation (Hartley, 1969) is based upon the assumption of evaporation from a soil surface and no account is taken for diffusion through the soil profile. This method states that the flux of a pure organic compound applied at the soil surface can be obtained from a knowledge of the evaporation flux of water vapor from the same surface.

$$J_i = J_w \ \frac{P_i \ (MW_i)^{\frac{1}{2}}}{(1 - RH) \ P_w \ (MW_w)^{\frac{1}{2}}} \qquad (2)$$

J_i = the evaporation flux of a surface applied organic (kg/m^2/day)

J_w = the evaporation flux of surface applied water (kg/m^2/day)

P_i = the partial pressure of the organic (atm)

P_w = the partial pressure of water (atm)

RH = the relative humidity of the air above the surface

MW_i = the molecular weight of the organic (g/mol)

MW_w = the molecular weight of water (g/mol)

In order to apply this simple model, the only parameters which must be known are the values of J_w , P_i , and MW for any given set of environmental conditions. The main advantage of this model is the ease in calculating evaporation rates for pure component organics. It is also appropriate to use this model to estimate the initial rate of vapor loss of a soil-incorporated organic compound. For larger periods, this model should not be used to estimate soil diffusion of organics, and has the disadvantage of not considering biodegradation and adsorption processes.

A model for soil incorporated organic compounds has been proposed by Thibodeaux (1979). In this model, a gradientless moving-front diffusion problem is considered and the vaporization rate is solved as a function of time. The final equation for the rate of volatilization is

$$J_i = \frac{D_E \ (p_i^* - p_i) \ (\frac{MW_i}{RT})}{2D_E \left[\dfrac{(p_i^* - p_i)MW_i}{m_i/(A \cdot h) \ RT} \cdot t \right]^{\frac{1}{2}}} \tag{3}$$

where

J_i = the volatilization flux of organic compound, i $(kg/m^2/day)$

D_E = the effective diffusion coefficient of i in the soil (m^2/day)

p_i^* = the vapor pressure of i in the wet soil zone (atm)

p_i = the vapor pressure of i at the wet-dry soil interface (atm)

m_i = the total mass of i applied to the soil (kg)

A = the cross-sectional area of the soil (m^2)

h = the depth of incorporation of compound i (m)

The advantages to using this model are that the diffusion process through the soil is controlling the volatilization rate, there are only a few parameters to consider, and it predicts a decrease of volatilization with time. On the other hand, this model neglects several important soil processes such as biodegradation and adsorption, and lacks sensitivity to atmospheric conditions such as wind speed, relative humidity of the air, and energy budgets. Again, as in the previous model, it is not acceptable for an accurate determination of vapor fluxes from soils which incorporate organic compounds.

The final model to be considered thus far is that of Jury et. al. (1983). This model describes the transport and loss of soil applied organic compounds and was derived to be used as a screening model for the development of new pesticides. The model assumes a linear, equilibrium partitioning between the vapor, aqueous, and adsorbed phases; net first order biodegradation; steady-state upward or downward movement of water due to evaporation or infiltration; and loss to the atmosphere by mass transfer through a stagnant air boundary layer at the soil surface. From these assumptions, an analytical solution for the soil concentration and volatilization flux was obtained:

$$C_T(Z_1t) = \tfrac{1}{2}C_0\exp(-\mu t)\left\{\left\{\left(erfc\left[\frac{(Z-L-V_Et)}{\sqrt{4D_Et}}\right] - erfc\left[\frac{(Z-V_Et)}{\sqrt{4D_Et}}\right]\right\}\right.\right.$$

$$+ (1 + V_E/H_E)\exp(V_EZ/D_E)$$

$$\left\{erfc\left[\frac{(Z+L+V_Et)}{\sqrt{4D_Et}}\right] - erfc\left[\frac{(Z+V_Et)}{\sqrt{4D_Et}}\right]\right\} \qquad (5)$$

$$+ (2+V_E/H_E)\exp\left(\left[H_E(H_E+V_E)t + (H_E+V_E)Z\right]/D_E\right)$$

$$\left\{erfc\left[\frac{Z+(2H_E+V_Et)}{\sqrt{4D_Et}}\right] - \exp(H_EL/D_E)erfc\left[\frac{Z+L+(2H_E+V_E)t}{\sqrt{4D_Et}}\right]\right\}\right\}$$

C_T = the total soil organic concentration (g/m^3)

C_0 = the initial soil organic concentration (g/m^3)

μ = a first order biodegradation rate constant (day^{-1})

t = time (day)

z = the depth below the soil-air interface (m)

L = the depth of initial incorporation of organic (m)

V_E = the effective solute convective velocity (m/day)

D_E = the effective diffusivity in the soil (m^2/day)

H_E = the effective transport coefficient across the stagnant air boundary layer at the surface (m/day)

$erfc$ = the complimentary error function (1-erf)

$$erf(x) = \frac{2}{\sqrt{\pi}} \int_0^x \exp(-J^2)dJ$$

The volatilization flux evaluated at the soil-air surface is given by differentiating the above equation with respect to z and evaluated at $z = o$,

$$J_S(0,t) = \frac{1}{2}C_0 \exp(-\mu t) \left\{ V_E \left(\text{erfc}\left[\frac{V_E t}{\sqrt{4D_E t}}\right] - \text{erfc}\left[\frac{(L+V_E t)}{\sqrt{4D_E t}}\right] \right. \right.$$

$$+ 2(H_E + V_E) \exp[H_E(H_E+V_E)t/D_E]$$

$$\exp(H_E L/D_E) \text{ erfc}\left[\frac{L+(2H_E+V_E)t}{\sqrt{4D_E t}}\right]$$

$$\left. \left. - \text{erfc}\left[\frac{(2H_E+V_E)t}{4d_E t}\right] \right) \right\}$$

where

$$J_S = \text{the flux of vapor to the atmosphere (g/m}^2\text{/day)}$$

The equation for J_S (0,t) can be greatly simplified for the special case of negligible mass transfer resistance at the soil-air interface, no biodegradation, and no evaporation-infiltration of water through the soil profile.

$$J_v \propto C_0 \, K_H^{1/2} \, a^{5/3} \, K_{oc}^{-1/2} \, f_{oc}^{-1/2} \, t^{-1/2}$$

where

J_v = the organic vapor flux to the atmosphere (g/m^2/day)

K_H = the dimensionless Henry's Law constant

a = the volumetric air content (m^3/m^3)

$$K_{oc} = K_D/f_{oc}$$

K_D = the solid-aqueous partition coefficient (m^3/kg)

f_{oc} = the fraction organic carbon in the soil

t = time (days)

The most important advantages to the Jury et. al. model are:

1. An analytical solution is available.

2. Parameter sensitivity can be easily determined.

3. In special cases, a large degree of simplification can occur.

4. The most important physical, chemical, and biochemical parameters of soil are considered.

The disadvantages of this model are that the biodegradation rate coefficient is modeled as a first order reaction and that this equation can only be applied to very small concentrations of organics in the soil. Landfarming of oily wastes commonly has much greater loadings of the organic than the part-per-million concentrations assumed in this model.

In considering all the soil volatilization models thus far, the model of Jury et.al. appears to hold the most promise for accurately determining the fluxes of VOC from soils amended with organic compounds, however, future research in this area will undoubtedly result in improved models.

REFERENCES

1. Antoine, C. (1888). C.R. 107:681, 836.

2. Britton, Larry N. (1984). "Microbial degradation of aliphatic hydrocarbons." In: Microbial Degradation of Organic Compounds (David T. Gibson, ed), 89-129, Marcel Dekker, Inc.

3. Dagley, Stanley, (1978). "Pathways for the utilization of organic growth substrates." In: The Bacteria. Vol. VI Bacterial Diversity (I.G. Gunsalus, L.N. Ornston, and J.R. Sokatch, eds), 303-388.

4. Dagley, Stanley, Ibid., 1-10.

5. Dibble, J.T. and Bartha, R. (1979). "Effect of environmental parameters on the biodegration of oil sludge," Appl. Environ. Microbiol., 37:729-739.

6. Ehlers, W., Letey, J., Spencer, W.F., and Farmer, W.J. (1969). "Lindane diffusion in soils: I. Theoretical considerations and mechanisms of movement." Soil Sci. Soc. Amer. Proc. 33:501-504.

7. Ehlers, W., Letey, J., Spencer, W.F., and Farmer, W.J. (1969). "Lindane diffusion in soils: II. Water content, bulk density, and temperature effects." Soil Sci. Soc. Amer. Proc. 33:505-508.

8. Erickson, L.E., and Humphrey, A.E. (1969). "Growth models of cultures in two liquid phases. II. Pure substrate in dispersed phase." Biotechnol. Bioeng. 11:467-487.

9. Farmer, W.J., Igue, K., Spencer, W.F., and Martin, J.P. (1972). "Volatility of organochlorine insecticides from soil: I. Effect of concentration, temperature, air flow rate, and vapor pressure." Soil Sci. Soc. Amer. Proc. 36:443-447.

10. Guenzi, W.D., and Beard, W.E. (1970). "Volatilization of Lindane and DDT from soils." Soil Sci. Soc. Amer. Proc. 34:443-447.

11. Hartley, G.S. (1969). "Evaporation of Pesticides." In: Pesticide Formulation Research, Adv. Chem. Series. 86:115.

12. Igue, K., Farmer, W.J., Spencer, W.F., and Martin, J.P. (1972). "Volatility of organochlorine insecticides from soils: II. Effect of relative humidity and soil water content on Dieldrin volatility." Soil. Sci. Soc. Amer. Proc. 36:447-450.

13. Jobson, A., McLaughlin, M., Cook, F.D., and Westlake, D.W.S. (1974). "Effect of amendments on the microbial utilization of oil applied to soil." Appl. Microbiol. 27:166-171 (1974).

14. Jury, W.A., Spencer, W.F., and Farmer, W.J. (1983). "Behavior assessment model for trace organics in soil: I. Model description." J. Environ. Qual. 12:558-564.

15. Jury, W.A., Grover, R., Spencer, W.F., and Farmer, W.F. (1980). "Modeling vapor losses of soil-incorporated Triallate." Soil Sci. Soc. Amer. J. 44:445-450.

16. Kennedy, R.S., Finnerty, W.R., Sadarsanan, K., and Young, R.A. (1975). "Microbial assimilation of hydrocarbons, I. The fine-structure of a hydrocarbon oxidizing Acinetobacter sp." Arch. Microbiol. 102:75-83.

17. Kennedy, R.S. and Finnerty, W.R. (1975). "Microbial assimilation of hydrocarbons, II. Intracytoplasmic membrane induction in Acinetobacter sp." Arch. Microbiol. 102:85-90.

18. Lyman, W.J., Reehl, W.F., and Rosenblatt, D.H. (1982). "Handbook of Chemical Properties Estimation Methods: Environmental Behavior of Organic Chemicals." Chpt. 16. McGraw-Hill, New York.

19. Scott, C.C.L., Makula, R.A., and Finnerty, W.R. (1976). "Isolation and characterization of membranes from a hydrocarbon-oxidizing Acinetobacter sp." Journal of Bacteriology, 127:469-480.

20. Scott, C.C.L. and Finnerty, W.R. (1976). "Characterization of intracytoplasmic hydrocarbon inclusions from the hydrocarbon-oxidizing Acinetobacter species HO1-N." Journal of Bacteriology, 127:48-489.

21. Scott, C.C.L. and Finnerty, W.R. (1976). "A comparative analysis of the ultrastructure of hydrocarbon-oxidizing microorganisms," Journal of General Microbiology, 94:342-350.

22. Shearer, R.C., Letey, J., Farmer, W.J., and Kute, A. (1973). "Lindane diffusion in soil." Soil Sci. Soc. Amer. Proc. 37:189-193.

23. Singer, M.E. and Finnerty, W.R. (1984). "Microbial metabolism of straight-chain and branched alkanes." In: Petroleum Microbiology (R.M. Atlas, ed.), 1-59, Macmillan Publ. Co.

24. Spencer, W.F., Claith, M.M., and Farmer, W.J. (1969). "Vapor density of soil-applied Dieldrin as related to soil-water content, temperature, and Dieldrin concentration." Soil. Sci. Soc. Amer. Proc. 33:509-511.

25. Spencer, W.F. (1970). "Distribution of pesticides between soil, water, and air." In: Pesticides in the Soil: Ecology, Degradation, and Movement, 120-128, Michigan State University.

26. Spencer, W.F. and Claith, M.M. (1973). "Pesticide volatilization as related to water loss from soil." J. Environ. Quality, 2:284-289.

27. Thibodeaux, L.J. (1979). Chemodynamics: Environmental Movement of Chemicals in Air, Water, and Soil. 339, John Wiley and Sons.

NOMENCLATURE

A	cross-sectional area of the soil (m^2)
a	volumetric air content of the soil (m^3/m^3)
C_g	concentration of organics in the gas phase (gm organic/cm^3)
C_ℓ	concentration of organics in the aqueous phase (gm organic/cm^3 aqueous)
C_o	initial soil organic concentration (gm/m^3 soil)
C_s	concentration of organics on the solid surface (gm organic/gm soil)
C_T	total soil organic concentration (gm/m^3 soil)
D_E	effective diffusion coefficient of organic i in the soil (m^2/day)
f_{oc}	fraction of organic carbon in the soil
H_E	effective transport coefficient across the stagment air boundary layer at the surface (m/day)
h	depth of incorporation of organic component i (m)
J_i	evaporation flux of organic i ($kg \cdot m^{-2} \cdot day^{-1}$)
J_s	flux of vapor to the atmosphere ($g \cdot m^{-2} \cdot day^{-1}$)
J_v	flux of organic vapor to the atmosphere ($g \cdot m^{-2} \cdot day^{-1}$)
J_w	evaporation flux of water ($kg \cdot m^{-2} \cdot day^{-1}$)
K_H	Henry's Law constant (y_i/x_i)

K_D solid-aqueous distribution coefficient $(m^3 \cdot kg)$

K_{oc} normalized distribution coefficient (K_D/f_{oc})

L depth of initial incorporation of organic into the soil (m)

MW   molecular weight

MW_i molecular weight of the organic i

MW_w molecular weight of water

m_i total mass of organic i applied to the soil (kg)

P vapor pressure of pesticide in the soil (atm)

p_i^* vapor pressure of organic i in the wet soil zone (atm)

p_i vapor pressure of organic i at the wet-dry soil interface (atm)

P_{max} maximum vapor pressure of pesticide in the soil at 30°C (atm)

P_i partial pressure of organic i (atm)

P_w partial pressure of water (atm)

RH   relative humidity

t time (day)

z depth below the soil-air interface (m)

Greek

μ first-order biodegradation rate constant (day^{-1})

ABBREVIATIONS

API	American Petroleum Institute
ASTM	American Society for Testing Materials
AT	attenuation
BPD	barrels per day
CARB	California Air Resources Board
ChE	Chemical Engineer(ing)
cp	centipoise
erf	error function
erfc	complimentary error function
FID	flame ionization detector
GC	gas chromatography
GCMS	gas chromatography/mass spectrometer
MS	mass spectrometer
NBS	National Bureau of Standards
ppm	parts per million
RVP	Reid Vapor Pressure
TIC	Total Ion Chromatogram
VOC	volatile organic compounds
w/w	weight/weight fraction
YSI	Yellow Springs Instrument Company, Incorporated

ADDENDUM A

Volume II

ORIGINS OF PETROLEUM AND ITS GENERAL CHEMISTRY

Kimiye Tanaka

TABLE OF CONTENTS

FIGURES

TABLES

ORIGINS OF CYCLOALKANES

INTRODUCTION

The most important contribution to the identification of hydrocarbons present in crude oil was Research Project 6: Analysis, Purification and Properties of Petroleum Hydrocarbons. This study, sponsored by the American Petroleum Institute (API) began in 1926, and involved analysis of petroleum fractions from seven locations in the United States. The University of California team in Davis, in a separate study, attempted to determine the identity and quantity of hydrocarbons in the fraction below 150°C, in heavy crude from Kern County. Frequent references to the API Project 6 data made it apparent that cycloalkanes play a significant role in the composition of crude oil (see Tables 1 and 2). Data sheets for the UCD study can be found in the Appendix. Interest in the biological origins of these cyclic compounds resulted in this brief review of their origins.

GENERAL ORIGINS AND CHEMISTRY OF PETROLEUM

Petroleum is primarily composed of three types of hydrocarbons: the paraffins, cycloalkanes and aromatics. The paraffin family consists mainly of C1 to C30 normal- and iso-alkanes with small degrees of branching. The cycloalkanes are primarily cyclopentane and cyclohexane rings with or without alkyl substitution, though higher boiling fractions contain cycloalkanes with one or more rings and longer alkyl side chains. Aromatics are present in lower relative quantities than paraffins or cycloparaffins and may, at higher molecular weights, contain both aromatic and cycloparaffins in the same molecule (Meinschein, 1959).

Table 1:   Relative amounts of the classes of hydrocarbons by peak area of
           identified components   (UCD study).

CLASSES OF HYDROCARBONS	Relative amounts of the identified compounds		
	31X	MONTE CRISTO	36W
Normal Paraffins	0	0	17.4
Branched Paraffins	6.4	36.5	30.8
Alkenes	0	0.5	2.6
Alkyl Cyclopentanes	39.4	44.8	24.5
Alkyl Cyclohexanes	52.3	18.1	7.5
Alkyl Benzenes	1.9	0	17.2
	100.0	100.0	100.0

Table 2:   Relative amounts of the five classes of hydrocarbons in the 40 to
           210°C fraction of each of the straight-run gasolines.

CLASS OF HYDROCARBONS	Relative amounts of the identified compounds						
	PONCA, OKLAHOMA	EAST TEXAS	BRADFORD, PENN.	GREENDALE-KAWKAWLIN, MICHIGAN	WINKLER, TEXAS	MIDWAY, CALIF.	CONROE, TEXAS
Normal Paraffins	35.3	24.6	34.1	62.2	9.5	9.9	17.6
Branched Paraffins	20.2	27.1	32.0	13.0	61.4	21.4	19.6
Alkyl Cyclopentanes	23.1	25.9	13.4	7.8	20.4	40.7	16.6
Alkyl Cyclohexanes	20.2	21.9	20.0	15.5	8.2	27.4	42.6
Alkyl Benzenes	1.2	0.5	0.5	1.5	0.5	0.6	3.6
	100.0	100 .0	100.0	100.0	100.0	100.0	100.0
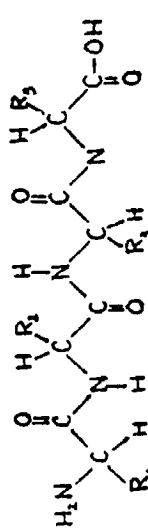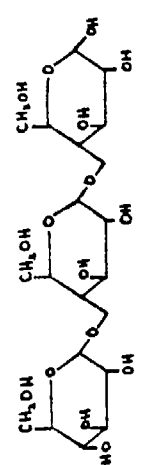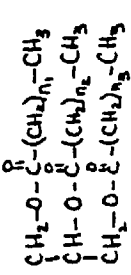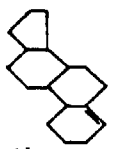
(Rossini, Mair, and Streiff, 1953).

Beginning about 2 billion years ago, during the Precambrian period, blue-green algae were amongst the first sources of organic matter. Along with marine phytoplankton and bacteria, they dominated until the appearance and proliferation of the terrestrial plants near the middle of the Devonian period, some 350 million years later. Although terrestrial plants have caused the production of increasing amounts of organic matter of a different nature, it is estimated that even today, approximately 50 to 60 percent of the organic carbon produced origi-nates from microorganisms such as bacteria and marine phytoplankton (which includes the blue-green algae) (Tissot and Welte, 1984). This is a very large percentage, but due to the fact that these organ-isms are capable of surviving extreme environmental conditions plus the fact that they are major contributors to the absence of huge piles of dead animals and plants across the face of the earth, this number is not unbelievable.

Additional support for the importance of microbes in the formation of petroleum comes from the research of Ourisson, Albrecht, and Rohmer (1984), who have been studying the genesis of fossil fuels and organic sedimentary deposits at the molecular level for the last 20 years. Every sediment sampled and ana-lyzed by these gentlemen contained one form or another of hopanes, a lipid found almost exclusively in the cell membrane of bacteria and cyanobacteria (blue-green algae). Such a striking similarity in the wide variety of sediments was a pleasant surprise and has strengthened the belief that the lipids of microbes are the main precursors of petroleum (Breger, 1960).

In general, all organisms contain three main types of molecules: pro-teins, carbohydrates and lipids, each of which has the potential of being a pre-cursor of petroleum, due to their organic nature (see figure 1). The most likely precursor, however, appears to be the lipids, due to their hydrocarbon nature,

Fig. 1: Examples of the three classes of molecules prominant in organisms: proteins, carbohydrates, and lipids.

PROTEINS	CARBOHYDRATES	LIPIDS
PRIMARY STRUCTURE:	CELLULOSE = β-1,4-glucose polymer found in plant cells	SATURATED FATTY ACIDS: $CH_3(CH_2)_n COH$
The R-groups are saturated hydrocarbons, alcohols, aromatics, phenols, carboxylic acids, imidazole groups, guanidino groups, sulfur groups, or amino groups		UNSATURATED FATTY ACIDS (e.g. oleic acid) $CH_3(CH_2)_7 CH=CH(CH_2)_7 COH$
		FATS (TRIGLYCERIDES)
		GENERAL STEROID BASE:

as well as their resistance to bacterial degradation. Erdman (1961) has specu-
lated on the possibility of low molecular weight hydrocarbons being formed if
large enough quantities of proteins were deposited in marine sediments; and Trask
(1932) has found that if carbohydrates did occur in sediments, their quantities
were small and decreased with depth. However, protein and carbohydrates are not
likely candidates for petroleum precursors because of their susceptibility to
hydrolysis by bacterial enzymes.

Data on sediment, such as that collected by Ourisson, et. al., have proved
to be of great importance in determining the presence or absence of petroleum
formations below as well as the type of petroleum likely to be found (Dott and
Reynolds, 1969). The main differences between sediment and the petroleum which
evolves from it are: sediments may contain only a fraction of a percent to
several percent organics (Breger, 1960); the relative amounts of paraffins,
cycloalkanes, and aromatics will differ from the sediment to the petroleum
evolved from it; and the size of the molecules found in the sediment will be
larger than those found in the petroleum (Dott and Reynolds, 1969). The changes
which occur in organic matter from the time it is laid down in the sediment to
the time of the actual formation and accumulation of petroleum are difficult to
follow due to the formation of an insoluble rock known as kerogen which is
formed during diagenesis (Tissot and Welte, 1984).

Organic matter in sediment goes through two stages of evolution: diagene-
sis and catagenesis. Diagenesis, or the first stage, is the transformation of
organics, via aerobic and anaerobic bacterial decomposition. Aerobic bacteria
grow faster than anaerobic bacteria, thus lowering the oxygen, nitrogen, sulfur
and phophorous content at a faster rate than the anaerobes (Trask, 1932).
However, the depth to which the aerobic bacteria survive depends on the nature

of the sediment which determines the efficiency of oxygen diffusion (Taylor, 1984). Once the oxygen runs out, the anaerobes take over and may survive for years, thus acting as important precursors for organic residues since they are the last living creatures to alter the organic matter (Trask, 1932).

The ultimate form of the organics after diagenesis is kerogen, a highly insoluble form of organic matter comprising approximately 90% of the 1.0×10^{16} tons of organic carbon estimated to occur in sediments. Its formation occurs in sedimentary rock due to chemical rearrangement, polycondensation, and insolubilization. The environment in which the organics were originally laid down (marine versus non-marine) will influence the relative amounts of paraffins, cycloalkanes, and aromatics that will be present in the hydrocarbon fraction of the resulting petroleum.

Catagenesis, the second stage of organic evolution of sediments, involves the formation of petroleum as a result of the thermal degradation of kerogen. The main reasons for this breakdown appear to be the higher temperatures and pressures encountered as the depth of burial increases (Trask, 1932).

As much as 90% of the crude oil hydrocarbons originate from kerogen. The rest is relatively intact geochemical fossils (or biological markers) which are organic molecules that have survived unchanged or little altered from their original structure. These molecules show pronounced resistance to chemical change and have been used in petroleum, sediments, coals, and crude oils as indicators of their biological origin (Eglinton and Calvin, 1967). Unfortunately, due to the insoluble nature of kerogen, it is very difficult to follow the evolution of crudes. The reactions occurring in the formation of petroleum depend upon the temperatures, pressures, and types of catalysts (e.g. clays and minerals) in the local environment of the kerogen, and the end pro-

duct is usually a much simpler molecule than that which went into the production of the organic kerogen.

ORIGINS OF THE CYCLOALKANES

The original goal of this paper was to determine the biological precursors of the cycloalkanes (also known as cycloparaffins or napthenes) found in the crude oil samples we analyzed. Before proceeding much further, the obstacles which are faced in making absolute correlations between a biological class or species of organism and the particular hydrocarbons resulting from them should be realized. They are: 1) knowledge of the chemistry of organisms, though known in a general sense, is incomplete -- the principal constituents of only a very few small groups of living things have been identified; 2) the biochemistry of ancient organisms may or may not be the same as that of present-day organisms; and 3) little is known of the chemical changes that occur as organics become petroleum (Eglinton and Calvin, 1967). As a result, the origins of the cycloalkanes discussed here will be stated in general terms.

In particular, the third obstacle listed above involves problems in determining the composition of kerogen and the loss of much information concerning the biological origins of petroleum due to bacterial and thermal degradation of organic matter. Despite such difficulties, several possible sources of the cycloparaffins have been suggested (Mair, 1964; Breger, 1960; Brooks, 1950; Eglinton and Calvin, 1967; Meinschein, 1959). The most probable source appears to be the cyclic terpenoids, though the cyclization of the acyclic terpenoids and fatty acids has also been considered (Breger, 1960).

The first mechanism to be discussed involves the fatty acids. These molecules belong to the lipid family and are long-chain saturated or unsaturated

$$CH_3-(CH_2)_n-\overset{\overset{\displaystyle O}{\|}}{C}-OH$$
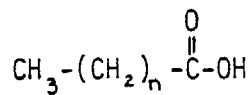
Figure 2a: Saturated Fatty
Acid.

$$CH_2-O-\overset{\overset{\displaystyle O}{\|}}{C}-(CH_2)_{n_1}-CH_3$$
$$CH-O-\overset{\overset{\displaystyle O}{\|}}{C}-(CH_2)_{n_2}-CH_3$$
$$CH_2-O-\overset{\overset{\displaystyle O}{\|}}{\underset{\underset{\displaystyle O^-}{|}}{P}}-O^-$$

Figure 2b: Phospholipid

(1) Hydrogenation

(2) Decarboxylation
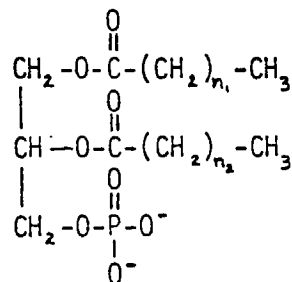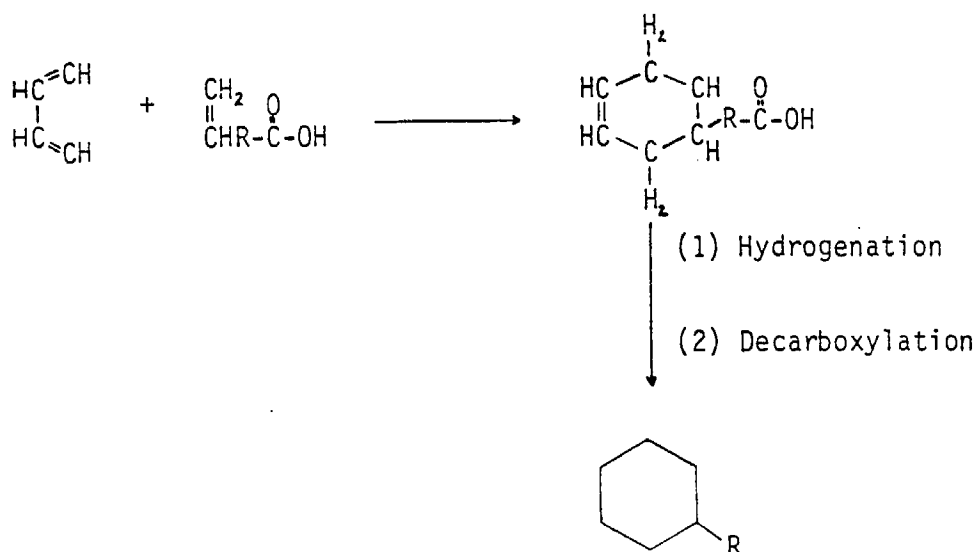
Figure 3: Cyclization of fatty acids via Diehls-Alder reaction
(Breger, 1960).

hydrocarbons attached to a carboxylic acid (Fig. 2a). One of the most common sources of fatty acids are the phospholipids -- amphipathic structural molecules found in cell membranes which are composed of two fatty acids and a phosphate group attached to a glycerol molecule, where R represents a polar group (see Figure 2b).

Breger (1960) suggested the cyclization of fatty acids via the Diehl-Alder reaction followed by a decarboxylation as a possible source of cyclic alkanes (Fig. 3). If fatty acids are a source of the cycloalkanes, they may justify the findings of comparatively vast sources of fatty acids in nature and napthenic acids in petroleum, in contrast with the scarcity of fatty acids in petroleum and cycloalkanes in biological sources. This mechanism, however would only justify the formation of single-substituted cyclic compounds (Mair, 1964). To determine how multi-substituted cyclic compounds have become so prominent in petroleum, we turn to the terpenoids.

Terpenoids comprise a large class of biological molecules synthesized from isoprene units, and include well known compounds as the steroids, such as cholesterol and some hormones; carotenoids such as beta-carotene; and the hopanoids. Classification is according to the number of isoprene units in the molecule (see Table 3 and Figure 4) and can be cyclic or acyclic (Mair, 1964).

TABLE 3: Classification of Terpenoids

Class	No. of C-atoms	No. of Isoprene units
Monoterpenoids	10	2
Sesquiterpenoids	15	3
Diterpenoids	20	4
Triterpenoids	30	6
Tetraterpenoids	40	8

$$CH_3-\overset{\overset{\displaystyle CH_3}{|}}{C}=CH-CH_3$$

Figure 4: Isoprene

(1) Oxidation

(2) Decarboxylation

(3) Saturation

Isomerization
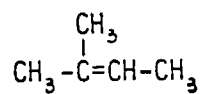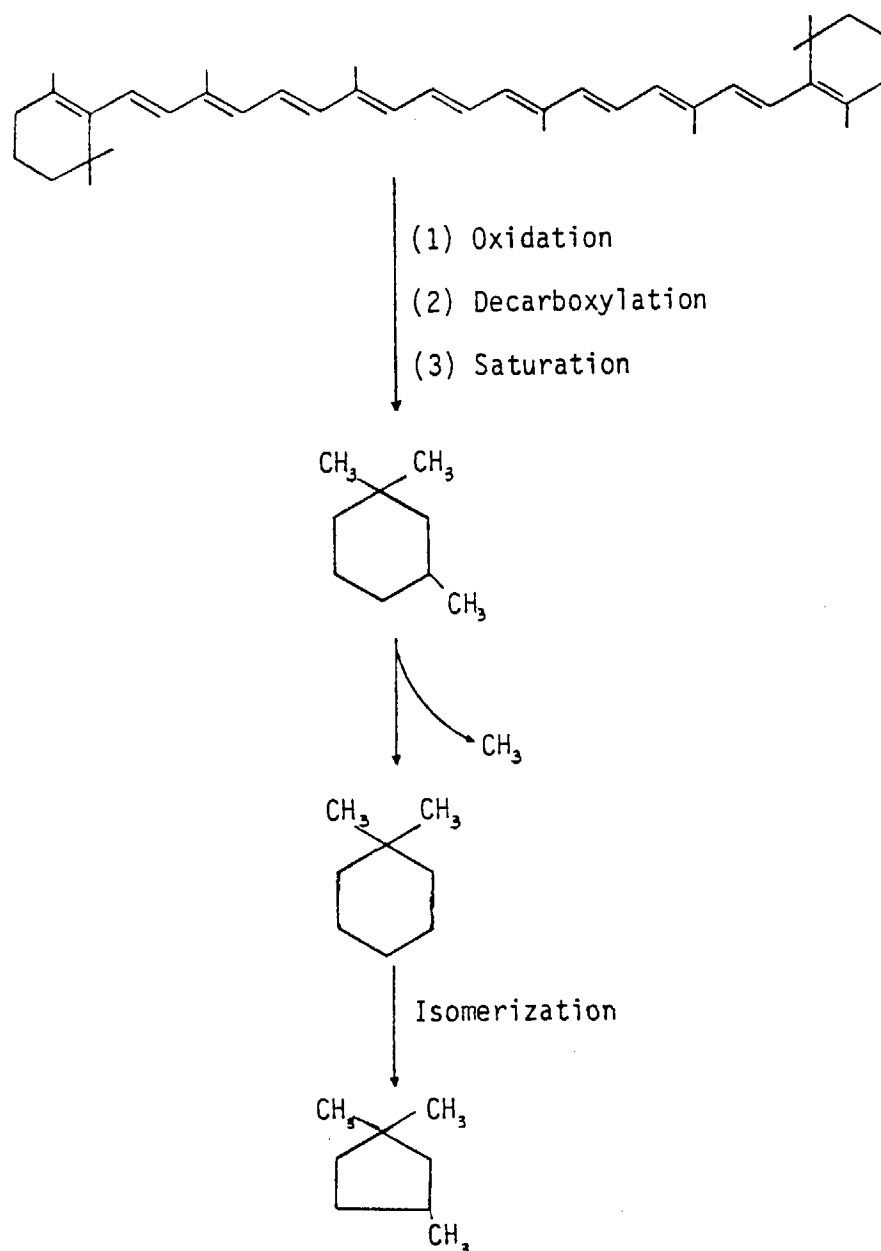
Figure 5: Formation of methyl-substituted cycloalkanes from β-Carotene.

The terpenoids are suspected of being the source of the majority of the branched alkanes, cyclic alkanes, and aromatics. Part of the evidence in favor of this theory is the preponderance of methyl-substituted compounds in the cycloalkanes and aromatics, and a high fraction of normal and iso-alkanes in the paraffins. According to Perry (1984), methylcyclopentane exceeds cyclopentane by approximately five times while the methylcyclohexane is found in quantities approximately double that of cyclohexane. Cyclopentane rings, though rare in nature, are found in quantities comparable to the cyclohexane rings, which would seem to indicate preferential preservation of the cyclopentane rings and/or isomerization of cyclohexane to cyclopentane rings (Mair, 1964). The latter mechanism has been found to occur in the lab fairly easily and at low temperatures in the presence of aluminum chloride for the conversion of cyclohexane to methylcyclopentane (Brooks, 1950).

Carotenoids is the name given to a class of carotenes and their oxygenated derivatives (xanthophylls) consisting of 8 isoprenoid units joined so that the orientation of these units is reversed at the center. Though the 40-carbon carotenoids, synthesized exclusively by microbes and plants, appear to be the most prevalent, 30-carbon carotenoids, found exclusively in non-photosynthetic bacteria, and 50-carbon carotenids have also been identified (Taylor, 1984). Beta-carotene, in particular is thought to be a precursor for 1,1,3-trimethylcyclohexane which in turn can form 1,1-dimethylcyclohexane and 1,1,3-trimethycyclopentane through demethylization and isomerization reactions respectively (Mair, 1964). See Figure 5.

Perhydro-beta-carotene, also known as carotane, is a tetraterpane found in the Green River bitumen (Anders and Robinson, 1970), derived by reduction of

beta-carotene, which is believed to produce petroleum constituents such as 1,1,3-trimethyl-2-(3-methylpentyl)cyclohexane and a number of its isomers (Eglinton and Calvin, 1967). See Figure 6.

Just by looking at the basic structures of the terpenoids, one can imagine cyclization of the acyclic forms, cleavage of the multi-ringed compounds, and hydrogenation of unsaturated compounds to form the mono-cyclic compounds. In addition, disproportionation-type reactions may also play a prominent role in the formation of the lower molecular weight cycloalkanes found in petroleum, since it is an energetically favorable reaction whose rate may be increased by the presence of sulfur (Mair, 1964 and Meinschein, 1959). For example:

$$\frac{3 \begin{array}{l} \text{alkylcyclohexane} \\ \text{isoprenoid} \\ \text{molecules} \end{array}}{\text{tionation}} \xrightarrow{\text{dispropor-}} \begin{array}{l} 1 \text{ alkylbenzene} \\ + \\ 2 \text{ alkylcyclo-} \\ \hspace{1em} \text{hexane} \end{array}$$
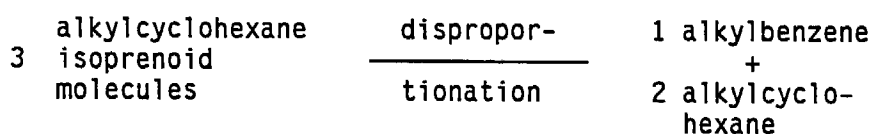
Unfortunately, most of the work involving the terpenoids has been focused on their significance as geochemical fossils, which implies an interest only in slightly degraded molecules, since the lower molecular weight compounds such as the monocyclicalkanes provide very little information as to the original bio-logical molecule (Ourisson, Albrecht and Rohmer, 1984; Tissot and Welte, 1984). A few of these will be discussed briefly for completeness, but no mechanisms will be offered, since none have been suggested in the literature.

The steroids are a very prominent group of geochemical fossils which are derivatives of a fused, reduced ring system, cyclopenta [α]-phenanthrene, comprising three fused cyclohexane rings (A, B, and C) in the phenanthrene arrangement and a terminal cyclopentane ring (D). Some of the general charac-teristics found in steroids are as follows: (1) each ring is completely
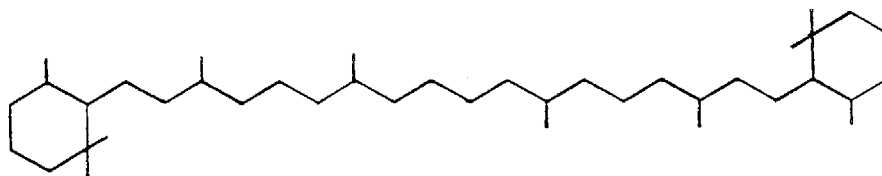
Figure 6: Carotane
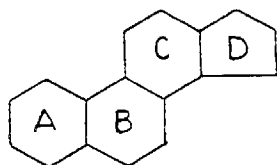
a) Perhydrocyclopenta-
   hopenanthrene
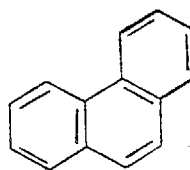
b) Phenanthrene
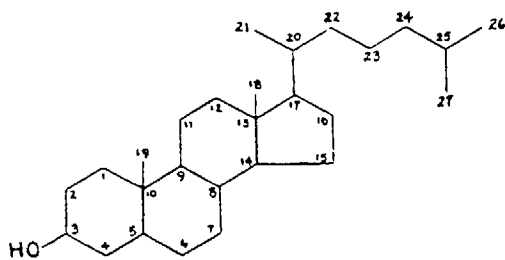
c) Cholestanol
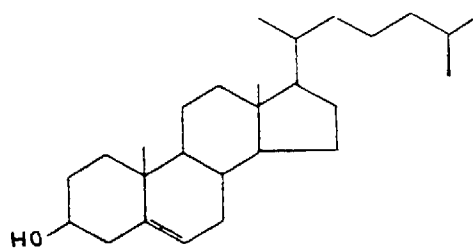
d) Cholesterol

Figure 7: Steroids

saturated; (2) there is an oxygenated substituent on carbon atom 3 in almost all naturally occurring steroids; (3) there are angular methyl groups (19 and 18) on carbons 10 and 11; (4) ring A is aromatic in some steroids, which implies an absence of a methyl group on carbon-atom 10; and (5) there may be an aliphatic substituent on carbon-atom 17 (Morrison and Boyd, 1973; Smith, 1983). Sterols, of which cholesterol is a popular example, are mainly found in eucaryotic cells functioning in the cell membrane to regulate the rigidity and selectivity of the cell membrane. Other sterols to be found are the steroid hormones, of which the sex hormones found in mammals is an example (see Figure 7).

The steranes, in general, are the hypothetical parent molecules of the steroid hormones. They are saturated hydrocarbons whose oxygenated counterparts (27 to 30 carbon atoms), may be constituents of the waxy coverings of the leaves and pollen of land plants (Eglinton and Calvin, 1967). The C-27, C-28, and C-29 steranes (cholestane, ergostane, and sitostane respectively) have been identified as 4-ring cycloalkanes in the Green River bitumen as geochemical fossils (Anders and Robinson, 1971; Williams and Wilkens, 1982). See Figure 9.

The family of hopanoids has already been mentioned as being a group of compounds found in most bacteria and some terrestrial plants. Being similar in size to cholesterol (see Figure 9) and a product of squalene cyclization (as is cholesterol), the hopanoids are believed to have a similar function in cell membranes, i.e., as rigidity regulators of the fluid lipid membranes (Ourisson, Albrecht, and Rohmer, 1979). According to analyses by Ourisson et. al. (1984), hopanoids account for about 5 to 10 percent of the earth's 1.0×10^{15} tons of soluble organic carbon. Due to their ubiquitous nature, they have been receiving increasing amounts of attention in the last few years, especially with regards to their usage as geochemical fossils. The most prevalent hopane is bacteriohopane, so called due to its biological source in bacteria.

a) CHOLESTANE

b) ERGOSTANE

c) SITOSTANE
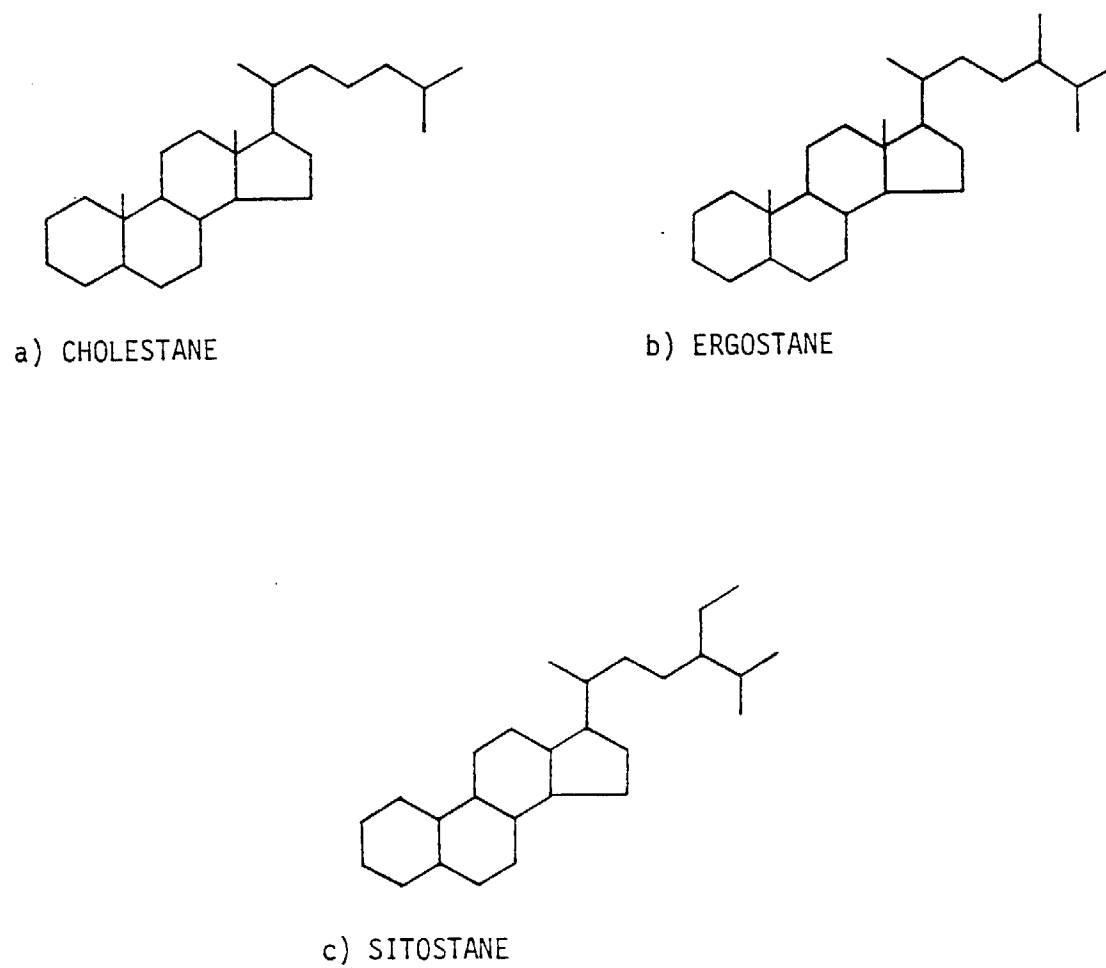
Figure 8: The C-27, C-28, and C-29 Steranes
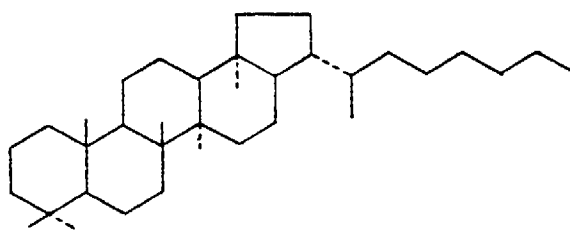
Figure 9: Bacteriohopane

SUMMARY

In summary, petroleum appears to have its biological origins in the lipid fractions of microorganisms and plants, with animals contributing negligible amounts. The bacterial and chemical degradation of these cell constituents results in a mass of insoluble rock known as kerogen, which upon thermal decomposition yields paraffins, cycloalkanes, and aromatics of lower molecular weight than their original biological precursors.

Specifically, cyclic alkanes have several possible origins: the cyclization of fatty acids and acyclic terpenoids, and the decomposition of cyclic terpenoids. Information as to the exact source of petroleum is incomplete due to the inability to follow the transformation of kerogen, from biological molecules to petroleum, in addition to the lack of knowledge the exact cellular composition of most organisms, past and present. Because of such a lack of knowledge, correlations between living creatures and the resulting petroleum have only been speculated.

REFERENCES

1. Anders, D.E. and Robinson, W.E. (1971). "Cycloalkane Constituents of the Bitumen from Green River Shale." Geochim. Cosmoch. 35(2): 661-678.

2. Andreev, P.F., Bogomolov, A.I., Dobryanskii, A.F. and Kartsev, A.A. (1968). Transformation of Petroleum in Nature. Pergamon Press, Oxford.

3. Breger, I.A. (1960). "Diagenesis of Metabolites and a Discussion of the Origin of Petroleum Hydrocarbons." Geochim. Cosmochim. 19(4); 207-308.

4. Brooks, T. (1950). The Chemistry of the Nonbenzenoid Hydrocarbons, second ed. Reinhold Publ.

5. Davis, J.B. (1967). Petroleum Microbiology. Elsevier Publ., Amsterdam.

6. Dott, R.H. and Reynolds, M.J. (1969). Sourcebook for Petroleum Geology. Am. Assoc. of Pet. Geol.

7. Eglinton, G. and Calvin, M. (1967). "Chemical Fossils." Scientific American's Organic Chemistry of Life. 344-355.

8. Erdman, J.G. (1961). "Some Chemical Aspects of Petroleum Genesis as Related to the Problem of Source Bed Recongnition." Geochim. Cosmochim. 22:16-36.

9. Mair, B.J. (1964). "Terpenoids, Fatty Acids and Source Materials for Petroleum Hydrocarbons." Geochim. Cosmochim., 28(2):1303-1321.

10. Meinschein, W.G. (1959). Origin of Petroleum. Bull. Am. Assoc. Petr. Geol. 43(5): 925-943.

11. Morrison, R., Boyd, R. (1973). Organic Chemistry, 3rd ed. Allyn and Bacon Inc., Boston.

12. Ourisson, G., Albrecht, P., Rohmer, M. (1979). "The Hopanoids." Pure and Appl. Chem. 51:709-729.

13. Ourisson, G., Albrecht, P., Rohmer, M. (1979). "The Microbial Origin of Fossil Fuels." Sci. Am. 251(2): 44-51.

14. Rossini, F.D., Mair, B.J. and Streiff, Anton J., A.J. (1953). Hydrocarbons from Petroleum. Reinhold Pub. Corp., New York.

15. Perry, J.J. (1984). "Microbial Metabolism of Cyclic Alkanes." Petroleum Microbiology. Macmillan Publ., N.Y.

16. Smith, E.L. et. al. (1983). Principles of Biochemistry, 7th ed. McGraw Hill Book Co., N.Y.

17. Taylor, R.F. (1984). "Bacterial Terpenoids." Microbiological Reviews 48(3):181-198.

18. Tissot, B.P. and Welte, D.H. (1984). Petroleum Formation and Occurrence, 2nd ed. Springer-Verlag, Berlin.

19. Trask, P.D. (1932). Origin and Environment of Source Sediments of Petroleum. Am. Petr. Inst., Houston.

20. Williams and Wilkens. (1982). Stedman's Medical Dictionary, 24th ed. Baltimore.

APPENDIX

Identified Compounds in the VOC

ADDENDUM A

Volume II

Table A1: 31X DATA

NAME OF COMPOUND IDENTIFIED	BOIL T	RET. TIME (MIN.)	N-PAR	BR-PAR	ALKENE	CYCLOC5	CYCLOC6	AROMATIC
METHYLCYCLOPENTANE	71.8	10.325				17023		
CYCLOHEXANE	80.7	12.561					38512	
2,3-DIMETHYLPENTANE	89.8	13.353		26255				
1,1-DIMETHYLCYCLOPENTANE	87.5	13.594				19879		
3-METHYLHEXANE	91.9	13.900	17790					
1-CIS-3-DIMETHYLCYCLOPENTANE	90.8	14.460				63657		
1-TRANS-3-DIMETHYLCYCLOPENTANE	91.7	14.701				78782		
1-TRANS-2-DIMETHYLCYCLOPENTANE	91.9	14.939				197401		
METHYLCYCLOHEXANE	100.9	17.994					436576	
1,1,3-TRIMETHYLCYCLOPENTANE	104.9	18.279				86082		
ETHYLCYCLOPENTANE	103.5	19.144				86594		
2,4-DIMETHYLHEXANE	109.4	19.447		27717				
1-TRANS-2-CIS-4-TRIMETHYLCYCLOPENTANE	109.3	20.064				204532		
1-TRANS-2-CIS-3-TRIMETHYLCYCLOPENTANE	110.4	20.840				374831		
TOLUENE	110.6	21.522						103165
2,3,4-TRIMETHYLPENTANE	113.5	21.133						
1,1,2-TRIMETHYLCYCLOPENTANE	113.7	22.408				120501		
1,1,3,3-TETRAMETHYLCYCLOPENTANE	118	22.728				26568		
2-METHYLHEPTANE	117.7	22.998						
4-METHYLHEPTANE	117.7	23.142						
3-METHYLHEPTANE	118.9	23.356						
1-TRANS-4-DIMETHYLCYCLOHEXANE	119.4	24.047					549732	
1,1-DIMETHYLCYCLOHEXANE	119.6	24.881					63504	
1-METHYL-TRANS-3-ETHYLCYCLOPENTANE	121.2	25.532				80897		
1-METHYL-TRANS-2-ETHYLCYCLOPENTANE	121.2	25.702				317327		
1-ETHYL-1-METHYLCYCLOPENTANE	121.5	25.911						
1-METHYL-CIS-3-ETHYLCYCLOPENTANE	121.1	25.29				87938		
1-TRANS-2-DIMETHYLCYCLOHEXANE	123.4	26.273					268216	
1,1-CIS-3-CIS-4-TETRAMETHYLCYCLOPENTANE	130.2	27.964				140477		
2,3,5-TRIMETHYLHEXANE	131.3	28.903						
N-PROPYLCYCLOPENTANE	131.0	29.131				62829		
1,1,4-TRIMETHYLCYCLOHEXANE	135.0	30.886					87524	
M-XYLENE	139.1	33.675						
2,3-DIMETHYLHEPTANE	140.5	33.882		185722				
3,4-DIMETHYLHEPTANE	140.6	34.120		86751				
1-METHYL-3-ISOPROPYLCYCLOPENTANE	142.0	34.400				160880		
1-TRANS-2-CIS-3-TRIMETHYLCYCLOHEXANE	144.0	35.742						
1,2,4-TRIMETHYLCYCLOHEXANE	144.0	36.155						
O-XYLENE	144.4	36.414						
1-METHYL-CIS-3-ETHYLCYCLOHEXANE	148.5	37.23					1372746	
1-METHYL-TRANS-3-ETHYLCYCLOHEXANE	151.1	37.364						

TOTAL =			0	344235	0	2126198	2816810	103165
PERCENT =			0	6.386065	0	39.44410	52.25597	1.913862

TOTAL IDENTIFIED PEAK AREA IN 31X = 5390408

Table A2: MONTE CRISTO DATA

NAME OF COMPOUND IDENTIFIED	BOIL T	RET. TIME (MIN.)	N-PAR	BR-PAR	ALKENE	CYCLOC5	CYCLOC6	AROMATIC
2-METHYLBUTANE (ISOPENTANE)	27.8	5.199						
2,2-DIMETHYLBUTANE	49.7	6.484		98029				
2,3-DIMETHYLBUTANE	58.0	7.403		680554				
3-METHYLPENTANE	63.3	8.101		35651				
HEXANE	68.7	8.860						
2,2-DIMETHYLPENTANE	79.2	10.222		115780				
METHYLCYCLOPENTANE	71.8	10.390						
2,4-DIMETHYLPENTANE	80.5	10.585		252107				
2,2,3-TRIMETHYLBUTANE	80.9	10.966		201184				
3,3-DIMETHYLPENTANE	86.1	12.326		141020				
CYCLOHEXANE	80.7	12.617					16065	
2-METHYLHEXANE	90.0	13.268						
2,3-DIMETHYLPENTANE	89.8	13.441		870324				
3-METHYL-1-HEXENE	83.9	13.669			71516			
3-METHYLHEXANE	91.9	13.975		33709				
1-CIS-3-DIMETHYLCYCLOPENTANE	90.8	14.777				352184		
1-TRANS-3-DIMETHYLCYCLOPENTANE	91.7	14.536				203641		
2,2,3-TRIMETHYLPENTANE	109.8	15.141		35323				
METHYLCYCLOHEXANE	100.9	18.042					44279	
2,5-DIMETHYLHEXANE	109.1	19.329						
2,4-DIMETHYLHEXANE	109.4	19.539		488299				
1-TRANS-2-CIS-4-TRIMETHYLCYCLOPENTANE	109.3	20.202				1969937		
1-TRANS-2-CIS-3-TRIMETHYLCYCLOPENTANE	110.4	20.909				438728		
2,3,4-TRIMETHYLPENTANE	113.5	21.679		234947				
2-METHYL-3-ETHYLPENTANE	115.7	22.552		440134				
1,1,3,3-TETRAMETHYLCYCLOPENTANE	118	22.831				68374		
4-METHYLHEPTANE	117.7	23.273		53563				
3-METHYLHEPTANE	118.9	23.427		195651				
1-TRANS-4-DIMETHYLCYCLOHEXANE	119.4	24.365					310563	
3-METHYLENEHEPTANE	120.0	23.762		221824				
1,1-CIS-3-TRANS-4-TETRAMETHYLCYCLOPENTANE	121.6	24.148				2020449		
1,1-DIMETHYLCYCLOHEXANE	119.6	24.977					221278	
1-METHYL-TRANS-3-ETHYLCYCLOPENTANE	121.2	25.379				155710		
1-METHYL-CIS-3-ETHYLCYCLOPENTANE	121.1	25.63				150073		
1,1-CIS-3-CIS-4-TETRAMETHYLCYCLOPENTANE	130.2	28.504				127266		
2,3,5-TRIMETHYLHEXANE	131.3	28.987		127714				
2,4-DIMETHYLHEPTANE	132.9	30.302		239725				
1,1,4-TRIMETHYLCYCLOHEXANE	135.0	30.598					566489	
1,1,3-TRIMETHYLCYCLOHEXANE	136.6	31.564					988792	
2,3-DIMETHYLHEPTANE	140.5	33.973		304145				
3,4-DIMETHYLHEPTANE	140.6	34.213		179034				
1-METHYL-3-ISOPROPYLCYCLOPENTANE	142.0	34.642				582834		
1-TRANS-2-CIS-3-TRIMETHYLCYCLOHEXANE	144.0	35.827					306173	
1-TRANS-2-CIS-4-TRIMETHYLCYCLOHEXANE	144.6	36.052						

| | TOTAL = | 0 | 4948717 | 71516 | 6069196 | 2453639 | 0 |
| | PERCENT = | 0 | 36.54059 | 0.528063 | 44.81404 | 18.11730 | 0 |

TOTAL IDENTIFIED AREA FOR MONTE CHRISTO = 13543068

Table A3: 36W DATA

NAME OF COMPOUND IDENTIFIED	BOIL T	RET. TIME (MIN.)	INLET PEAK AREA					
			N-PAR	BR-PAR	ALKENE	CYCLOC5	CYCLOC6	AROMATIC
2-METHYLPENTANE	60.3	7.539						
3-METHYLPENTANE	63.3	8.121						
HEXANE	68.7	8.866	32584					
METHYLCYCLOPENTANE	71.8	10.382				36030		
2,2,3-TRIMETHYLBUTANE	80.9	10.956		19580				
BENZENE	80.1	11.919						76614
CYCLOHEXANE	80.7	12.637					21459	
2-METHYLHEXANE	90.0	13.262		57303				
2,3-DIMETHYLPENTANE	89.8	13.420		58325				
3-METHYLHEXANE	91.9	13.981		92965				
1-CIS-3-DIMETHYLCYCLOPENTANE	90.8	14.543				40748		
1-TRANS-3-DIMETHYLCYCLOPENTANE	91.7	14.77				47674		
1-TRANS-2-DIMETHYLCYCLOPENTANE	91.9	15.021				66597		
HEPTANE	98.4	16.129	256045					
METHYLCYCLOHEXANE	100.9	18.062					129427	
1,1,3-TRIMETHYLCYCLOPENTANE	104.9	18.346				37034		
ETHYLCYCLOPENTANE	103.5	19.233						
1-TRANS-2-CIS-4-TRIMETHYLCYCLOPENTANE	109.3	20.126				61558		
3-METHYL-2,4-HEXADIENE	110.4	21.25			78415			
TOLUENE	110.6	21.615						338678
2,3-DIMETHYLHEXANE	115.6	22.405		20697				
1,1,3,3-TETRAMETHYLCYCLOPENTANE	118	22.84				213569		
2-METHYLHEPTANE	117.7	23.008		356721				
4-METHYLHEPTANE	117.7	23.242						
3-METHYLHEPTANE	118.9	23.925						
1-TRANS-4-DIMETHYLCYCLOHEXANE	119.4	24.342						
1,1-DIMETHYLCYCLOHEXANE	119.6	24.981						
1-METHYL-TRANS-3-ETHYLCYCLOPENTANE	121.2	25.362				123555		
1-METHYL-CIS-3-ETHYLCYCLOPENTANE	121.1	25.618						
4-TRANS-OCTENE	122.3	25.744						
1-TRANS-2-DIMETHYLCYCLOHEXANE	123.4	26.328						
OCTANE	125.7	27.035	241464					
1,1-CIS-3-CIS-4-TETRAMETHYLCYCLOPENTANE	130.2	28.052				122330		
2,4-DIMETHYLHEPTANE	132.9	29.874		34708				
2,6-DIMETHYLHEPTANE	135.2	30.652		162541				
1,1,3-TRIMETHYLCYCLOHEXANE	136.6	31.211					77720	
M-XYLENE	139.1	33.769						111464
2,3-DIMETHYLHEPTANE	140.5	33.929		138507				

```
TOTAL =    530093   941347    78415   749095   228606   526756
PERCENT =17.35556 30.82026 2.567353 24.52581 7.484697 17.24630
```

TOTAL IDENTIFIED PEAK AREA IN 31X = 3054312

ADDENDUM B

Volume II

DEVELOPMENT OF THE THEORY FOR THE HEAT AND MASS TRANSFER PROCESSES

Christine Laban

TABLE OF CONTENTS

ADDENDUM B

Volume II

DEVELOPMENT OF THE THEORY FOR THE MASS AND HEAT TRANSFER PROCESSES

INTRODUCTION

Mass transfer and heat transfer processes occur simultaneously at the air/oil interface of the oil sumps due to the large difference in temperature between the oil (60 to 70°C) and the atmosphere. Mathematically, one can separate these two problems to make it easier to solve them. Linked by the temperature dependence of the transport of material into the atmosphere, the two models can then be used in a computerized reiteration scheme.

At this point in time, the isothermal, single-component mass transfer model has been solved, and work is in progress to determine the solution to the heat transfer problem. Derivations of the governing differential equation and boundary conditions for both are given in their respective sections.

1.0 Mass Transfer Process

The governing differential equation describing the evaporation process (Figure 1) is derived starting with the continuity equation describing mass transport of a single molecular species at a point in the oil:

$$\frac{\partial c_A}{\partial t} = - \nabla \cdot \underset{\sim}{N}_A + R_A \quad , \tag{1}$$

where c_A is the molar concentration of species A, $\underset{\sim}{N}_A$ is the flux of A at a point and R_A is the homogeneous reaction rate of A and in this case zero.

The flux $\underset{\sim}{N}_A$ at a point is given by

$$\underset{\sim}{N}_A = c_a \underset{\sim}{v}^* + \underset{\sim}{J}_A^* \quad , \tag{2}$$

where the velocity v* is zero since convection is assumed to be negligible in the oil phase due to the high viscosity in the range of 1000 cp . The diffusion flux $\underset{\sim}{J}_A^*$ is

$$\underset{\sim}{J}_A^* = - cD_{AB}\nabla x_A \quad , \tag{3}$$

where c is the total molar concentration, D_{AB} is the binary diffusion coefficient and x_A is the mole fraction. Substituting Equations (2) and (3) into (1) yields:

$$\frac{\partial c_A}{\partial t} = - \nabla \cdot [cD_{AB}\nabla x_A] \quad . \tag{4}$$

Further assuming that diffusion is one-dimensional and normal to the free surface, and that c and D_{AB} are constant, yields the governing differential equation:

$$\frac{\partial c_A}{\partial t} = - D_{AB} \frac{\partial^2 c_A}{\partial z^2} \quad . \tag{5}$$

The initial and boundary conditions are:

Initial Condition: When the oil enters the sump, the concentrations of the evaporating components are uniform throughout the oil.

$$c_A = c_{A_o} \quad \text{at} \quad t = 0 \quad . \tag{6}$$

Boundary Condition (1):   There is no flux of volatile components at the oil/water interface.

$$N_A = - D_{AB} \frac{\partial c_A}{\partial z} = 0 \tag{7}$$

or

$$\frac{\partial c_A}{\partial z} = 0 \quad \text{at} \quad z = 0 \quad . \tag{8}$$

The second boundary condition requires continuity of flux at the air/oil interface. Therefore the flux from the bulk oil to the interface equals the flux from the interface to the bulk air. The flux from the bulk oil is

$$N_A^{oil} = - D_{AB} \frac{\partial c_A}{\partial z} \quad \text{at} \quad z = L \tag{9}$$

and the flux from the bulk air is

$$N_A^{air} = K_G (c_{AG}^i - c_{AG}^\infty) , \tag{10}$$

where c_{AG}^i is the molar concentration of A in the air at the interface and c_{AG}^∞ is the bulk concentration of A in the air. Since c_{AG}^∞ is taken to be zero,

$$N_A^{air} = K_G c_{AG}^i \quad . \tag{11}$$

In order to express the interfacial gas phase concentration in terms of the liquid phase concentration, interfacial equilibrium is assumed. This equilibrium can be stated in terms of Henry's law:

Figure 1:   Schematic of a pad of oil in a sump, floating
            on a layer of water.
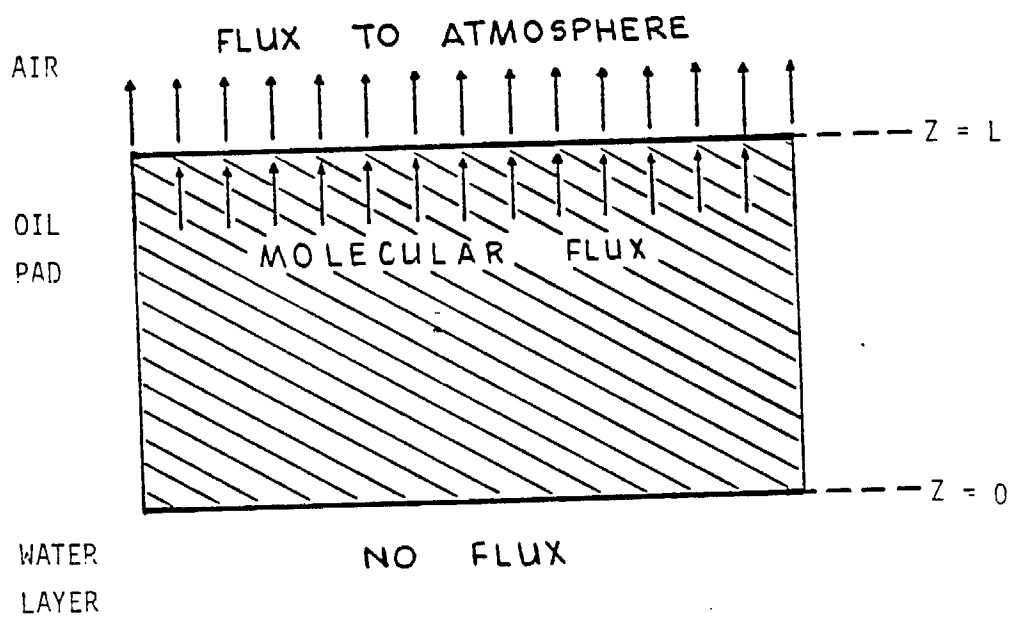
$$y_A/x_A = H \quad , \tag{12}$$

where y_A and x_A are mole fractions of A in the gas and liquid.

Assuming that the liquid and gas phases are ideal, Raoult's law applies and H is given by p_A^{sat}/p where p_A^{sat} = pure component saturation vapor pressure and P is the total pressure. Equation (12) can be rearranged in terms of concentrations:

$$y_A = \frac{c_{AG}^i}{c_G} = \frac{Hc_{AL}^i}{c_L} = Hx_A \quad , \tag{13}$$

where c_L and c_G are the total molar concentrations of the liquid and gas phases respectively.

Therefore, $$c_{AG}^i = (H \frac{c_G}{c_L})c_{AL}^i \quad . \tag{14}$$

Substituting into equation (11):

$$N_A^{air} = (K_G H \frac{c_G}{c_L}) \, c_{AL}^i = K_G \tilde{H} c_A^i \quad , \tag{15}$$

where $\tilde{H} = \frac{HC_G}{c_L}$ and the L subscript is dropped on c_{AL}^i . Boundary condition (2) in its final form can now be written:

$$- D_{AB} \frac{\partial c_A}{\partial z} = K_G \tilde{H} c_A^i \quad \text{at} \quad z = L \quad . \tag{16}$$

The solution to Equation (5) with initial condition, Equation (6) and boundary conditions Equations (8) and (16) is (see Appendix A):

$$\frac{c_A}{c_{A_0}} = 2\sum_{n=1}^{\infty} \exp\left(-\lambda_n^2 D_{AB} t\right) \left(\frac{\sin \lambda_n L}{(\sin\lambda_n L)(\cos\lambda_n L) + \lambda_n L}\right) \cos \lambda_n z \quad . \tag{17}$$

The boundary conditions yield the following eigenvalue condition from which the eigenvalues $(\lambda_n L)$ were determined:

$$\cot \lambda_n L = \frac{\lambda_n L}{\beta} \quad , \tag{18}$$

where β is a dimensionless group representing the ratio of liquid-to-air resistance:

$$\beta = \frac{K_G \tilde{H} L}{D_{AB}} \quad . \tag{19}$$

The flux at the interface is found by differentiating equation (17):

$$N_A \Big|_L = -D_{AB} \frac{\partial c_A}{\partial z} \Big|_L \tag{20}$$

$$= 2c_{A_0} D_{AB} \sum_{n=1}^{\infty} \exp\left(-\lambda_n^2 D_{AB} t\right) \left(\frac{\lambda_n \sin^2 \lambda_n L}{\lambda_n L + (\sin\lambda_n L)(\cos\lambda_n L)}\right) \quad .$$

As will be shown later, the flux becomes independent of β as the liquid-phase resistance increases.

1.1 Estimation of Parameters for Mass Transfer

As was mentioned in the theory section, the flux of volatiles from the bulk oil at the air-oil interface may be expressed in terms of the liquid diffusivity, D_{AB} (eqn. 9):

$$N_A^{oil} = - D_{AB} \ \frac{\partial C_A}{\partial Z}$$

and the flux into the bulk air at the air-oil interface be given by (eqn. 15)

$$N_A^{air} = K_G \ \tilde{H} \ C_A$$

In order to determine the primary source of resistance to mass transfer, it is necessary to compute the contributions to the overall mass transfer coefficient, $K_{o\ell G}$:

$$K_{o\ell G} = \frac{1}{\dfrac{1}{K_G} + \dfrac{1}{D_{AB} / L}} \tag{21}$$

where $\frac{1}{K_G}$ represents the gas-phase resistance and $\frac{1}{D_{AB}/L}$ represents the liquid-phase resistance. The mass-transfer parameters D_{AB} (liquid diffusivity), K_G (gas-phase mass transfer coefficient), and H (Henry's Law Constant) will be discussed and related to the overall mass transfer coefficient in this section.

Diffusion Coefficient, D_{AB}

Early correlations developed for liquid diffusion coefficients were based on the Stokes-Einstein relation (Reid, Sherwood and Prausnitz, 1955; Bird, Stewart and Lightfoot, 1960). These previous relationships in liquids between the diffusion coefficient D and the viscosity μ have commonly included an inverse dependence:

$$D \alpha \mu^{-1} \tag{22}$$

Equation (22) has been shown to be very accurate for the limiting case of a large solute molecule in a solvent consisting of small molecules, where the proportionality constant in the equation is a function only of solute radius.

Hiss and Cussler (1973) explored the relation between diffusion and viscosity for a small solute diffusing in a high viscosity liquid (solvent of relatively large molecules). They found that the diffusion coefficient, D , for a small solute diffusing in a viscous solvent of larger molecules is proportional to the (- 2/3) power of the solvent's viscosity:

$$D \alpha \mu^{-2/3} \tag{23}$$

In practice, diffusion varies with the inverse of the solvent viscosity below 10^{-3} kg/m-s (poise) and with the (-2/3) power from 5×10^{-3} to at least 5 kg/m-s.

Equation (23) is not necessarily in conflict with previously published rules for predicting diffusion which assume that diffusion is inversely proportional to viscosity. However, the proportionality constant is a function of both solute and solvent properties, such as molar volume of the solute or molecular weight of the solvent, and therefore may implicitly involve the viscosity in an unknown manner.

If diffusion is assumed proportional to the inverse of viscosity, estimates will be 1000% in error at a viscosity of 1 kg/m-s (1000 cp). The exponent of (-2/3) on the other hand, is applicable only to high viscosity liquids of moderate molecular weight. Such are the conditions of the sump oil pad.

Hiss and Cussler have presented data on hexane and naphthalene in viscous, transparent hydrocarbon oils. A least squares analysis of this data yields simple relationships for hexane and naphthalene:

$$D\mu^{0.66} = \text{constant (hexane)} \tag{24}$$

$$D^{0.69} = \text{constant (naphthalene)} \tag{25}$$

Thus a plot of log (diffusion coefficient) vs. log (viscosity) for each compound is expected to yield a straight line.

Hiss and Cussler found the diffusion coefficients of hexane and napthalene in viscous solvents to be on the order of 10^{-11} m^2/sec at 25°C. The hydrodynamic theory predicts a direct proportionality between temperature and liquid diffusivity, therefore higher values would be expected at the temperatures of the sump which range from 60 to 95°C. Nevertheless, diffusivities higher than one would expect would be required to predict the observed level of emissions. Measured liquid diffusivities of hydrocarbons in viscous solvents have not been found above 25°C. For this reason, a procedure is presently being developed by Ms. Castronovo (Addendum C).

MASS TRANSFER COEFFICIENT, K_G

The expression used to estimate the value of K_G for the model comes from the correlation of MacKay and Yuen (1983). The correlation is expressed in terms of the air friction velocity and the Schmidt number of the compound in air and water. Such a correlation provides characterization of the effects of solute diffusivity, temperature and also windspeed, by means of a drag coefficient correlation with friction velocity.

In developing the mass transfer coefficient correlation, MacKay and Yuen first noted that the logarithmic velocity law

$$U/U^* = (1/K) \ln (Z/Z_0) \tag{26}$$

described their data adequately, where

U = velocity (m/sec) at an anemometer height of Z(m)

U* = air side friction velocity (m/sec)

Z_0 = roughness height (m)

K = von Karman constant = 0.4

The average drag or friction coefficient C_D can be calculated from the friction velocity and the windspeed and is defined as

$$C_D = \tau_a/\rho_a U_\infty^2 = (U*/U_\infty^2) \tag{27}$$

where τ_a (N/m^2) is the wind shear stress, ρ_a (kg/m^3) is the air density, and U_∞ is the free stream velocity.

From examination of their gas-phase resistance water evaporation data, MacKay and Yuen were able to show that K_G is well correlated with the friction velocity U* . It was then necessary to correct K_G for the solute diffusivity, molecule size, or molecular weight. Overwhelming evidence suggests that the correct quantity is the Schmidt number (Sc_G) , which is the dimensionless ratio of kinematic viscosity/diffusivity and is typically in the range 0.5-2.0 for gases.

From their data, related studies and the work of other researchers, McKay and Yuen concluded that the most likely relationship is

$$K_G \, \alpha \, Sc_G^{-0.67} \quad . \tag{28}$$

Fitting correlation equations containing this dependence to the entire data set yielded

$$K_G = 46.2 \times 10^{-3} u^* Sc_G^{-0.67} \tag{29}$$

Further combining these correlations with the C_D correlations relating U_∞ to U^* yields:

$$K_G = 46.2 \times 10^{-5} (6.1 + 0.63\ U_{10})^{0.5}\ U_{10} Sc_G^{-0.67} , \tag{30}$$

where U_{10} is the wind speed at a height of 10 meters.

It is believed that this equation applies to windspeeds above approximately 5 m/sec or to U^* greater than 0.3 m/sec . At lower windspeeds, the equations may be inaccurate.

In addition it was found that K_G tends to a still-air value at zero windspeed. Based on their data and other literature, MacKay and Yuen estimated the still-air value as

$$K_G = (1.0 \pm 0.5) \times 10^{-3} \text{ m/sec} \tag{31}$$

Therefore, the final expression for K_G is:

$$K_G = 1.0 \times 10^{-3} + 46.2 \times 10^{-3}\ U^* Sc_G^{-0.67} \tag{32}$$

where $U^* = (6.1 + 0.63\ U_{10})^{0.5}\ U_{10} \times 10^{-2}$.

Values for K_G were calculated for a low and a high wind speed: 5 m/sec (11 mph) and 20 m/sec (45 mph). The Schmidt number for gases is usually

about 2 at room temperature. Using $Sc_G = 2.0$ and the above wind speeds, a range for K_G was obtained:

$$K_G = 5 \times 10^{-3} \text{ to } 2.5 \times 10^{-2} \text{ m/sec} \tag{33}$$

Henry's Law Constant $\tilde{H}$

As stated previously, $\tilde{H} = \dfrac{Hc_G}{c_L}$, where c_L and c_G are the total molar concentrations of the liquid and gas and H is the Henry's Law Constant. Using an approximated liquid concentration of 5000 gmol/m^3 and gas concentration for a perfect gas of 50 gmol/m^3 , the ratio of c_G/c_L is 0.01.

Assuming ideal gas conditions, $y_A P = x_A \gamma_A P_A^{sat}$. Activity coefficients, γ_A , are presently assumed equal to unity. This expression may be rearranged to obtain a dimensionless expression for H :

$$\frac{P_A^{sat}}{P} = \frac{y_A}{x_A} = H \tag{34}$$

Experimental work is presently under way to measure vapor pressures of individual components in crude oil (see Addendum D). Until experimental values are available, however, P_A^{sat} will be calculated from the Antoine equation:

$$P_A^{sat} = \exp\left[A - \frac{B}{T+C} \right] \tag{35}$$

where A , B and C are the Antoine constants, T is the temperature in degrees Kelvin and P_A^{sat} is in mm Hg . The Henry's Law constant may then be calculated by dividing P_A^{sat} by P , the total pressure of the atmosphere which is estimated as 760 mm Hg (1 atm) .

In order to explore the effect of temperature on vapor pressure, a temperature range of 273 K to 373 K was chosen in order to bracket all experimental conditions. In addition, two compounds -- n-pentane and n-decane -- which are not in abundance in the crude oil mixture, but bracket the boiling point range, were chosen to calculate a range of values for $\tilde{H}$. The P_A^{sat} values for these two compounds are:

temp	n-pentane	n-decane
273 K	182 mm Hg	0.17 mm Hg
373 K	4429 mm Hg	71 mm Hg

Using these values, $\tilde{H}$ varies between 2.24×10^{-6} and 5.83×10^{-2}.

Using an average oil pad thickness of 0.1 meters, it is now possible to compare the gas-phase and liquid- phase resistances. The range of mass transfer parameters are shown in the table below:

Ranges of Mass Transfer Parameters

	K_G (m/sec)	H	D_{AB} (m^2/sec)
minimum	5.0×10^{-3}	2.24×10^{-6}	10^{-9}
maximum	2.4×10^{-2}	5.83×10^{-2}	10^{-7}

Calculations of $1/K_G$ and $\dfrac{1}{D_{AB}/L}$ shows the liquid phase resistance to be controlling mass transfer.

$$1/K_G \approx \frac{1}{.005} = 200$$

$$\frac{1}{D_{AB}/L} \approx \frac{0.1}{10^{-8}} = 10^7$$

1.2 Initial Concentration, Density and Molecular Weight of Crude Oil

A complication which arises when complex mixtures such as crude oils evaporate is that there is some doubt about the initial concentration (c_{A_0}) of each species present at the inlet to the sump.

From an analysis of the Monte Cristo crude oil, an initial concentration of approximately 100 mol/m^3 was determined. Comparison of the inlet and outlet concentrations then yields a loss of VOC ranging from 15 to 20 mol/m^3 .

Physical properties important to the analysis are the density and molecular weight of the crude oil. The density may be experimentally measured. This resulted in a value of 0.8 x 10^6 g/m^3 at 60°C. The molecular weight, however, must be approximated due to the unknown composition of the crude oil. Considering the four most abundant components present in the crude oil mixture (toluene, trimethyleyclopentane, n-heptane and octane) an average molecular weight of 100 g/mol is estimated.

2.0 Computer Program

Computer programs were developed to calculate the mass flux and concentration as functions of temperature, time and oil depth. The program for the flux, found in Appendix B, calculates mass flux of a single component as a function of time, given the conditions of the sump. Integrated in the program is the Newton-Raphson reiteration method (Appendix C) which is used to find 100 eigenvalues where eigenvalues are the values of $\lambda_n L$ which satisfy the boundary conditions

$$\cot \lambda_n L = \frac{\lambda_n L}{\beta}$$

Although an infinite number of eigenvalues exist, only a few are necessary to yield an accurate plot of the concentration profile. However, since determination of the flux involves taking the derivative at a point on the curve describing the concentration profile, enough eigenvalues must be used to adequately describe the slope at areas where the concentration curves are sharp.

The Newton-Raphson method involves driving $f(\lambda_n L) = \cot\lambda_n L - \frac{\lambda_n L}{\beta}$ to zero. The formula $\lambda_n L(k + 1) = \lambda_n L(k) - f(\lambda_n L)/f'(\lambda_n L)$ provides a means of going from one guess of $\lambda_n L(k)$ to the next guess, $\lambda_n L(k + 1)$. Iterations were made until $f(\lambda_n L)$ was sufficiently close to zero, within a tolerance of 0.001.

A plot of $\cot\lambda_n L$ vs. $\lambda_n L/\beta$ (Figure 2) shows the source of some problems in obtaining the eigenvalues. Notice the clear intersection of $\lambda_n L/\beta$ and $\cot\lambda_n L$ for large β. When β is small ($\beta<20$), however, it is harder to estimate the eigenvalues using the Newton-Raphson method because the two functions, $\cot\lambda_n L$ and $\lambda_n L/\beta$ tend to coincide and do not yield a clear intersection. The iteration method shown in Appendix C was used for these values of β.

3.0 Heat Transfer Process

The mass and heat transfer processes occurring at the air/oil interface are linked through the mass flux of components which depends on temperature. The governing differential equation describing heat transfer was derived beginning with the thermal energy equation in terms of the internal energy. This derivation is given in Appendix (D).

Noting that thermal diffusivity $= \alpha = \dfrac{k}{\rho \hat{C}_p}$, the governing differential equation is:
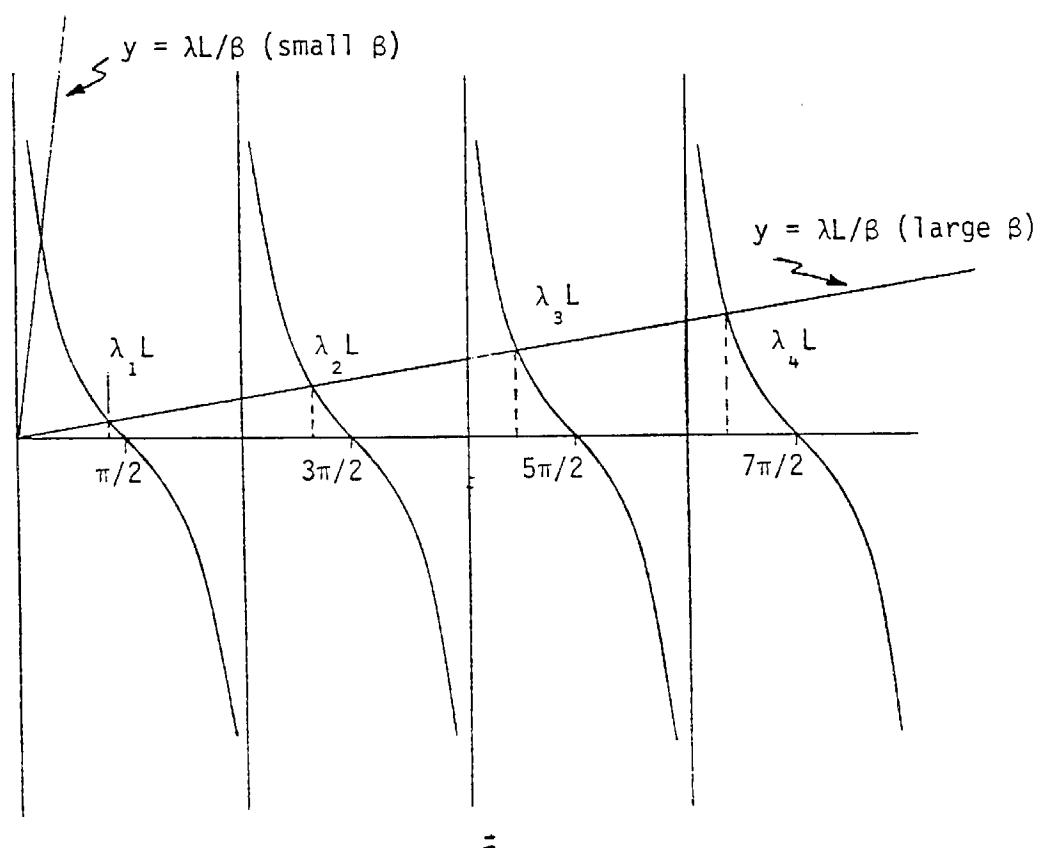
Figure 2: Intersection of $\lambda_n L/\beta$ and cot $\lambda_n L$
for Large β and Small β.

$$\frac{\partial T}{\partial t} = \alpha \frac{\partial^2 T}{\partial z^2} - \frac{1}{\rho \hat{c}_p} \sum_{i=1}^{n} \hat{c}_{pi} (T-T_0) D_{ij} \frac{\partial^2 c_i}{\partial z^2} \quad . \tag{1}$$

The first term on the right-hand-side represents the energy due to conduction and the second term represents the energy due to diffusion.

The initial and boundary conditions are:

Initial Condition: When the oil enters the sump, it is at temperature T_0 throughout the pad.

$$T = T_0 \quad \text{at} \quad t = 0 \quad . \tag{2}$$

Boundary Condition (1): The temperature is constant at the water/oil interface.

$$T = T_0 \quad \text{at} \quad z = 0 \quad . \tag{3}$$

The second boundary condition at the air/oil surface requires continuity of energy:

$$-k \frac{\partial T}{\partial z}\bigg|_{liq} + \sum_{i=1}^{n} N_i H_i \bigg|_{liq} = -k \frac{\partial T}{\partial z}\bigg|_{vap} + \sum_{i=1}^{n} N_i H_i \bigg|_{vap} - Q_{rad} \tag{4}$$

where,

$$-k \frac{\partial T}{\partial z}\bigg|_{vap} = \text{convective heat flux} = h(T-T_\infty) \tag{5}$$

Q_{rad} = net flux of long and short wave radiation

T_∞ = temperature of the air

Therefore,

$$- k \left. \frac{\partial T}{\partial z} \right|_{liq} = h(T-T_\infty) + \sum_{i=1}^{n} N_i \left(H_i \Big|_{vap} - H_i \Big|_{liq} \right) - Q_{rad} \qquad (6)$$

Boundary Condition (2): at air/oil interface:

$$- k \left. \frac{\partial T}{\partial z} \right|_{liq} = h(T-T_\infty) + \sum_{i=1}^{n} N_i \Delta H_{vap} - Q_{rad} \qquad at \quad z = L \qquad (7)$$

In considering the solution of the governing differential Equation (1) with boundary conditions Equations (3) and (7), the approach was to first look at a limiting case that would allow for an analytical solution. Such a solution was desired in order to provide both a quick description of the heat transfer process occurring at the oil surface and a means for determining the accuracy of a more complex numerical solution that will be developed in future work. With these considerations in mind, certain simplifications were made to the model.

The time dependent behavior of the coefficients was not accounted for in this preliminary model. Instead, the boundary condition at the air/oil interface uses a temperature that may be viewed as the daily averaged surface oil temperature for estimating $\sum_{i=1}^{n} N_i \Delta H_{vap}$ and $Q_{radiation}$.

From an order of magnitude analysis of the terms in the governing differential equation, the diffusion term was found to be about three orders of magnitude less than the conduction term. Thus, in striving for an analytical solution, the diffusion term was neglected when solving the governing differential equation. The diffusion term would tend to increase surface temperature. Therefore, ignoring this term results in minimizing interfacial temperatures thus providing a limiting case.

The simplified version of Equation (1) is then:

$$\frac{\partial T}{\partial t} = \alpha \frac{\partial^2 T}{\partial z^2} \qquad (8)$$

Work on the solution to equation (8) is presently in progress.

3.1 Estimation of Parameters for Heat Transfer Net Flux of Radiation, Q_{rad}

One method used to determine long-wave radiation received at a water surface uses Stefan's law which depends on the temperature of the ambient air (Brunt, 1944). The method is described by the expression:

$$Q_{LW} = \sigma T_\infty^4 (c + d\sqrt{e_a}) \qquad (11)$$

where

Q_{LW} = radiation received, cal cm^{-2} day^{-1}

σ = Stefan-Boltzmann constant, 1.355×10^{-1} cal sec^{-1} cm^{-2} K^{-4}

T_∞ = air temperature, K

e_a = vapor pressure of water in the air, millibars

c = constant

d = constant

Evaporation studies were conducted by Koberg to obtain long-wave radiation-data, which in turn generated a value of 0.0263 for the constant d. The constant c was found to vary with air temperature and cloud cover. The effect of cloud cover is related to the ratio of the measured solar radiation to that received on a clear day. The value of c varies from 0.48 to 0.74 for air temperatures 0 to 36°C.

The atmospheric conditions of Bakersfield results in a small value for e_a, the vapor pressure of water in air. The term $d\sqrt{e_a}$ will then be negligible

when compared to c . The expression for Q_{LW} is then

$$Q_{LW} = c\sigma T_\infty^4 \tag{12}$$

Since the surface of the oil is a black surface, the total emitted energy is given by the Stefan-Boltzmann law:

$$Q_B^{(e)} = \sigma T^4 \tag{13}$$

where the temperature T is the temperature of the oil surface. Therefore, the net flux of radiation is:

$$Q_{rad} = \sigma(cT_\infty^4 - T_{avg}^4) \tag{14}$$

THERMAL DIFFUSIVITY AND THERMAL CONDUCTIVITY

Thermal diffusivity α and the thermal conductivity k were estimated from the value for lubricating oil at 60°C as approximately 8×10^{-8} m^2/sec for α and 3.4×10^{-2} cal/sec m K for k (Whitaker, 1983). These parameters are relatively constant over short temperature ranges.

HEAT TRANSFER COEFFICIENT

A table of heat transfer coefficient vs. air velocity was generated from a correlation for convection heat transfer with air flow at atmospheric pressure over external surfaces (Boltz and Tuve, 1976):

$$h = \text{constant} \times \frac{k}{D} \times (\frac{DV\rho}{\mu})^{0.6} (\frac{c\mu}{k})^{0.3} \tag{15}$$

where temperature = 70° F (mean air temperature).

For air properties and air velocity at mean mixed air temperature, h is approximately 15 cal/m^2 s K for an air velocity of about 15 m/s.

TEMPERATURES OF AIR AND WATER

Temperature T_0 is the temperature of the water and T_∞ is the ambient air temperature. Calculations were made at the temperatures considered to be the two extremes possible for the oil and water and the air, between 273 and 373 K.

HEAT OF VAPORIZATION

The heat of vaporization ΔH_{vap} was calculated from the Watson correlation (Reid, Sherwood and Prausnitz, 1976):

$$\Delta H_{vap} = \Delta H_{vap_{(b.p.)}} \left[\frac{1 - T_r}{1-T_{r_{(b.p.)}}} \right]^{0.38} \tag{16}$$

where $\Delta H_{vap_{(b.p)}}$ = ΔH_{vap} of compound at its boiling point

$T_r = T/T_c$ = reduced temperature of the compound

$T_{r_{(b.p.)}}$ = reduced temperature of the compound at its boiling point

REFERENCES

1. Bird, R.B., Stewart W.E. and Lightfoot, E.W. 1960. <u>Transport Phenomena</u>. Wiley and Sons, Inc., New York, p. 515.

2. Bolz, R. and Tuve, G. 1976. <u>CRC Handbook of Tables for Applied Engineering Science</u>. CRC Press, Inc., Ohio, p. 538.

3. Brunt, D., 1944. <u>Physical and Dynamical Meterology</u>. Cambridge Univ. Press. p. 105.

4. Hiss, T.G. and Cussler, E.L. 1973. [5]Diffusion in High Viscosity Liquids[5]. <u>AIChE J.</u>, (19): 698-703.

5. Koberg, G. [5]Methods to Compute Lang-Wave Radiation from the Stratosphere and Reflected Solar Radiation from a Water Surface. Geological Survey Professional Paper 272-F.

6. MacKay, D. and Yuen, A. 1983. <u>Environ. Sci.</u> Technol., (17):211.

7. Reid, R., Sherwood, J., and Prausnitz, T. 9176. <u>The Properties of Liquids and Gases</u>. 3rd. edition. McGraw-Hill Inc., N.Y. p. 210.

8. Whitaker, S. 1983. <u>Fundamental Principles of Heat Transfer</u>. Robert E. Krieger. Malabar, Florida. p. 539.

NOMENCLATURE

B_i Biot number = hL/k (dimensionless number)

C total molar concentration ($gmol \cdot cm^{-3}$)

C_A molar concentration of species A

C_{A_o} initial molar concentration of species A

$C_{A_G}^i$ molar concentration of A in the air at the oil-air interface

$C_{A_G}^\infty$ molar concentration of A in the air for from the oil-air interface

C_L total molar concentration of the liquid phase

C_G total molar concentration of the gas phase

C_D average drag or friction coefficient (dimensionless)

C_p molar heat capacity or specific heat at constant pressure ($energy \cdot temp^{-1} \cdot mole^{-1}$)

D_{AB} binary diffusion coefficient ($cm^2 \cdot sec^{-1}$)

e_a vapor pressure of air (millibar)

H Henry's Law Constant (dimensionless)

$\tilde{H}$ $H(C_G/C_L)$

h heat transfer coefficient ($cal \cdot m^{-2} \cdot s^{-1} \cdot K^{-1}$)

ΔH_{vap} heat of vaporization ($cal \; mole^{-1}$)

$\Delta H_{vap(b.p.)}$ heat of vaporization of a compound at its boiling point

J_A^* molar diffusion flux of species A $(gmol \cdot cm^{-2} \cdot s^{-1})$

K von Karman constant (0.4)

K_G mass transfer coefficient in the gas phase

k thermal conductivity $(cal \cdot s^{-1} \cdot m^{-1} \cdot K^{-1})$

L thickness of the oil pad (cm)

N_A flux of species A $(gmol \cdot cm^{-2} \cdot s^{-1})$

N_A^{air} flux of species A from the bulk air

N_A^{oil} flux of species A from the bulk oil

P total pressure (mm Hg or atm)

P_A^{sat} pure component saturation vapor pressure

Q_A radiation received $(cal \cdot m^{-2} \cdot day^{-1})$

Q_B radiation emitted from a black body

Q_{rad} net radiation

R_A homogeneous reaction rate of component A $(gmol \cdot s^{-1})$

Sc_G Schmidt number $= \mu/\rho D$

T temperature (K)

T_{avg} average daily temperature at the surface of the oil

T_c critical temperature of a compound

T_o initial temperature of crude oil

T_∞ ambient air temperature

T_r reduced temperature (T/T_c) (dimensionless)

$T_{r(b.p.)}$ reduced temperature of a compound at its boiling point

t time

U_z wind velocity at an anemometer height of z $(m \cdot s^{-1})$

$U*$ air side friction velocity

U_∞ free stream velocity

$U*$ air side friction velocity

U_∞ free stream velocity

$v*$ local molar average velocity $(m \cdot s^{-1})$

x_A mole fraction of A in the liquid phase

y_A mole fraction of A in the gas phase

z height at which anemometer is reading (m)

z_o roughness height (m)

Greek

α thermal diffusivity $(k/\rho \ C_p)$ $(m^2 \cdot s^{-1})$

β dimensionless group $(K_G \tilde{H} \ L/D_{AB})$

γ_A activity coefficient of   A   (dimensionless)

λ_n n$\underline{\text{th}}$ eigenvalue

ρ density $(gm \cdot cm^{-3})$

ρ_a density of air

σ Stefan-Boltzmann constant $(1.355 \times 10^{-12} \ cal \cdot s^{-1} \cdot cm^{-2} \cdot K^{-4})$

τ_a wind shear stress $(N \cdot m^{-2})$

μ viscosity $(gm \cdot cm^{-1} \cdot s^{-1})$

Subscripts

A   organic component

a   air

B   crude oil residue

b.p.   boiling point

c   critical

G   gas phase

L   liquid phase

o   initial (time zero)

r   reduced

rad   radiation

vap   vapor

∞ reading taken far from the oil-air interface

Superscripts

i   reading taken at an interface

sat   saturation

APPENDIX A

ADDENDUM B

Volume II

Solution to the Governing Differential (G.D.E.) Equation Describing Mass Transfer:

$$D_{AB} \frac{\partial^2 c_A}{\partial z^2} = \frac{\partial c_A}{\partial t}$$

Boundary Condition (1): $\frac{\partial c_A}{dz} = 0$ at $z = 0$

Boundary Condition (2): $-D_{AB} \frac{\partial c_A}{\partial z} = K_G \tilde{H} c_A$ at $z = L$

Initial Condition: $c_A = c_{A_0}$ at $t = 0$

let $c_A = F(z) \tau(t)$

G.D.E. becomes: $F''\tau = \frac{1}{D_{AB}} F\tau'$

or $\frac{F''}{F} = \frac{1}{D_{AB}} \frac{\tau'}{\tau} = -\lambda^2$

B.C. 1: $\tau F' = 0$ at $z = 0$

B.C. 2: $-D_{AB}\tau F' = K_G \tilde{H} F \tau$

or $-\frac{F'}{F} = \frac{K_G \tilde{H}}{D_{AB}}$ at $z = L$

let $\beta = \frac{K_G \tilde{H} L}{D_{AB}}$

$$\frac{F'}{F} = -\lambda^2$$

solution: $F = C_1 \sin\lambda z + C_2 \cos\lambda z$

$$F' = C_1\lambda\cos\lambda z - C_2\lambda\sin\lambda z$$

From boundary conditions:

B.C. 1: $0 = C_2$ therefore $F = C_1\cos\lambda z$

B.C. 2: $\dfrac{C_1 \; \lambda\sin\lambda L}{C_1 \; \cos\lambda L} = \dfrac{\beta}{L}$

$\cot \lambda L = \dfrac{\lambda L}{\beta}$ eigenvalue condition

$\dfrac{\tau'}{\tau} = -\lambda^2$ yields $\tau = e^{-\lambda^2 D_{AB} t}$

Therefore $c_A = \sum\limits_{n=1}^{\infty} C_n e^{-\lambda_n^2 D_{AB} t} \cos\lambda_n z$

I.C. $c_A = c_{Ao}$ at $t = 0$

$$c_{Ao} = \sum\limits_{n=1}^{\infty} C_n \cos\lambda_n z$$

so $C_n = \dfrac{c_{Ao} \displaystyle\int_0^L \cos \lambda_n z \; dz}{\displaystyle\int_0^L \cos^2\lambda_n z \; dz} = \dfrac{2c_{Ao}\sin\lambda_n L}{\lambda_n L + (\sin\lambda_n L)(\cos\lambda_n L)}$

$$\frac{c_A}{c_{Ao}} = 2 \sum_{n=1}^{\infty} e^{-\lambda_n^2 D_{AB} t} \frac{\sin\lambda_n L}{\lambda_n L + (\sin\lambda_n L)(\cos\lambda_n L)} \cos\lambda_n z$$

Flux: $-D_{AB} \dfrac{\partial c_A}{\partial z} = 2c_{Ao} D_{AB} \displaystyle\sum_{n=1}^{\infty} e^{-\lambda_n^2 D_{AB} t} \dfrac{\lambda_n \sin^2\lambda_n L}{\lambda_n L + (\sin\lambda_n L)(\cos\lambda_n L)}$

```
*
*          APPENDIX B: COMPUTER PROGRAM TO CALCULATE
*                     FLUX AS A FUNCTION OF TIME
*
*
           DIMENSION X(100), XNEW(100), TEMP(16), VP(16), T(16), XKH(16)
           OPEN(UNIT=2, FILE='FLUX3', STATUS='NEW')
           TYPE*, 'ENTER CA, S'
           READ(5,*) CA,S
           WRITE(2,*)' '
           WRITE(2,*)'CAO=',CA,'       S=',S
           WRITE(2,*)' '
           TYPE*, 'ENTER A, B, C, K'
           READ(5,*)A,B,C,XK
           TYPE*, 'ENTER TEMP'
           READ(5,*) TEM
           DO 123 I=1,16
           TEMP(I)=TEM
  123      CONTINUE
           DO 13 L=1,16
           VP(L)=EXP(A-B/(TEMP(L)+C))
           XKH(L)=XK*(.01/760)*VP(L)
   13      CONTINUE
           WRITE(2,*)'A=',A,'B=',B,'C=',C
           WRITE(2,*)'K=',XK,'M/S'
           WRITE(2,*)' '
           WRITE(2,1)
    1      FORMAT(3X,'DAB',8X,'KH',7X,'TEMP',7X,'BETA',7X,'DEPTH',5X,
          $'TIME',7X,'FLUX',9X,'INT FLUX',5X,'AVE FLUX')
           WRITE(2,7)
    7      FORMAT(1X,'(M^2/S)',4X,'(M/S)',6X,'DEG K',18X,'(M)',7X,'(S)',
          $5X,'MOL/M^2-S)',5X,'M^-2')
           WRITE(2,*)' '
           TYPE*, 'ENTER DAB, DEPTH'
           READ(5,*)DAB,XL
           T(1)=1.
           T(2)=2.
           T(3)=5.
           T(4)=10.
           T(5)=20.
           T(6)=50.
           T(7)=100.
           T(8)=200.
           T(9)=500.
           T(10)=1000.
           T(11)=2000.
           T(12)=5000.
           T(13)=100000.
           T(14)=200000.
           T(15)=500000.
           T(16)=600000.
           DO 29 M=1,16
           BETA=XKH(M)*XL/DAB
           IF (BETA.LT.20.)GO TO 66
           DO 10 J=1,100
   18      IF (J.GT.1)GO TO 2
           X(1)=1.1*3.1415927/2.
```

```fortran
      GO TO 17
2     X(J)=XNEW(J-1)+3.1415927
17    F=1./TAN(X(J))-X(J)/BETA
      FF=-1./SIN(X(J))**2-1./BETA
22    D=F/FF
      XNEW(J)=X(J)-D
      TEST=F
      IF(ABS(TEST).LT.S)GO TO 20
      X(J)=XNEW(J)
      GO TO 17
20    XLHS=XNEW(J)/BETA
      RHS=1./TAN(XNEW(J))
      DIFF=XLHS-RHS
10    CONTINUE
      GO TO 222
66    X(1)=1.1*3.1415927/2.
77    F=1./TAN(X(1))-X(1)/BETA
      FF=(-1./(SIN(X(1)))**2)-(1./BETA)
88    D=F/FF
      XNEW(1)=X(1)-D
      TEST=F
      IF(ABS(TEST).LT.S)GO TO 200
      X(1)=XNEW(1)
      GO TO 77
200   DO 111 J=2,100
      ALPHA1=XNEW(J-1)+(3.1415927*(J-1))/BETA
      GO TO 700
69    ALPHA1=GAMMA2+(3.1415927*(J-1))/BETA
700   GAMMA1=ATAN(1./ALPHA1)
      ALPHA2=GAMMA1+(3.1415927*(J-1))/BETA
      GAMMA2=ATAN(1./ALPHA2)
      TEST=GAMMA2-GAMMA1
      IF(ABS(TEST).LT..00001)GO TO 80
      GO TO 69
80    XNEW(J)=GAMMA2+(3.1415927*(J-1))
111   CONTINUE
222   SUM=0.
      SUMM=0.
      DO 30 N=1,100
      P=(XNEW(N)/XL)*SIN(XNEW(N))**2
      Q=XNEW(N)+(SIN(XNEW(N))*COS(XNEW(N)))
      R=(XL/XNEW(N))*SIN(XNEW(N))**2
      U=((XNEW(N)/XL)**2)*SIN(XNEW(N))*COS(XNEW(N))
      SUMM=SUMM+(1.-EXP(-((XNEW(N)/XL)**2)*DAB*T(M)))*R/Q
      SUM=SUM+EXP(-((XNEW(N)/XL)**2)*DAB*T(M))*P/Q
30    CONTINUE
      FLUX = 2.*SUM*CA*DAB
      FLUXX = 2.*SUMM*CA
      AVE = FLUXX/T(M)
      WRITE(2,40)DAB,XKH(M),TEMP(M),BETA,XL,T(M),FLUX,FLUXX,AVE
40    FORMAT(1X,E8.1,3X,E8.2,3X,F6.2,3X,E7.2,6X,F5.3,3X,F8.1,
     $3X,3(E11.4,3X),/)
      WRITE(2,*)' '
      WRITE(5,*)'M=',M
29    CONTINUE
      CLOSE(UNIT=2, DISPOSE='KEEP')
      STOP
      END
```
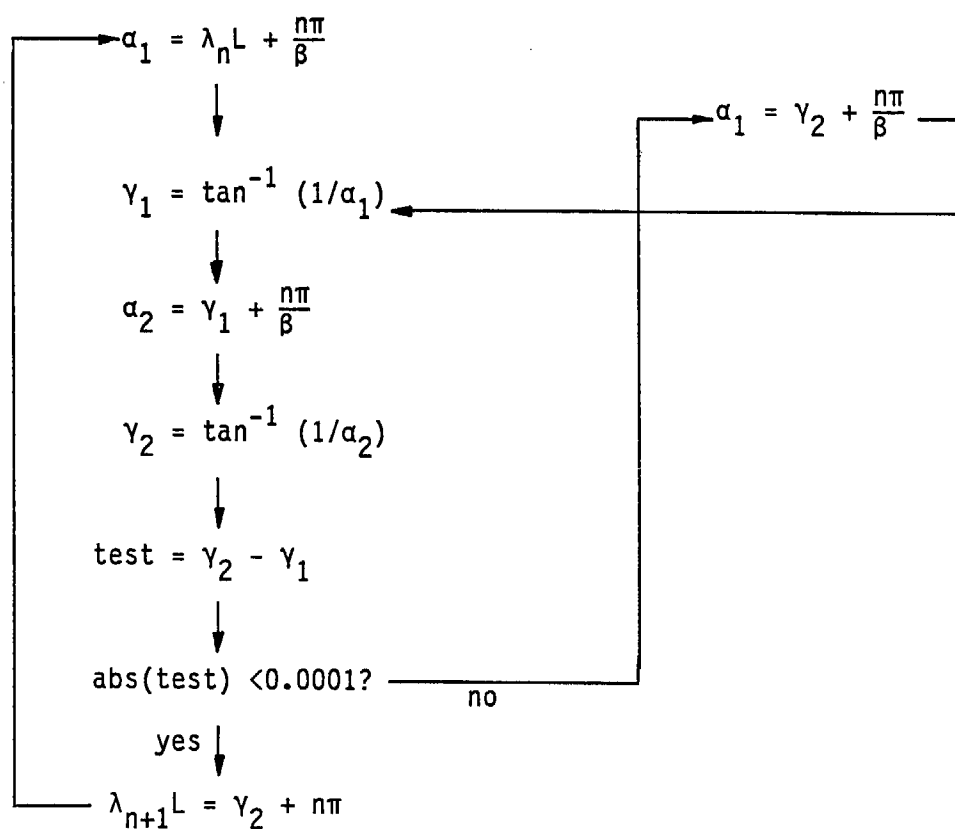
APPENDIX C

ADDENDUM B

Volume II

Iteration Method to Calculate $\lambda_n L$ for $\beta < 20$

$n = 1, 2, \ldots, 100$

$$\alpha_1 = \lambda_n L + \frac{n\pi}{\beta}$$

$$\gamma_1 = \tan^{-1}(1/\alpha_1)$$

$$\alpha_1 = \gamma_2 + \frac{n\pi}{\beta}$$

$$\alpha_2 = \gamma_1 + \frac{n\pi}{\beta}$$

$$\gamma_2 = \tan^{-1}(1/\alpha_2)$$

$$\text{test} = \gamma_2 - \gamma_1$$

$$\text{abs(test)} < 0.0001?$$

no

yes

$$\lambda_{n+1}L = \gamma_2 + n\pi$$

APPENDIX D

ADDENDUM B

Volume II

Derivation of the Governing Differential Equation Describing Heat Transfer

Starting with the thermal energy equation in terms of the internal energy $\hat{U}$:

1) $\quad \rho\frac{D\hat{U}}{Dt} = - (\nabla \cdot q) - (\underset{\approx}{\pi}:\nabla\underline{v}) + \sum_{i=1}^{n} (\underline{j}_i \cdot \underline{g}_i)$

It can be shown that:

2) $\quad \underset{\approx}{\pi} = \underset{\approx}{\tau} + \underset{\approx}{\delta}p$

3) $\quad \rho\frac{D\hat{U}}{Dt} = \rho\frac{D\hat{H}}{Dt} - \rho\frac{D_p\hat{V}}{Dt} = \rho\frac{D\hat{H}}{Dt} - \rho\frac{D\hat{V}}{Dt} - \rho\frac{\hat{V}Dp}{Dt}^1$

4) $\quad \rho p\frac{D\hat{V}}{Dt} = p\nabla \cdot \underline{v}$

5) $\quad \underset{\approx}{\delta}p:\nabla\underline{v} = p\nabla \cdot \underline{v}$

where "∧" means per unit mass.

Substituting 2), 3), 4) and 5) into 1) and rearranging:

6) $\quad \rho\frac{D\hat{H}}{Dt} = - (\nabla \cdot q) - (\underset{\approx}{\tau}:\nabla\underline{v}) + \frac{Dp}{Dt} + \sum_{i=1}^{n} (\underline{j}_i \cdot \underline{g}_i)$

Note that $\hat{H} = \hat{H}(T,p,n_i)$ may be expressed as the total differential (n_i = mol/1000 g):

7) $\quad \rho\frac{D\hat{H}}{Dt} = \rho\left(\frac{\partial\hat{H}}{\partial T}\right)_{p,n_i} \frac{DT}{Dt} + \rho\left(\frac{\partial\hat{H}}{\partial p}\right)_{T,n_i} \frac{Dp}{Dt} + \rho \sum_{i=1}^{n} \left(\frac{\partial\hat{H}}{\partial n_i}\right)_{p,T} \frac{Dn_i}{Dt}$

It can be shown that:

8) $\rho\left(\frac{\partial\hat{H}}{\partial T}\right)_{p,n_i} = \rho\hat{C}_p \frac{DT}{Dt}$

9) $\rho\left(\frac{\partial\hat{H}}{\partial p}\right)_{T,n_i} \frac{Dp}{Dt} = \rho[-T\left(\frac{\partial\hat{V}}{\partial T}\right)_{p,n_i} + \hat{V}] \frac{Dp}{Dt} = \rho v^1 [-\left(\frac{\partial\ln\hat{V}}{\partial\ln T}\right)_{p,n_i} + 1] \frac{Dp}{Dt}$

Letting $\left(\frac{\partial\eta\hat{H}}{\partial n_i}\right)_{p,T,n_i} = \bar{H}_i$

where "___" means partial molal, then:

10) $\rho\frac{D\hat{H}}{Dt} = \rho\hat{C}_p \frac{DT}{Dt} - \left(\frac{\partial\ln\hat{V}}{\partial\ln T}\right)_{p,n_i} \frac{Dp}{Dt} + \frac{Dp}{Dt} + \rho \sum_{i=1}^{n} \bar{H}_i \frac{Dn_i}{Dt}$

Substituting this expression for $\rho \frac{D\hat{H}}{Dt}$ into the previous expression 6) and rearranging yields:

11) $\rho\hat{C}_p \frac{DT}{Dt} = -(\nabla\cdot\underset{\sim}{q}) - (\underset{\approx}{\tau}:\nabla\underset{\sim}{v}) + \left(\frac{\partial\ln\hat{V}}{\partial\ln T}\right)_{p,n_i} \frac{Dp}{Dt} + \sum_{i=1}^{n} \underset{\sim}{j}_i\cdot\underset{\sim}{g}_i - \rho \sum_{i=1}^{n} \bar{H}_i \frac{Dn_i}{Dt}$

Consider $\rho\frac{Dn_i}{Dt}$:

12) $\rho\frac{Dn_i}{Dt} = \rho\frac{\partial n_i}{\partial t} + \rho \underset{\sim}{v}\cdot\nabla n_i = \left(\frac{\partial\rho n_i}{\partial t} - n_i\frac{\partial\rho}{\partial t}\right) + (\nabla\cdot\rho n_i\underset{\sim}{v} - n_i\nabla\cdot\rho\underset{\sim}{v})$

13) $\rho\frac{Dn_i}{Dt} = \frac{\partial\rho n_i}{\partial t} + \nabla\cdot\rho n_i\underset{\sim}{v} - n_i [\frac{\partial\rho}{\partial t} + \nabla\cdot\rho\underset{\sim}{v}]$

Noting that since $\rho = g/m^3$ and $n_i = mol/1000 g$,

14) $\rho n_i = mol/m^3 = c_i$.

From the continuity equation:

15) $\dfrac{\partial \rho \eta_i}{\partial t} = \dfrac{\partial c_i}{\partial t} = -\nabla \cdot \underset{\sim}{N}_i + R_i = -\nabla \cdot c_i \underset{\sim}{v}_i + R_i$

16) $\nabla \cdot \rho \eta_i \underset{\sim}{v} = \nabla \cdot c_i \underset{\sim}{v}$

Substituting 15) and 16) into 13):

17) $\rho \dfrac{D\eta_i}{Dt} = R_i - [\ \nabla \cdot c_i\ v - \nabla \cdot c_i \underset{\sim}{v}\ ]$

$\qquad\qquad = R_i - \nabla \cdot c_i\ (\underset{\sim}{v} - \underset{\sim}{v}_i)$

18) $\rho \dfrac{D\eta_i}{Dt} = R_i - \nabla \cdot \underset{\sim}{J}_i$

Therefore,

19) $\rho \sum\limits_{i=1}^{n} \bar{H}_i \dfrac{D\eta_i}{Dt} = \sum\limits_{i=1}^{n} \bar{H}_i [\ R_i - (\nabla \cdot \underset{\sim}{J}_i)\ ]$

Finally,

20) $\rho c_p \dfrac{DT}{Dt} = -(\nabla \cdot \underset{\sim}{q}) - (\underset{\approx}{\tau} : \nabla \underset{\sim}{v}) + \left(\dfrac{\partial \ln V}{\partial \ln T}\right)_{p,\eta_i} \dfrac{Dp}{Dt} + \sum\limits_{i=1}^{n} \underset{\sim}{J}_i \cdot \underset{\sim}{g}_i + \sum\limits_{i=1}^{n} \bar{H}_i\ [\ \nabla \cdot \underset{\sim}{J}_i) - R_i J]$

Assumptions:

1) zero velocity, $\dfrac{DT}{Dt} = \dfrac{\partial T}{\partial t} + \overset{0}{\underset{\sim}{v} \cdot \nabla T}$

2) constant thermal conductivity, $-\nabla \cdot \underset{\sim}{q} = \nabla \cdot (k\nabla T) = k\nabla^2 T$

3) no viscous dissipation, $\underset{\approx}{\tau} : \nabla \underset{\sim}{v} = 0$

4) no gravitational forces, $\sum\limits_{i=1}^{n} \underset{\sim}{j}_i \cdot \underset{\sim}{g}_i = 0$

5) $\left(\dfrac{\partial \ln V}{\partial \ln T}\right)_{p,\eta_i} \dfrac{Dp}{Dt} = -\dfrac{T}{\rho}\left(\dfrac{\partial \rho}{\partial T}\right)_{p,\eta_i} \dfrac{Dp}{Dt} = 0$

6) no reactions, $R_i = 0$

7) one dimensional, $\nabla^2 T = \dfrac{\partial^2 T}{\partial z^2}$

8) molecular weight of VOC's = molecular weight of non-volatile compounds,

$$\underset{\sim}{J}_i = \dfrac{{}_\star M_B}{M} \underset{\sim}{J}_i = -D_{ij}\nabla c_i$$

9) $\overline{H}_i = H_i = c_{pi}(T - T_0)$

Therefore, the governing differential equation is:

21) $\rho \hat{C}_p \dfrac{\partial T}{\partial t} = k\dfrac{\partial^2 T}{\partial z^2} - \sum\limits_{i=1}^{n} \hat{c}_{pi}(T - T_0)D_{ij}\dfrac{\partial^2 c}{\partial z^2}$

ADDENDUM C

Volume II

*DIFFUSIVITIES OF VOLATILE ORGANIC COMPOUNDS IN
HIGH VISCOSITY SOLVENTS*

Cynthia L. Castronovo

TABLE OF CONTENTS

FIGURES

LIST OF TABLES

ADDENDUM C

DIFFUSIVITIES OF VOLATILE ORGANIC COMPOUNDS IN HIGH VISCOSITY SOLVENTS

Introduction:

The model developed to describe the organic compound emissions from crude oil sumps depends on several parameters, including Henry's law coefficients, gas phase mass transfer coefficients, and liquid diffusion coefficients. The assumption that the crude oil layer behaves as a semisolid supports the idea that the dominant mechanism of transport through the oil pad is molecular diffusion. It is likley that, in many cases, this diffusion process is the limiting factor in VOC emissions. This section will describe work done so far to determine the liquid diffusivities of volatile organic compounds (VOCs) in the crude oil.

Our previous work has included speciation of the portion of the crude oil that distills at or below 220 deg C. Comparision of this distillate fraction from an inlet sump sample with the distillate obtained from an outlet sample has revealed that the compounds being lost from the crude oil to the atmosphere have boiling points of 150 deg C or less. These compounds are the ⁵VOCs⁵ as defined in this work. From our speciation results, a typical VOC emitted from a sump might be a cycloparaffin containing 7 carbon atoms.

A review of the literature reveals two primary classes of experimental techniques to determine diffusion coefficients, optical methods and Taylor diffusion methods. Both of these techniques would be difficult to apply to a crude oil system. The optical methods measure concentration gradients of a solute in a relatively transparent solvent by determining the changes in refractive index or other optical property. The fact the crude oil is opaque prevents the use of these methods. The Taylor diffusion technique generally measures the extent

of "band spreading" of a pulse of solute (VOC) into a stream of solvent (crude oil). Several types of detectors can be used to determine the shape of the outlet "pulse," but as a slow diffusion process is expected, the "band spreading" may be difficult to measure. In addition, there are problems in creating a reproducible and definable initial pulse.

The literature also offers little experimental data on diffusion through viscous liquids. Diffusion coefficients of hexane and naphthalene in viscous ils are reported by Hiss and Cussler (1973). They used an optical technique, thus necessitating the use of ⁵transparent⁵ viscous oils.

A common method of obtaining an estimate of liquid diffusion coefficients is estimation through use of a predictive equation. For liquids, the most commonly used is the Wilke-Chang equation (Wilke and Chang, 1955). Unfortunately, these correlations give large errors for viscous solvents. The literature contains a vast amount of physical data on petroleum, but we have yet to find any data on liquid diffusion coefficients of hydrocarbons in heavy crude oil.

These factors prompted development of our own experimental method, which is based on measurement of diffusion through a stagnant layer, familiarly known as a Stefan tube model (Stefan and Wein, 1973). Our adaptation provides for the transient measurement of the VOC flux from a premixed oil layer using a diffusion cell and a flame ionization detector (FID). The oil used as substrate is a crude oil residium obtained from a distillation to remove compounds boiling below 220°C. This distilled fraction is approximately 5% of the original crude oil. The VOC of interest is then mixed with the residium in pre-determined proportions. A carrier gas (N_2) is passed over a stagnant layer of oil containing the uniformly mixed VOC. The VOC emissions from the oil layer are swept

by the carrier gas to the FID. The mass of the VOC is measured by the FID from which the flux from the oil surface can be found using the equation below.

The theory and working equations for determining diffusion coefficients from flux data is described below.

Development of Working Equation:

To illustrate the development of the working equation, it is helpful to review the sump emissions mathematical model. The governing differential equation and associated boundary conditions are

$$\frac{\partial C}{\partial t} = - D_{AB} \frac{\partial^2 C}{\partial z^2}$$

B.C.1 $\qquad C = 0 \quad at \quad Z = \infty$

B.C.2 $\qquad - D \frac{\partial C}{\partial z} = k_g \tilde{H} (C_{Ao} - C) \quad at \quad Z = 0$

IC $\qquad C = 0 \quad at \quad t = 0$

In these equations, $C = C_{Ao} - C_A$ (the concentration of component A initially in the sump, minus the concentration of A at any time). Since C_A is always less than C_{Ao}, C is a positive value. The concentration of A is uniform at time zero. In these equations, A is the VOC component and B is the crude oil residue.

Also note that the first boundary condition assumes that the concentration of A at the bottom of the oil layer does not change over the time period of the experiment. This assumption is supported by calculations reported earlier which

estimate that the concentration profile penetrates to the bottom of a 1 cm oil pad in 17 minutes. Oil layers used in the experiment are approximately 2 cm and only the data obtained in the first 30 minutes are used.

The equations above can be solved analytically to provide an expression for C_A:

$$C_A = -e^{zK/D} + e^{(\frac{K^2 t}{D_{AB}})} \; erfc \left[K \; \sqrt{t/D} + \frac{z}{\sqrt{4Dt}} \right] + \left[erfc \; \frac{z}{\sqrt{4Dt}} \right]$$

Note that $K = k_g H$

This expression can be used to solve for the flux at z=0 (at the air-oil interface):

$$FLUX = - D \; \frac{\partial C_A}{\partial z} \Big|_{z=0} = C_{Ao} \; exp \left[K^2 t/D \right] \; erfc \; K \sqrt{\frac{t}{D}}$$

The error function can be replaced by a series approximation to give:

$$FLUX = C_{Ao} \; \sqrt{\frac{D}{\pi t}} \left[1 - \frac{D}{2K^2 t} + \frac{3}{4} \frac{D^2}{K^4 t^2} - \quad \ldots\ldots \quad \right]$$

We can estimate the order of magnitude of the second term in the parentheses by estimating values of K, D, and t. From a correlation for k_g taken from Cussler (1984), k_g is approximately 10^{-2} m/sec in the cell. $\tilde{H}$ is on the order of 10^{-2}. Thus K is on the order of 10^{-5}. D, the diffusivity, is estimated to be on the order of 10^{-9} m^2/sec. t is exposure time in seconds At t = 60 seconds, this term is on the order of 10^{-1}. But after 180 seconds, it is on the order of 10^{-2}. Thus, the assumption that this term is negligible after the first few minutes of a run appears valid. The other terms in the series are

even smaller and can also be discarded. Thus we arrive at the following expression which corresponds to a penetration theory model and is independent of the gas phase resistance.

$$\text{FLUX} = C_{Ao} \sqrt{D/\pi t}$$

and squaring both sides

$$(\text{FLUX})^2 = \left[\frac{c_{Ao}^2 D}{\pi} \right] \frac{1}{t}$$

This is the working equation being used to calculate diffusion coefficients. Note that if the square of the flux is plotted against 1/time, the slope is equal to $c_{Ao}^2 D/\pi$.

Before continuing, we should consider the physical significance of neglecting these smaller terms. The absence of K (k_gH) signifies no resistance to the diffusion process in the gas phase passing over the cell. Put another way, it assumes that all of the diffusion resistance lies in the liquid oil. The cell has been designed so that these conditions will hold, however it should be emphasized that these assumptions are not necessarily valid in other cases. A case in point is the actual sump in the field. At a particular sump, under particular weather conditions, liquid and gas phase resistances may both be affecting the VOC emissions although there is substantial evidence that the liquid phase resistance is controlling.

Description of Experimental Approach:

The design of the experimental method required the consideration of many factors. These factors are discussed below:
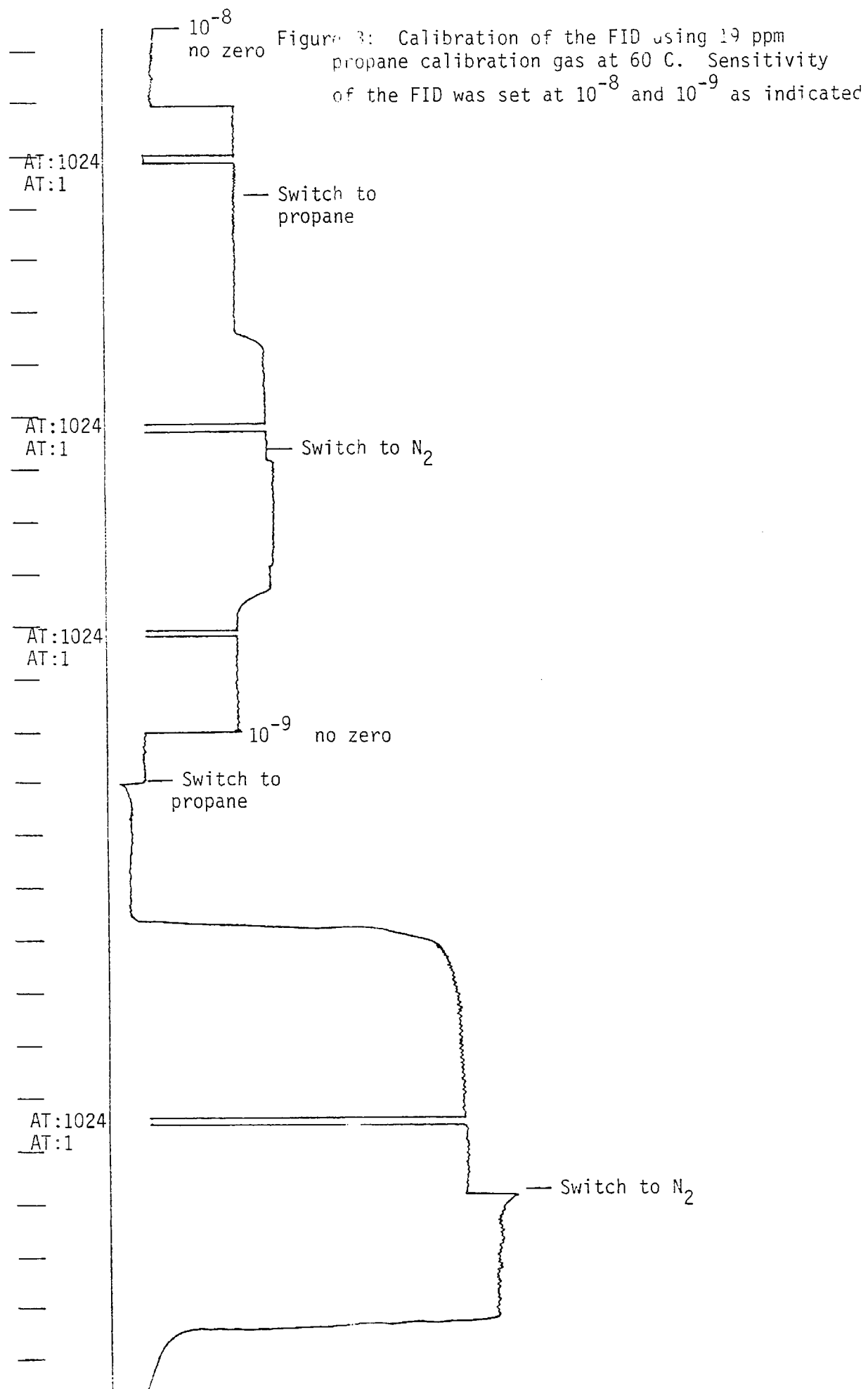
1. Choice of Detector

The method required a detector that was sensitive to ppm concentrations

of hydrocarbons. Initial plans called for a mass selective detector, however quantitation problems became apparent. Some preliminary runs were made using a mass selective detector, to ensure that only the VOC of interest was being emitted to the detector. A viscous oil of known properties, which had been used by Cussler (1984) for diffusion experiments, was used as the solvent and n-heptane was used as the solute. The chromatograms are shown in Figures 1 and 2. As can be seen, the total ion chromatogram (TIC) is similar to the molecular ion trace (100) of heptane. Also, no ions having molecular weights greater than 100 were detected. Thus, we can assume that the viscous oil is not volatilizing in the diffusion cell.

Subsequent runs have utilized a flame ionization detector (FID). The sensitivity of the FID can be varied and even the least sensitive setting was adequate to detect the 19 ppm propane calibration gas (See Figure 3). The FID was calibrated by measuring the difference in response between the calibration gas and the pure N_2 . The response of the FID is printed during the run and is also stored on a floppy disk for later manipulation if desired. The difference in response is measured in millimeters using a ruler.

Due to the configuration of the FID, there is only a narrow band of carrier gas flow rate for which the FID remains an accurate quantitative detector. This flowrate is 30 ml/min. The average velocity of the carrier gas is determined by the channel in the diffusion cell. This channel is cut in a neoprene gasket and its dimensions can be varied by substitution of different gaskets. Thus it possible to vary the average velocity of the carrier gas above the sample vial without changing the total flowrate to the FID. This will allow validation of the relationship between VOC flux and gas phase mass transfer.

10^{-8}
no zero

Figure 3: Calibration of the FID using 19 ppm propane calibration gas at 60 C. Sensitivity of the FID was set at 10^{-8} and 10^{-9} as indicated

AT:1024
AT:1

— Switch to propane

AT:1024
AT:1

— Switch to N_2

AT:1024
AT:1

10^{-9} no zero

— Switch to propane

AT:1024
AT:1

— Switch to N_2
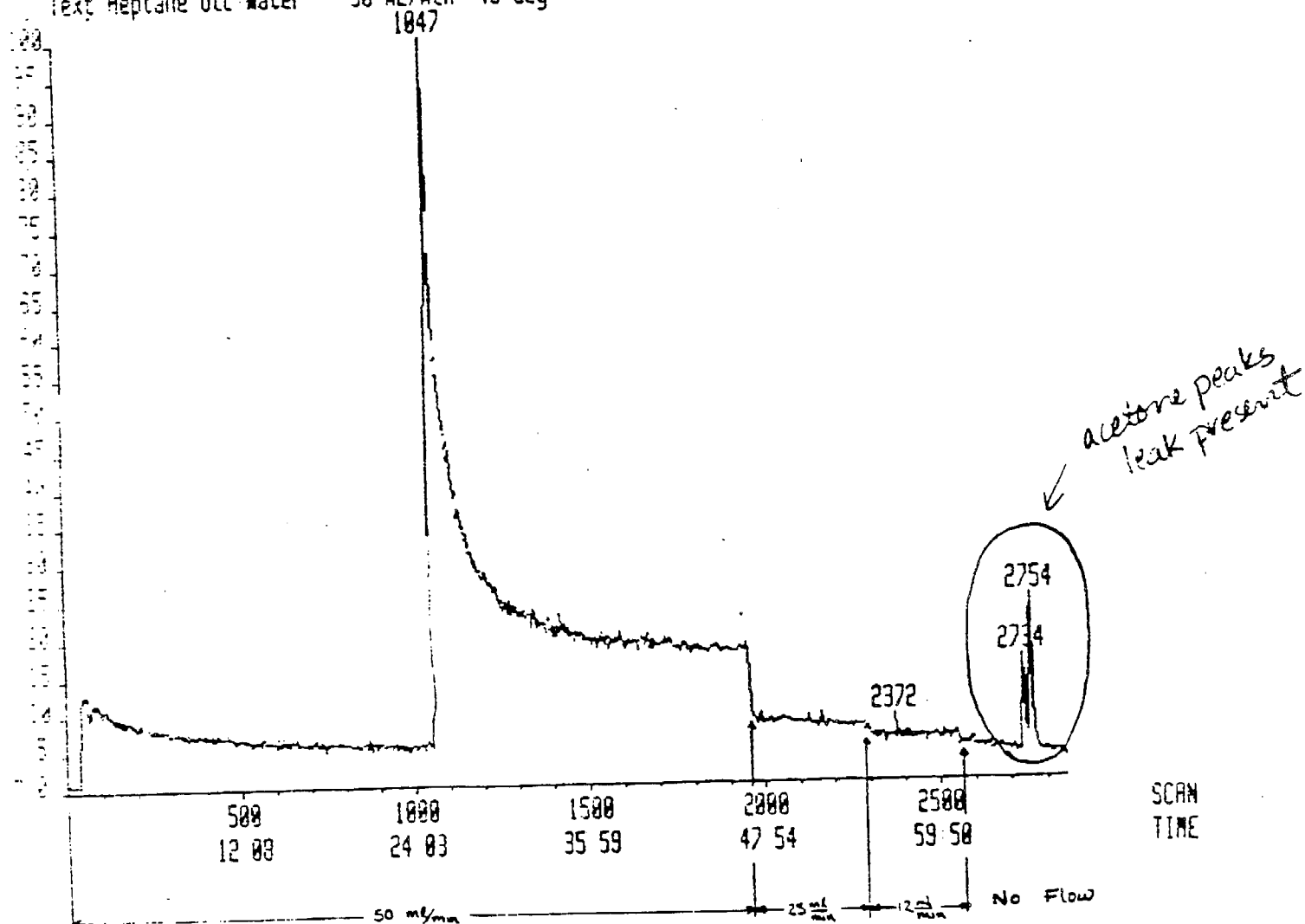
Figure 1: Total ion chromatogram (TIC) of n-heptane in viscous oil.

1181CCl #1-2851   1-NOV-85 09 38 ZRB-HS   acnt UCD/FRI   System GCSYS   IHP
Chromatogram Identifiers :   B1 188   B: 82418888
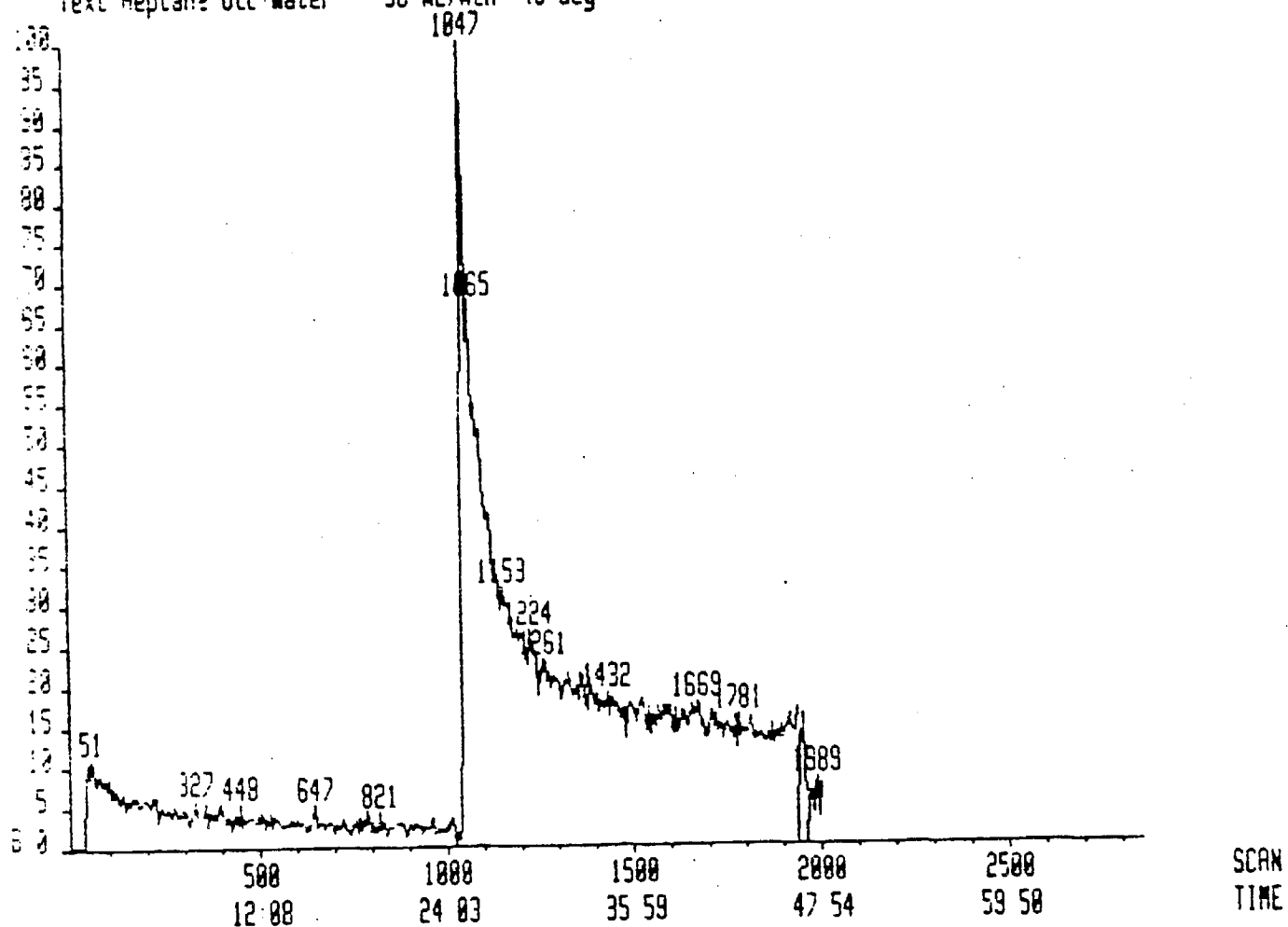Text Heptane Oil Water -- 58 mL/min 48 deg

Figure 2: Molecular ion trace of heptane in viscous oil.

2. Diffusion Cell Design

The diffusion cell was designed to accomodate small sample sizes, provide a definable mass transfer interface, allow easy insertion of samples without loss of the VOC and be small enough to be completely contained in a small GC oven.

Figures 4 and 5 depict the side and top views of the diffusion cell. The sample vial is attached to the cell by screwing it into a vial cap which has been cemented into the bottom plate of the cell. The top of the cap has been machined away, so that the surface area available for mass transfer is the cross-sectional area of the vial. The gas flow in and out of the cell are controlled by valves. The distance between the vial and the detector have been minimized to avoid axial diffusion of the VOC in the carrier gas.

3. VOC/Crude Oil Samples

The preparation of samples required mixing of the crude oil without the loss of the VOC component. Also , it was necessary to ascertain when uniform mixing had been achieved.

The sample vials are prepared by first placing crude oil into 1 dram tared vials until about half full. The vials are weighed and chilled. A known amount (usually 50 μl) of a known chilled VOC compound is injected into the oil layer through a septum. The vials are then capped securely, then heated in a water bath at about 75 deg C, to facilitate mixing of the VOC in the crude. The vials are occasionally taken out of the bath and placed on a tube rotator. An organic dye has been added to the VOC on trial runs in a somewhat transparent viscous oil to act as an indicator of complete mixing. This mixing process generally takes place over 2 to 3 days.

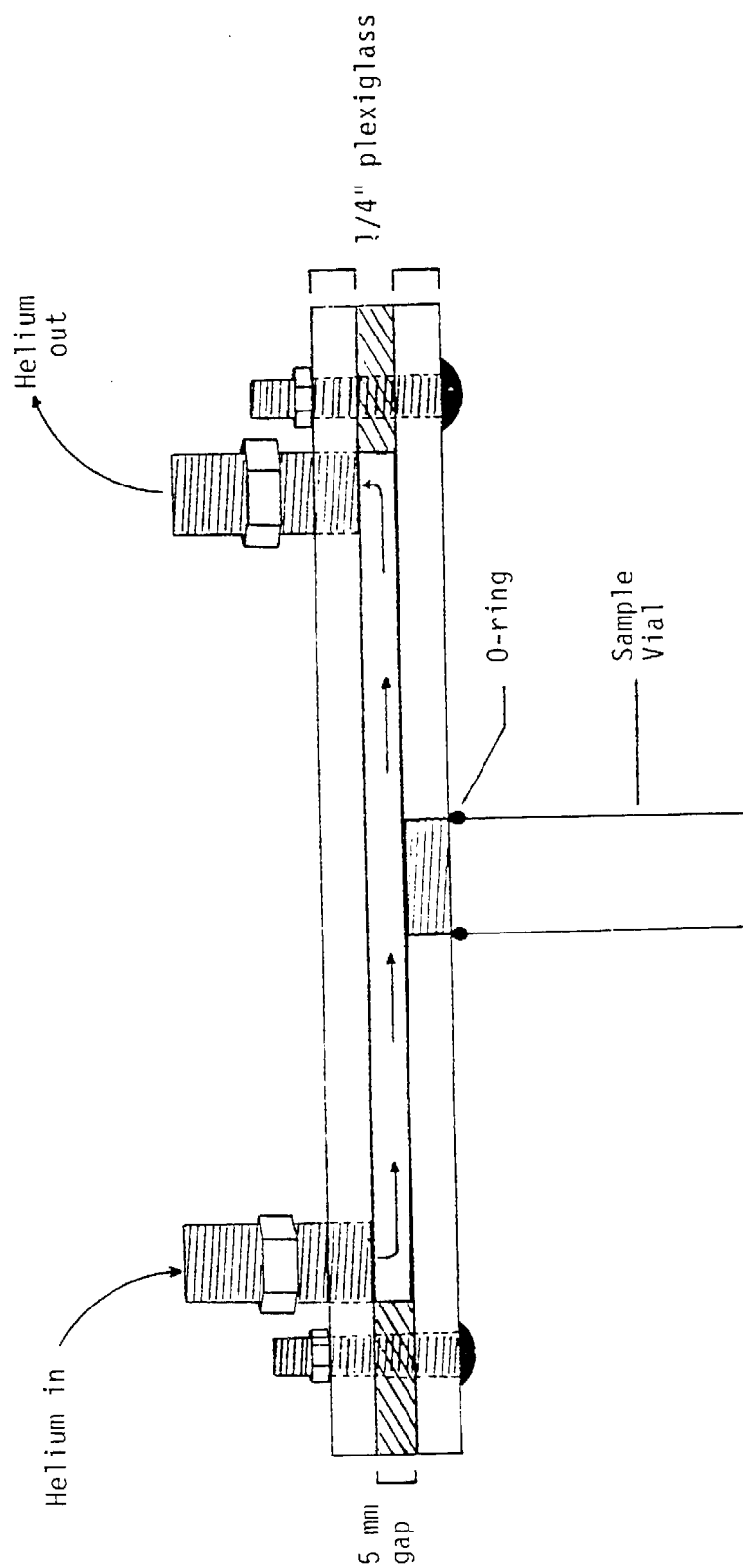Figure 4: Side view of the diffusion cell (helium flow rate of 40 ml/min)

Figure 5:   Top View of the Diffusion Cell
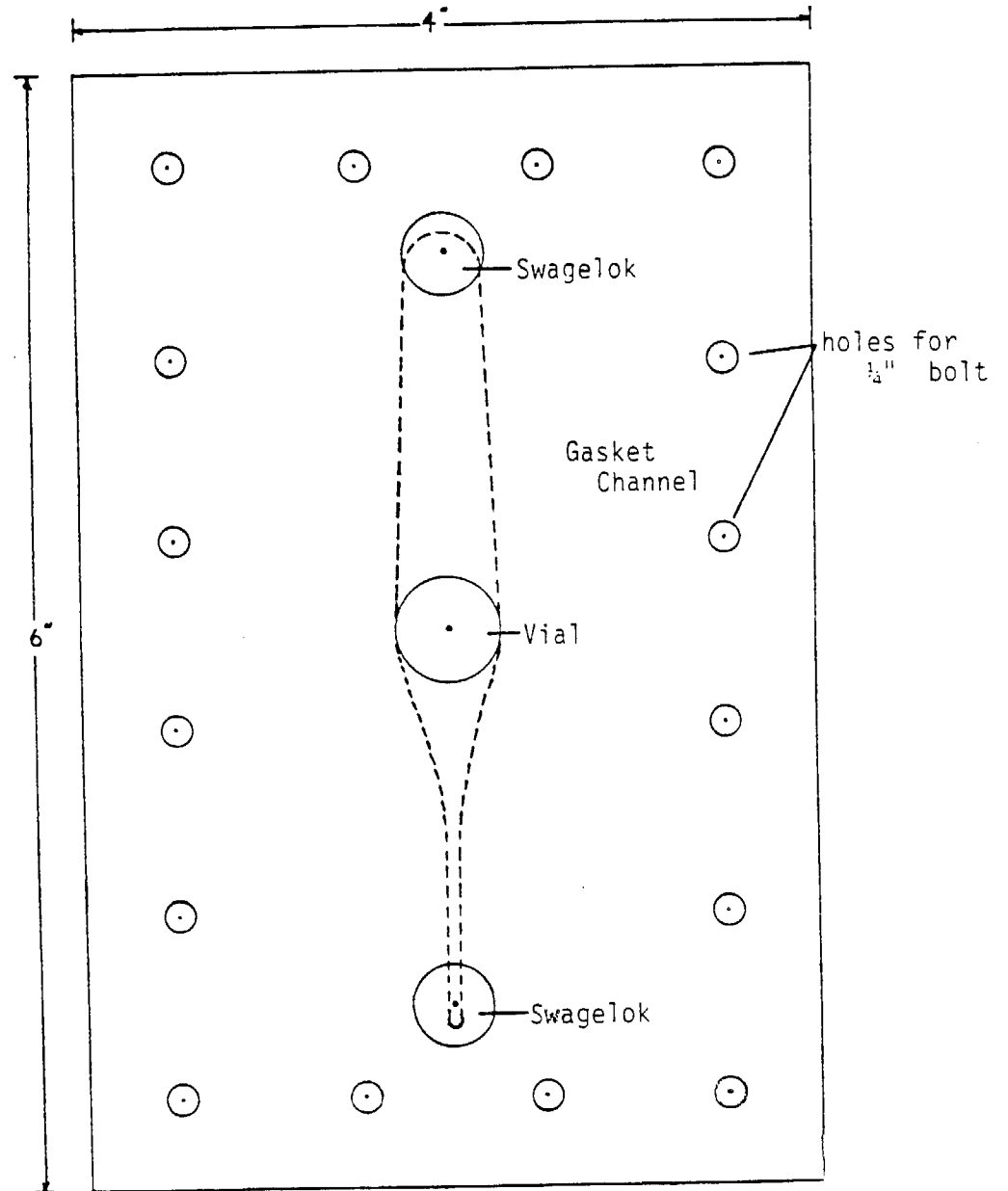
After the VOC compound is deemed uniformly mixed, the vials are chilled in an ice bath. Chilled distilled water is injected through a septum to fill the vial to the brim. The vials are capped again, and the water settles to the bottom of the vial, with the uniform viscous oil layer on top. The vials are kept refrigerated until ready to run.

Immediately before the run, the sample vial is placed in an ice bath. Then it is quickly screwed into the bottom plate of the diffusion cell, which has its valves closed to prevent loss of the VOC. The cell is designed so that the top of the oil layer is flush with the bottom of the carrier gas channel. The diffusion cell is brought up to run temperature in the GC oven. The FID is calibrated using the bypass line. The run commences upon opening the valves so that the carrier gas (N_2) can pass over the sample.

Figure 6 shows a diagram of the experimental apparatus. Note that it allows for easy switching (A) between the calibration gas and the carrier gas to allow a calibration before and after a test run. Also note the cell bypass (B) which allows constant flow to the detector. This was found to be necessary as the flame in the detector would extinguish upon sudden flow changes.

Preliminary Results

To test our method, it was decided to first run experiments using Cannon viscosity standard oils, to allow comparison with Hiss and Cussler's results.

It should be noted that the ⁵viscous⁵ oils used by Hiss and Cussler are not as viscous as the crude oil from the sumps. Thus the most viscous oil used by Hiss and Cussler is the least viscous oil of the three being used in our experiments. Also, Hiss and Cussler determined diffusivities at room temperature, while our temperatures range from room temperature to 80 deg C.

Figure 6: Dynamic VOC Flux Measurement Experimental Apparatus (not drawn to scale).
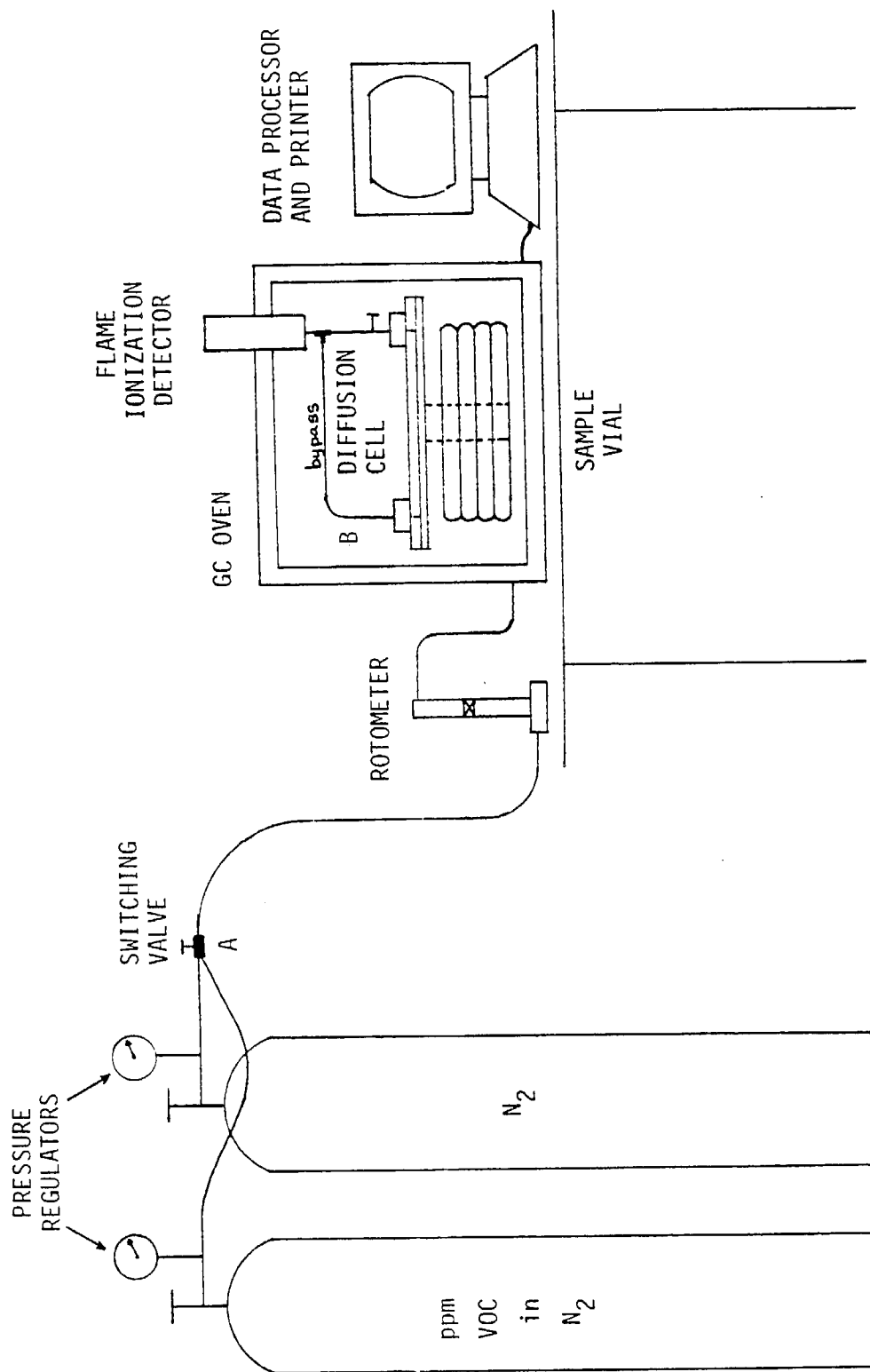
153

TABLE 1

PROPERTIES OF VISCOUS OILS

OIL ID	S2000	S8000	S30000
NUMBER AVE MOLECULAR WEIGHT	730	950	1400
VISCOSITY AT 25 DEG C (CP)	6008	24140	81670
CRUDE OIL ID	36W	31X	MONTE CRISTO
VISCOSITY AT 23 DEG C (CP)	7100	16300	3150

TABLE 2

CELL023

HEPTANE IN S30000 AT 60 DEG C

TIME (min)	HEIGHT (mm)	AT	ADJ HT (mm)	MASS RATE (ug/min)	FLUX (mol/min/cm2)	1/TIME (min-1)	(FLUX)2
3	67	4	20.95	6.1	2.36E-07	3.3E-01	5.59E-14
4	54.5	4	15.95	5.3	2.05E-07	2.5E-01	4.21E-14
5	96	2	13.35	4.9	1.89E-07	2.0E-01	3.58E-14
6	86	2	11.35	4.6	1.77E-07	1.7E-01	3.12E-14
7	78.5	2	9.85	4.3	1.67E-07	1.4E-01	2.80E-14
8	73	2	8.75	4.2	1.60E-07	1.2E-01	2.57E-14
9	69	2	7.95	4.0	1.55E-07	1.1E-01	2.42E-14
10	65	2	7.15	3.9	1.50E-07	1.0E-01	2.26E-14
11	62.5	2	6.65	3.8	1.47E-07	9.1E-02	2.17E-14
12	60	2	6.15	3.8	1.44E-07	8.3E-02	2.08E-14
13	58	2	5.75	3.7	1.42E-07	7.7E-02	2.01E-14
14	56	2	5.35	3.6	1.39E-07	7.1E-02	1.94E-14
15	108.5	1	5	3.6	1.37E-07	6.7E-02	1.88E-14
16	105.5	1	4.7	3.5	1.35E-07	6.2E-02	1.83E-14
17	102.5	1	4.4	3.5	1.33E-07	5.9E-02	1.78E-14
18	100	1	4.15	3.4	1.32E-07	5.6E-02	1.74E-14
20	95.5	1	3.7	3.4	1.29E-07	5.0E-02	1.66E-14
22	93	1	3.45	3.3	1.27E-07	4.5E-02	1.62E-14
24	89.5	1	3.1	3.3	1.25E-07	4.2E-02	1.57E-14
26	87	1	2.85	3.2	1.24E-07	3.8E-02	1.53E-14
28	84.5	1	2.6	3.2	1.22E-07	3.6E-02	1.49E-14
30	83	1	2.45	3.2	1.21E-07	3.3E-02	1.47E-14

```
                   Regression Output:
          Constant                 9.8E-15
          Std Err of Y Est         6.1E-16
          R Squared               0.996597
          No. of Observations           22
          Degrees of Freedom            20

          X Coefficient(s)         1.33E-13
          Std Err of Coef.         1.7E-15
```

(flux)2 = (c2 D/pi)* (1/t)
         slope

c = moles/cm3 = (g/cm3)/(g/mole)
              density   MW

          density   0.87 g/cc
           MW =   1400 g/mol

          c = 6.21E-04 mol/cc

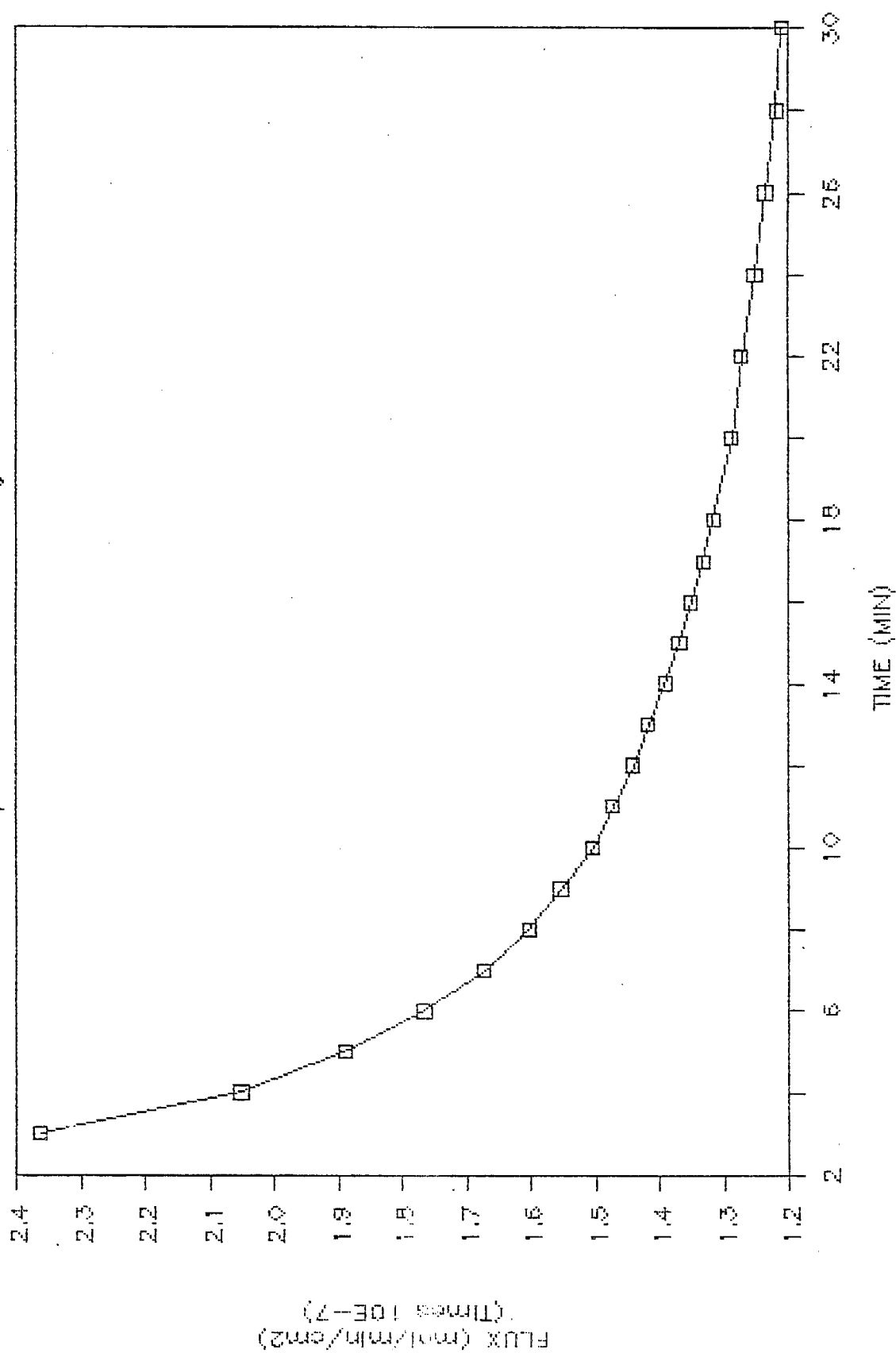D = (pi)(slope)/(c2) = 1.08E-06 cm2/min
              D =   1.80E-12 m2/sec

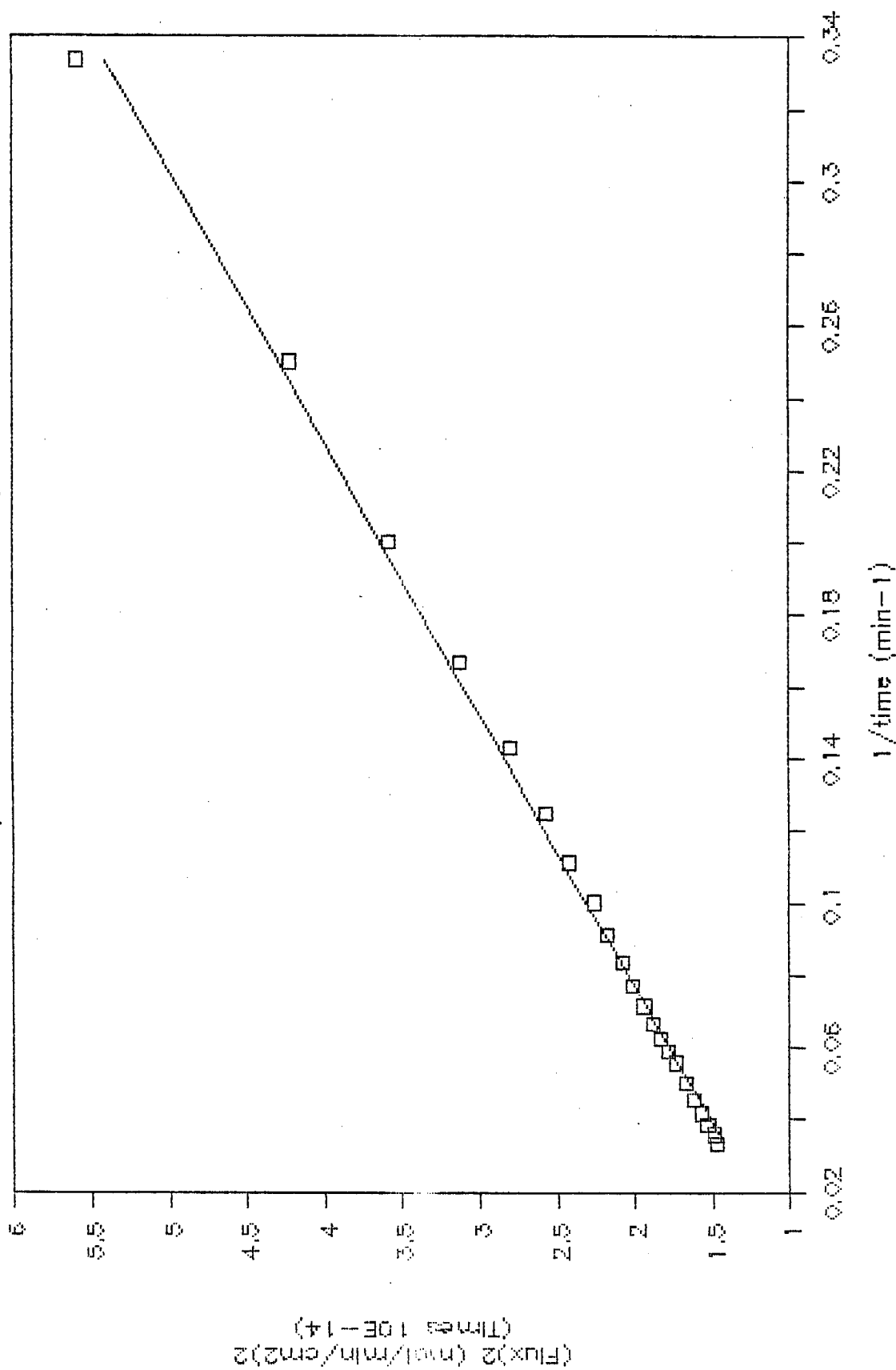Figure 7: Plot of the flux of n-heptane from the S30000 viscous oil as a function of time at 60 degrees centigrade.

Figure 8: Plot of the (flux)^2 of n-heptane from S30000 viscous oil as a function of the inverse of time at 60 degrees centigrade. The line through the data is the linear regression fit of the data.

Some information on the viscosity standard oils is given in Table 1. Also listed is some viscosity data on three crude oils for comparison.

It should be mentioned that the viscosity standard oils are primarily polybutene molecules of various lengths. The diffusion of small VOC molecules through these polymer solutions may differ from diffusion through crude oil of the same viscosity.

An example of a typical run data sheet is presented in Table 2. (Data sheets for other runs are contained in Appendix A). The height is the measurement of the FID response at a given time. AT is the attentuation on the printer. The adjusted height accounts for attenuation and subtracts any background. The mass rate is calculated by multiplying the adjusted height by a factor determined by a previous calibration run. The flux is calculated by dividing by the molecular weight of the VOC and the mass transfer area (the cross-sectional area of the sample vial). The relationship observed for the change of VOC flux with time is depicted in Figure 7.

The last two columns in Table 2 are the values required for determination of D using the working equation previously derived. A plot of these values is presented in Figure 8. Recall that the slope of this line is equal to $c_{Ao}^2 D/\pi$. The calculations for D are listed near the bottom of the run data sheet.

The results of the regression analysis for this last plot is also contained on the data sheet. The X coefficient is the slope of the line and is the value used to determine D. Note the goodness of fit of the line as illustrated by the R-squared value, or correlation factor (a perfectly straight line would have a value of 1.00000). Although the results of only one run is discussed here, all of the runs analyzed have R squared values greater than 0.95.

TABLE 3: DIFFUSIVITY OF N-HEPTANE (x 10^{13}) m^2/sec

OIL ——	S8000		S30000	
TEMP ——	60 deg	80 deg	60 deg	80 deg
D (m^2/sec) for n-heptane in standard oils (x 10^{13})	10.4	4.3	18	40
D (m^2/sec) for n-hexane in same viscosity at 25 deg C (x 10^{13})	119	297	52	128
VISCOSITY (cp)	1434	361	4992	1285

Table 3 compares some of the preliminary results with the data reported by Hiss and Cussler. Values are compared on the basis of viscosity, as the temperatures used in obtaining the data are different. Although no correlation between diffusivity and oil viscosity can be drawn from these results, some of our data show agreement with Hiss and Cussler's data within an order of magnitude. It should be kept in mind that these data represent results of trial runs used to develop the experimental method.

Work in Progress

More experiments with the viscosity standards are underway to test the repeatibility of the method. Although heptane is the only VOC test compound used so far, it is likely that a cycloparaffin and an aromatic compound will also be investigated. Upon completion of these tests, experiments with the VOC compounds in crude oil residues will begin.

Conclusions

The preliminary experiments have shown that flux data from viscous oils conform extremely well to the form of our working equation and can thus be used to calculate diffusion coefficients. A diffusion cell has been designed and constructed that will allow calibration before and after each sample run. The flame ionization detector has proven sufficiently sensitive to allow detection of the hydrocarbons emitted in the cell. A sample preparation technique has been developed to ensure uniform mixing of a VOC in a viscous oil without loss of the VOC.

REFERENCES

1. Cussler, E.L. (1984). Diffusion and Mass Transfer in Fluid Systems. 230.

2. Hiss, T.G., Cussler, E.L. (1973). Diffusion in High Viscosity Liquids, AIChE Journal, 19(4):698-703.

3. Stefan, J., Wein, J. (1873). 11(68):385.

4. Wilke, C.R., Chang, P. (1955). AIChE J., Vol. I. 264-270.

NOMENCLATURE

C   molar concentration ($gmole/cm^{-3}$)

C_A molar concentration of component A

C_{Ao} initial molar concentration of component A in the crude oil

C_G molar concentration of component A in the gas phase

C_L molar concentration of component A in the liquid phase

D   diffusion coefficient ($m^2 \cdot s^{-1}$)

H   Henry's Law Constant (dimensionless)

$\tilde{H}$ $H \dfrac{C_G}{C_L}$

k_g mass transfer coefficient in the gas phase ($m \cdot s^{-1}$)

K $k_g \tilde{H}$

t   time

z   directional coordinate

APPENDIX

Data Sheets for the Diffusion Cell

ADDENDUM C

Volume II

TABLE A1

VOCCELL015

HEPTANE IN S2000 AT 30 DEG C

TIME (min)	HEIGHT (mm)	AT	ADJ HT(mm)	MASS RATE (ug/min)	FLUX (mol/min/cm2)	1/TIME (min-1)	(FLUX)2
3	92.5	2	118	0.2	8.24E-09	3.3E-01	6.79E-17
4	84	2	101	0.2	7.05E-09	2.5E-01	4.98E-17
5	78.5	2	90	0.2	6.29E-09	2.0E-01	3.95E-17
6	74	2	81	0.1	5.66E-09	1.7E-01	3.20E-17
7	139.5	1	72.5	0.1	5.06E-09	1.4E-01	2.56E-17
8	134.5	1	67.5	0.1	4.71E-09	1.2E-01	2.22E-17
9	129	1	62	0.1	4.33E-09	1.1E-01	1.87E-17
10	123.5	1	56.5	0.1	3.95E-09	1.0E-01	1.56E-17
11	119.5	1	52.5	0.1	3.67E-09	9.1E-02	1.34E-17
12	116	1	49	0.1	3.42E-09	8.3E-02	1.17E-17
13	112.5	1	45.5	0.1	3.18E-09	7.7E-02	1.01E-17
14	109.5	1	42.5	0.1	2.97E-09	7.1E-02	8.81E-18
15	107.5	1	40.5	0.1	2.83E-09	6.7E-02	8.00E-18
16	104.5	1	37.5	0.1	2.62E-09	6.2E-02	6.86E-18
18	100.5	1	33.5	0.1	2.34E-09	5.6E-02	5.47E-18
20	96.5	1	29.5	0.1	2.06E-09	5.0E-02	4.24E-18
22	93	1	26	0.0	1.82E-09	4.5E-02	3.30E-18
24	90.5	1	23.5	0.0	1.64E-09	4.2E-02	2.69E-18

Regression Output:

Constant	-4.48449E-16
Std Err of Y Est	3.45423E-17
R Squared	0.9991443828
No. of Observations	18
Degrees of Freedom	16

X CoX Coeff	1.5E-14	1.61133E-14
Std Std Err	1.1E-16	3.06268E-16

$$(flux)2 = (c2\ D/pi) * (1/t)$$
$$slope$$

$$c = 1.13E-04\ mol/cc$$

$$D = (pi)(slope)/(c2) = 4.00E-06\ cm2/min$$
$$D = 6.66E-12\ m2/sec$$

VOCCELL019

HEPTANE IN S8000 AT 40 DEG C

TIME (min)	HEIGHT (mm)	AT	ADJ HT(mm)	MASS RATE (ug/min)	FLUX (mol/min/cm2)	1/TIME (min-1)	(FLUX)2
3	103	2	155	2.3	9.02E-08	3.3E-01	8.14E-15
4	93.5	2	136	2.1	7.92E-08	2.5E-01	6.26E-15
5	86	2	121	1.8	7.04E-08	2.0E-01	4.96E-15
6	80	2	109	1.6	6.34E-08	1.7E-01	4.02E-15
7	76	2	101	1.5	5.88E-08	1.4E-01	3.46E-15
8	72	2	93	1.4	5.41E-08	1.2E-01	2.93E-15
9	138	1	87	1.3	5.06E-08	1.1E-01	2.56E-15
10	133.5	1	82.5	1.2	4.80E-08	1.0E-01	2.31E-15
11	129	1	78	1.2	4.54E-08	9.1E-02	2.06E-15
12	124.5	1	73.5	1.1	4.28E-08	8.3E-02	1.83E-15
13	122	1	71	1.1	4.13E-08	7.7E-02	1.71E-15
14	118.5	1	67.5	1.0	3.93E-08	7.1E-02	1.54E-15
15	116	1	65	1.0	3.78E-08	6.7E-02	1.43E-15
16	113.5	1	62.5	0.9	3.64E-08	6.2E-02	1.32E-15
17	111	1	60	0.9	3.49E-08	5.9E-02	1.22E-15
18	108.5	1	57.5	0.9	3.35E-08	5.6E-02	1.12E-15
19	106.5	1	55.5	0.8	3.23E-08	5.3E-02	1.04E-15
20	105.5	1	54.5	0.8	3.17E-08	5.0E-02	1.01E-15
22	101.5	1	50.5	0.8	2.94E-08	4.5E-02	8.64E-16
24	98.5	1	47.5	0.7	2.76E-08	4.2E-02	7.64E-16
26	96	1	45	0.7	2.62E-08	3.8E-02	6.86E-16
28	93.5	1	42.5	0.6	2.47E-08	3.6E-02	6.12E-16
30	92	1	41	0.6	2.39E-08	3.3E-02	5.69E-16

Regression Output:
Constant	-2.88224E-16
Std Err of Y Est	5.18205E-17
R Squared	0.9993224644
No. of Observations	23
Degrees of Freedom	21

X Coefficie 2.6E-14
Std Err of 1.5E-16

$$(flux)2 = (c2\ D/pi) * (1/t)$$
$$\underset{slope}{}$$

c = 1.12E-04 mol/cc

D = (pi)(slope)/(c2) = 6.50E-06 cm2/min
D =   1.08E-11 m2/sec

VOCCELLO20

HEPTANE IN S8000 AT 60 DEG C

TIME (min)	HEIGHT (mm)	AT	ADJ HT (mm)	MASS RATE (ug/min)	FLUX (mol/min/cm2)	1/TIME (min-1)	(FLUX)2
3	122.5	4	437.5	6.1	2.34E-07	3.3E-01	5.48E-14
4	110.5	4	389.5	5.4	2.08E-07	2.5E-01	4.35E-14
5	102.5	4	357.5	5.0	1.91E-07	2.0E-01	3.66E-14
6	96.5	4	333.5	4.6	1.79E-07	1.7E-01	3.19E-14
7	92	4	315.5	4.4	1.69E-07	1.4E-01	2.85E-14
8	87.5	4	297.5	4.1	1.59E-07	1.2E-01	2.54E-14
9	84.5	4	285.5	4.0	1.53E-07	1.1E-01	2.34E-14
10	81.5	4	273.5	3.8	1.46E-07	1.0E-01	2.14E-14
11	79	4	263.5	3.7	1.41E-07	9.1E-02	1.99E-14
12	77	4	255.5	3.6	1.37E-07	8.3E-02	1.87E-14
13	148.5	2	244.5	3.4	1.31E-07	7.7E-02	1.71E-14
14	145.5	2	238.5	3.3	1.28E-07	7.1E-02	1.63E-14
15	143	2	233.5	3.2	1.25E-07	6.7E-02	1.56E-14
16	140	2	227.5	3.2	1.22E-07	6.2E-02	1.48E-14
17	137.5	2	222.5	3.1	1.19E-07	5.9E-02	1.42E-14
18	135	2	217.5	3.0	1.16E-07	5.6E-02	1.36E-14
19	133	2	213.5	3.0	1.14E-07	5.3E-02	1.31E-14
20	130.5	2	208.5	2.9	1.12E-07	5.0E-02	1.25E-14
22	127.5	2	202.5	2.8	1.08E-07	4.5E-02	1.17E-14
24	123.5	2	194.5	2.7	1.04E-07	4.2E-02	1.08E-14
26	120.5	2	188.5	2.6	1.01E-07	3.8E-02	1.02E-14
28	118	2	183.5	2.6	9.82E-08	3.6E-02	9.65E-15
30	116	2	179.5	2.5	9.61E-08	3.3E-02	9.23E-15

Regression Output:

Constant	5.14806E-15
Std Err of Y Est	8.13388E-16
R Squared	0.9953857736
No. of Observations	23
Degrees of Freedom	21

X Coefficie 1.5E-13
Std Err of 2.3E-15

$$(flux)2 = (c2\ D/pi)* (1/t)$$
$$\text{slope}$$

$$c = 1.06E-04\ mol/cc$$

$$D = (pi)(slope)/(c2) = 4.33E-05\ cm2/min$$
$$D = 7.22E-11\ m2/sec$$

VOCCELL026

HEPTANE IN S2000 AT 31 DEG C   0.015236

TIME (min)	HEIGHT (mm)	AT	ADJ HT(mm)	MASS RATE (ug/min)	FLUX (mol/min/cm2)	1/TIME (min-1)	(FLUX)2
3	79	2	151	2.1	8.14E-08	3.3E-01	6.62E-15
4	68	2	129	1.8	6.95E-08	2.5E-01	4.83E-15
5	121	1	114	1.6	6.14E-08	2.0E-01	3.77E-15
6	109	1	102	1.4	5.50E-08	1.7E-01	3.02E-15
7	100.5	1	93.5	1.3	5.04E-08	1.4E-01	2.54E-15
8	94	1	87	1.2	4.69E-08	1.2E-01	2.20E-15
9	88	1	81	1.1	4.36E-08	1.1E-01	1.90E-15
10	83.5	1	76.5	1.1	4.12E-08	1.0E-01	1.70E-15
11	79.5	1	72.5	1.0	3.91E-08	9.1E-02	1.53E-15
12	76	1	69	1.0	3.72E-08	8.3E-02	1.38E-15
13	73	1	66	0.9	3.56E-08	7.7E-02	1.26E-15
14	70	1	63	0.9	3.39E-08	7.1E-02	1.15E-15
15	68	1	61	0.9	3.29E-08	6.7E-02	1.08E-15
16	66	1	59	0.8	3.18E-08	6.2E-02	1.01E-15
17	63.5	1	56.5	0.8	3.04E-08	5.9E-02	9.27E-16
18	62	1	55	0.8	2.96E-08	5.6E-02	8.78E-16
19	60.5	1	53.5	0.7	2.88E-08	5.3E-02	8.31E-16
20	58	1	51	0.7	2.75E-08	5.0E-02	7.55E-16
22	56	1	49	0.7	2.64E-08	4.5E-02	6.97E-16

```
         Regression Output:
Constant              -3.04869E-16
Std Err of Y Est       5.41743E-17
R Squared             0.9988836082
No. of Observations             19
Degrees of Freedom              17

X Coefficie 2.0E-14
Std Err of  1.7E-16
```

$$(flux)2 = (c2 \ D/pi)* \ (1/t)$$
$$slope$$

$$c = 1.15E-04 \ mol/cc$$

$$D = (pi)(slope)/(c2) = 4.89E-06 \ cm2/min$$
$$D = 8.16E-12 \ m2/sec$$

VOCCELL028

HEPTANE IN S2000 AT 40 DEG C

TIME (min)	HEIGHT (mm)	AT	ADJ HT(mm)	MASS RATE (ug/min)	FLUX (mol/min/cm2)	1/TIME (min-1)	(FLUX)2
3	67	4	247.5	4.0	1.54E-07	3.3E-01	2.38E-14
4	117	2	213.5	3.5	1.33E-07	2.5E-01	1.77E-14
5	104	2	187.5	3.0	1.17E-07	2.0E-01	1.36E-14
6	95.5	2	170.5	2.8	1.06E-07	1.7E-01	1.13E-14
7	89.5	2	158.5	2.6	9.87E-08	1.4E-01	9.74E-15
8	83.5	2	146.5	2.4	9.12E-08	1.2E-01	8.32E-15
9	79.5	2	138.5	2.2	8.62E-08	1.1E-01	7.44E-15
10	76	2	131.5	2.1	8.19E-08	1.0E-01	6.70E-15
11	73	2	125.5	2.0	7.81E-08	9.1E-02	6.11E-15
12	70.5	2	120.5	2.0	7.50E-08	8.3E-02	5.63E-15
13	68.5	2	116.5	1.9	7.25E-08	7.7E-02	5.26E-15
14	66.5	2	112.5	1.8	7.01E-08	7.1E-02	4.91E-15
15	132	1	111.5	1.8	6.94E-08	6.7E-02	4.82E-15
16	129	1	108.5	1.8	6.76E-08	6.2E-02	4.56E-15
17	128	1	107.5	1.7	6.69E-08	5.9E-02	4.48E-15
18	127	1	106.5	1.7	6.63E-08	5.6E-02	4.40E-15
19	125	1	104.5	1.7	6.51E-08	5.3E-02	4.23E-15
20	125.5	1	105	1.7	6.54E-08	5.0E-02	4.27E-15

Regression Output:
Constant	1.06228E-16
Std Err of Y Est	3.85009E-16
R Squared	0.9951622011
No. of Observations	18
Degrees of Freedom	16

X Coefficie 6.9E-14
Std Err of 1.2E-15

$$(flux)2 = (c2\ D/pi) * (1/t)$$
$$\qquad\qquad slope$$

$$c = 1.06E-04\ mol/cc$$

$$D = (pi)(slope)/(c2) = 1.94E-05\ cm2/min$$
$$D = 3.23E-11\ m2/sec$$

TABLE A6

VOCCELL029

HEPTANE IN S2000 AT 60 DEG C

TIME (min)	HEIGHT (mm)	AT	ADJ HT(mm)	MASS RATE (ug/min)	FLUX (mol/min/cm2)	1/TIME (min-1)	(FLUX)2
5	83	4	261	4.0	1.54E-07	2.0E-01	2.36E-14
6	78	4	241	3.7	1.42E-07	1.7E-01	2.02E-14
7	74	4	225	3.4	1.33E-07	1.4E-01	1.76E-14
8	70	4	209	3.2	1.23E-07	1.2E-01	1.52E-14
9	136	2	201	3.1	1.18E-07	1.1E-01	1.40E-14
10	131.5	2	192	2.9	1.13E-07	1.0E-01	1.28E-14
11	126.5	2	182	2.8	1.07E-07	9.1E-02	1.15E-14
12	123	2	175	2.7	1.03E-07	8.3E-02	1.06E-14
13	120	2	169	2.6	9.95E-08	7.7E-02	9.91E-15
14	117.5	2	164	2.5	9.66E-08	7.1E-02	9.33E-15

```
            Regression Output:
Constant              1.36953E-15
Std Err of Y Est      1.65785E-16
R Squared             0.9989016602
No. of Observations          10
Degrees of Freedom            8

X Coefficie 1.1E-13
Std Err of  1.3E-15
```

$$(flux)2 = (c2\ D/pi) * (1/t)$$
$$\text{slope}$$

$$c = 1.04E-04\ mol/cc$$

$$D = (pi)(slope)/(c2) = 3.24E-05\ cm2/min$$
$$D = 5.40E-11\ m2/sec$$

ADDENDUM D

Volume II

VAPOR-LIQUID EQUILIBRIUM OF PURE COMPONENTS
IN CRUDE OIL

Gloria Lindner

TABLE OF CONTENTS

FIGURES

TABLES

ADDENDUM D

VAPOR-LIQUID EQUILIBRIUM OF PURE COMPONENTS IN CRUDE OIL

INTRODUCTION

The mass transfer model for a given binary pair of solvent and solute defined an interfacial condition at which there was continuity of flux. Because this boundary condition also required that the flux from the bulk oil to the interface be equal to the flux from the interface to the bulk air, it became necessary to express the interfacial gas phase concentration in terms of the interfacial liquid phase concentration. This was done by first assuming equilibrium at the interface, and then proposing a relationship to characterize this equilibrium.

It was proposed that a satisfactory analysis could be obtained by treating the residual fraction of the crude oil as a single high molecular weight compound, so that the crude oil could be represented as a multicomponent mixture of binary pairs, and the total mass transfer as the sum of evaporation of the binary pairs. Total vapor pressure would then be the sum of the vapor pressure of each binary pair. This approximation reduces the fundamental thermodynamic problem to one of a binary system of non-reacting chemical species, the mathematical solution to which is given by Smith and Van Ness (1975) and by Prausnitz (1969).

If a solute is present in vapor and liquid phases at equilibrium, and at constant temperature and pressure, then the fugacity of the solute must be the same in both phases. This equilibrium criterion is given by:

$$f_i^{liq} = f_i^{vap} \tag{1}$$

The fugacity of the solute (i) in the vapor mixture is

$$f_i^{vap} = \phi_i y_i P \tag{2}$$

where y_i is the mole fraction of solute in the vapor phase, ϕ_i is the fugacity coefficient, and P is the total pressure. In the liquid phase, the fugacity is given by

$$f_i^{liq} = \gamma_i x_i f_i^0 \tag{3}$$

where x_i is the mole fraction in the liquid phase, f_i^0 is the reference fugacity, and γ_i is the activity coefficient which characterizes the degree of non-ideality between the solute and the residual fraction of the oil. Substitution of Equation (3) into Equation (1) yields:

$$y_i \phi_i P = x_i \gamma_i f_i^0 \tag{4}$$

However, this general solution to the fundamental problem of vapor-liquid equilibrium is of limited use since there is no equation of state which adequately describes liquid-phase behaviour. These equations are reduced to tractable forms by making appropriate simplifying assumptions.

At pressures of 1 atmosphere and less, the assumption that the vapor phase is an ideal gas introduces little error. Therefore ϕ_i can be assumed very close to unity and the fugacity is then equal to the partial pressure of the solute. The term f_i^0 represents the fugacity exerted by the solute (i) in a standard state at the same temperature and pressure as that of the mixture. If the pure solute is a liquid at the system temperature and pressure, the saturation vapor pressure P_i^{sat} can be substituted for f_i^0 , and the vapor-liquid equilibrium equation is simplified to:

$$y_i P = x_i \gamma_i P_i^{sat} \quad . \tag{5}$$

If the critical region is not approached, it can be assumed that γ_i and P_i^{sat} are independent of pressure. So γ_i becomes a function of temperature and liquid phase composition, while P_i^{sat} is a function of temperature only.

Ordinarily, experimental vapor-liquid equilibrium data or mutual solubility data are used to calculate the activity coefficient of a solute in a solvent. When these are not available, γ_i is predicted by equations like those of Van Laar or Wilson (Prausnitz, 1969; Smith and Van Ness, 1975).

We require some knowledge of the functional dependence of γ_i on the temperature and composition of the liquid mixture for a rigorous thermodynamic analysis of the problem. Since this information was not be available, the analysis must be kept simple. The activity can be combined with P_i^{sat} in a single term which is a form of Henry's constant.

$$y_i P / x_i = H_M = \gamma_i P_i^{sat} \tag{6}$$

where H_M , the Henry's constant states a direct proportionality between the solubility of the volatile component (x_i) in the liquid phase and the pressure at constant temperature.

Equation (5) can also be written as

$$y_i / x_i = K_i = \gamma_i P_i^{sat} / P \tag{7}$$

where K_i is a distribution coefficient which gives the equilibrium ratio of species (i) between the vapor and liquid phases. K_i is a complex function of temperature, pressure and vapor composition, and differs from H_M in being

dimensionless where H_M has units of pressure. Combination of equations (6) and (7) yields:

$$K_i = H_M/P \qquad (8)$$

which allows calculation of the distribution coefficient from Henry's constant. The model required that the air-liquid partitioning of solute be expressed as a dimensionless ratio of concentration rather than mole fractions. If C_L and C_G are the total molar concentrations of the liquid and gas phases respectively, Equation (7) can be written as

$$c_i^G / c_i^L = K_i C_G/C_L \qquad (9)$$

where c_i^G and c_i^L are the concentrations of solute (i) in the gas phase and liquid phase, respectively. The term on the right hand side of Equation (9) is defined as $\tilde{H}$ in the second boundary condition at the air-oil interface (Addendum B).

The object of this part of the project is to obtain enough experimental information to derive a useful empirical relation for the distribution of any volatile component between the vapor and liquid phase. The approach is to batch distill the crude oil at 220°C to drive off all of the volatile organic carbon compounds which would be active under ambient conditions. Speciation of this volatile portion was completed in the first part of the project. Varying amounts of a pure component can then be added back to this residue and the vapor pressure measured in the apparatus described in the next section.

Because of the difficulties in directly determining true vapor pressures, the Reid vapor pressure (RVP) is most often used to express the vapor pressure of petroleum mixtures. The RVP is the absolute pressure in pounds per square

inch determined at 100°F and V/L (ratio of vapor volume to liquid volume, as defined in ASTM Designation: D323-72), using the apparatus and procedures by the American Society for Testing Materials. Thus the RVP differs from the true vapor pressure because of the presence of water vapor and air in the confined space. Correlations to relate true vapor pressure to Reid vapor pressure (API nomographs) have not been successful.

When Bryan (1981) reviewed potential methods to determine volatilities of heavy crude oils, there was no support for direct measurement of true vapor pressure. The method required use of an air-free sample and a V/L ratio approaching zero. There was no established method, the cost of developing one would be too high, and there was concern that laboratory costs might be too high depending on the care needed to obtain accurate and reproducible results.

Bryan recommended further studies on the vapor composition method. This method involves analysis of the headspace vapor in equilibrium with a liquid crude oil sample. The vapor pressure is assumed to be a product of the mole fraction of hydrocarbon vapor in the headspace times the absolute pressure. However this method like the RVP also measures the contribution of air and water in the headspace. The utility of this approach has yet to be demonstrated.

The method used in this study is an isoteniscopic technique in which air and water have been eliminated and is applicable down to approximately 1 mm Hg (0.04 in. Hg).

EXPERIMENTAL

Apparatus

Vapor pressure was measured by a static method in the apparatus shown in Figure 1. This is a minor modification of the system described by Hermsen (1962).

An isoteniscope assembly consisting of a glass vapor pressure cell and a null manometer was immersed in a glass thermostat vessel. The temperature bath was a 35 cm (13.75 in.) diameter x 42 cm (16.5 in.) high glass battery jar which could be raised and lowered when necessary. An immersion heater was suspended in the bath which was vigorously stirred to eliminate any temperature gradients. The heater was operated from a Yellow Springs Instrument Co. Inc. (YSI) proportional controller, Model 72, and the temperature was sensed by a YSI Model 403 thermistor probe.

Manometers

The null manometer consisted of two identical glass legs 8-mm (0.31 in.) in diameter each with a 25 cc (1.53 in.^{3}) surge bulb and joined at the bottom by a 2-mm (0.08 in.) capillary. The manometer was filled approximately half full with mercury and could support a pressure difference of approximately 20 cm (7.9 in.) Hg. The surge bulbs and capillary section were designed to prevent the mercury from being forced rapidly into either the vapor pressure cell or up the barometer leg should the manometer inadvertently be subjected to a pressure difference greater than 20 cm (7.9 in.) of Hg. The second leg of the null manometer was connected to the measuring leg of the mercury barometer through a high-vacuum teflon valve and a 3-litre (0.79 gal) surge bottle.
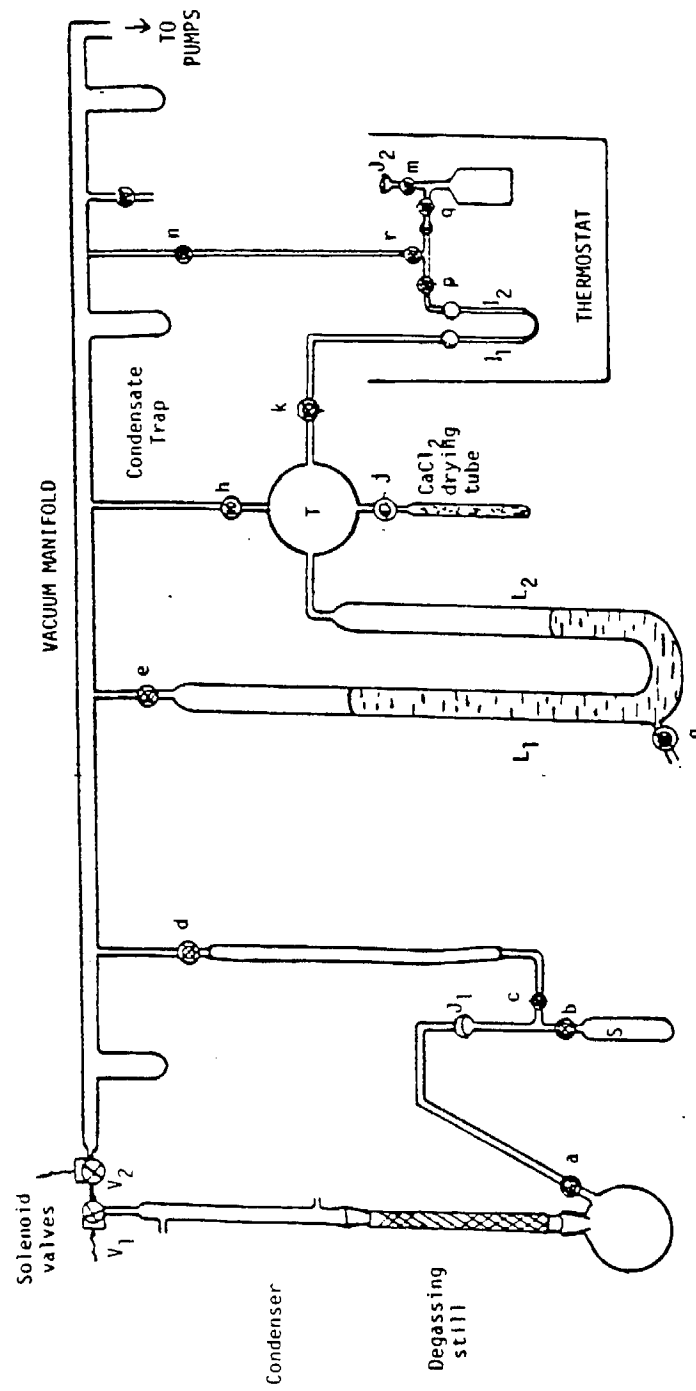
FIGURE 1. DIAGRAM OF APPARATUS

The most widely used manometer for the measurement of moderately low pressure is a U-shaped glass tube with one end sealed and filled with mercury. An extremely high vacuum above the mercury in the closed reference limb is essential for precise measurement of absolute pressure. In this study, the reference limb L_1 , instead of being sealed at the top, is connected directly to the vacuum manifold. The indicating limb, L_2 , is connected to the vacuum line and the isoteniscope assembly. L_1 was 107 cm (42 in.) long while L_2 was 79 cm (31 in.). Each limb had a diameter of 1.9 cm (0.75 in). This relatively wide diameter reduces considerably the errors caused by surface tension.

Vapor Pressure Cell

Because the residual fractions of the crude oils are so viscous, they cannot be introduced into the cell or removed by distillation after measurements. Therefore, a vapor pressure cell had to be designed which would allow transfer of material into the cell simply by pouring it in. The vapor pressure cell is shown in Figure 2. It is a flat-bottomed tube of glass 40 mm (1.51 in.) in diameter and 80 mm (3.15 in.) long. A tapered section at the top is closed by an O-ring joint which is connected to the loading vessel (S) and null manometer through a side arm and ball and socket joints. High vacuum valves, (q) and (m), allow isolation of the vapor pressure cell from the null manometer and loading vessel, respectively. Since the cell had to be detached after each series of measurements, this increased the amount of degassing necessary with each measurement.

FIGURE 2

VAPOR PRESSURE CELL
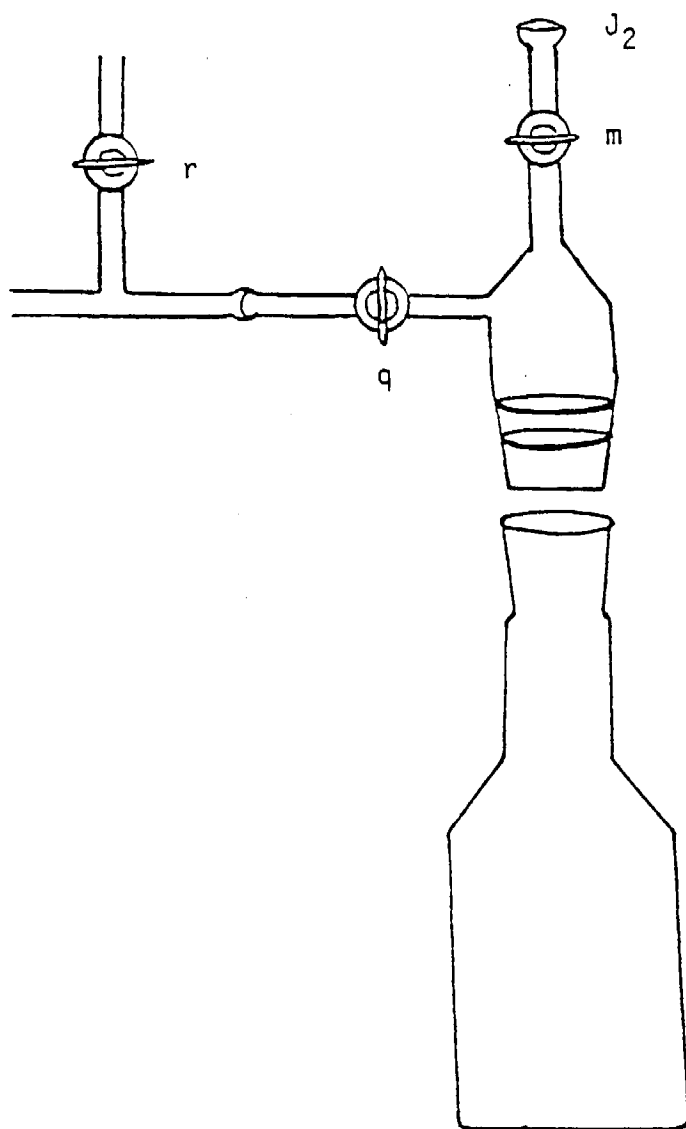
Degassing

After the apparatus was assembled, it was evacuated. The mechanical pump was used directly, without the diffusion pump, to evacuate it sufficiently to test for leaks with a Tesla coil. After leaks were located and repaired and the apparatus retested, the diffusion pump was started. The apparatus was then heated until a constant pressure of 6×10^{-4} mm (2.36×10^{-5} in.) Hg was obtained, whereupon the manometer was filled with mercury which was then degassed.

Filling and Degassing of the Mercury Manometer

Redistilled mercury was drawn into the U-tube through valve (g) by opening valves (e), (f), and (h) and carefully applying vacuum from the manifold to legs L_1 and L_2 until they were about half full. Valve (g) was then closed and the U-tube heated to free it from moisture and air. This refluxing of the mercury inside the tubes was continued for about 3 hours, by the end of which time, the total vapor pressure of contaminants in the system was 5×10^{-4} mm (1.97×10^{-3} in.) Hg when measured by an ionization gauge. Degassing was considered complete when this pressure held for approximately the last hour of the degassing period. The system was then allowed to cool to room temperature while maintaining the high vacuum.

Degassing of the Isoteniscope

The isoteniscope was degassed for several days by evacuating through both valves (p) and (r). All portions of the isoteniscope were gently heated with an air gun to drive off gases adsorbed on the walls or dissolved in the mercury of the isoteniscope. Leak rates were measured to check the progress of the

degassing and to test for leaks in the assembly. This was done by closing valve (p) and recording the levels of the mercury in legs l_1 and l_2 of the null manometer as a function of time. A maximum tolerable leak rate was then established using the same method described by Hermsen (1962). First, an accuracy limit on the pressure measurements was set at + 0.05 mm (0.002 in.) Hg. If a complete series of runs takes as long as 1 day, then a leak rate of less than 0.05 mm/day is the maximum tolerable. Once all the leaks in the assembly had been stopped, leak rates of less than 0.05 mm (0.002 in.)/day were easily attained, and no run was expected to take longer than 1 day to carry out.

After a good vacuum has been obtained, the apparatus could be closed to the pumps and the vacuum maintained for several days. However, since days of degassing are necessary even after a few minutes of exposure to air, the apparatus was opened only when necessary for repairs.

Degassing of Materials

Pure materials were degassed in the degassing still shown in Figure 1. The boiler was a 700-cc (0.025 ft^{-3}) pyrex flask which was connected by a ground glass joint to the column (C), and by a high vacuum teflon valve to the vacuum manifold. The pyrex glass column was 30 mm (1.18 in.) in diameter, and 40 cm (15.75 in.) long, and contained a section packed with 4-mm glass beads approximately 25 cm (9.84 in.) deep. A water-jacketed condenser was connected to the column by a ground glass joint and by a Teflon, Swagelok to two solenoid valves in series. The solenoid valves were Skinner Type V5 explosion-proof valves. V1 is normally closed and V2 is normally open. The valves were controlled by a programmed time switch so that regular periodic samples of the vapor above the

condenser could be removed. The volume of this sample was the same as the 10-cc (0.61 in.^{3}) volume within the pipe between V1 and V2.

The progress of the degassing was checked by transferring some of the material to the loading vessel (S) and freezing it slowly. Degassing is considered complete when no bubbles of gas can be expelled from the liquid by freezing. The efficiency of degassing was checked by comparing the vapor pressure of the material with that reported in the literature.

Because the residual fraction cannot be distilled it was degassed in the vapor pressure cell.

Transfer of Degassed Material to Vapor Pressure Cell

The loading vessel (S) was attached to the still at joint J_1, and with valve (a) closed, it was evacuated through valves (b) and (c) and the rubber tubing leading to the vacuum manifold. The loading vessel and glass tubing were heated to drive off adsorbed gases, and to prevent condensation of hydrocarbon vapors in the glass tubing during the following steps.

Valve (c) was closed, the loading vessel was immersed in a Dewar flask containing liquid nitrogen, and valve (a) was opened. This resulted in a vapor phase transfer of degassed material from the boiler to the loading vessel where it is frozen. After the desired amount of material had been transferred, valve (a) was closed, and the manifold and space above the frozen hydrocarbon were again evacuated through valve (c). Valves (b) and (c) were then closed and joint J_1 was disconnected. The material was allowed to melt, and the loading apparatus inverted and connected to the vapor pressure cell at J_2. Valves (q) and (m) were closed since the vapor pressure cell and its contents had already been evacuated. Valve (c) was opened long enough to evacuate the space between

valve (b) and (m) after which (c) was closed, and (b) and (m) were opened. If the material did not flow readily into the cell it was heated in order to create sufficient head. Valve (m) was closed after the cell was loaded.

The vapor pressure cell was weighed, and then connected to the isoteniscope assembly. With valves (p) and (q) closed, valve (r) was opened long enough to evacuate the space between valves (p) and (q). Valve (r) was then closed, so that measurements could be made.

Measurement of Vapor Pressure

After the cell was loaded, the thermostat bath was raised into place and set to the desired temperature, if this had not already been done. At a given temperature, the external pressure is adjusted so that both arms of the null manometer are at the same height. This was done by opening valve (k) and evacuating through (h) or by admitting dried air through valve (j). This balancing was also done during loading, and while changing the bath temperature so that no vapor escaped from the cell, C, and no air entered the cell through the manometer. After about 2 hours the mercury levels in l_1 and l_2 became steady, and the external pressure, which is equal to the pressure of the vapor in the isoteniscope was measured with the mercury manometer.

The heights of the mercury in L_1, L_2, l_1, and l_2 were then read with a Gaertner M-911 cathetometer. The readings were then converted to pressure in mm Hg at 0°C according to the method of Brombacher et al (1960). There was no correction to standard gravity. An example of the calculation for a typical run is given in the appendix.

RESULTS AND DISCUSSION

The performance of the apparatus and the experimental technique were checked by measuring the vapor pressure of methylcyclopentane, methylcyclohexane and heptane at 4 temperatures. The measured values are compared in Table 1 to those predicted by the Antoine equation using the constants reported in the API Research Project 44. The observed values are believed to lie within the limits of experimental measurement if the difference between observed and literature values is within 10 %. Although the results for methylcyclohexane did not satisfy this criterion, the results in general demonstrate that one can measure vapor pressure with this apparatus with a satisfactory degree of accuracy.

The plots of ln (P) versus 1/T for each of the 3 compounds tested are shown in Table 2 and Figure 3. They indicate that the results did not deviate significantly from the linear relationship predicted by the Clausius-Clapeyron equation.

The results of one run with the 31X residual fraction are also shown in Table 2 and Figure 4. These values are higher than expected, and may have been due to incomplete degassing of the sample. There was so much foaming during the freeze-thaw-evacuate cycles that it was not possible to determine by inspection when degassing was complete. The deviation of the semi-log plot (Figure 3) from linearity, and the linear nature of the plot of P versus T (Figure 4) suggest that the vapor pressure might have been due in large part to the presence of incompressible gases dissolved in the residue. An experiment has been planned to measure the vapor pressure after each cycle to determine how many are necessary before the sample is completely degassed. The vapor pressure is expected to decrease after each cycle until it reaches a constant value once all dissolved gases are expelled. The inclusion of an immersible magnetic stirrer in

TABLE 1

COMPARISON OF PREDICTED AND MEASURED VAPOR PRESSURES
Three Test Compounds

	t (deg C)	P (mm Hg)		
		Calculated	Experimental	% error
Methylcyclopentane	30.0	170.04	170.38	.20
	45.2	309.12	303.79	-1.72
	60.1	522.19	512.93	-1.77
	69.9	716.29	710.33	-.83
Methylcyclohexane	30.0	58.69	66.88	13.95
	40.0	91.61	109.47	19.50
	50.0	138.36	139.13	.56
	60.0	202.95	200.73	-1.09
Heptane	30.1	58.80	62.36	-6.05
	45.2	116.11	115.26	.74
	60.1	211.30	204.63	3.15

TABLE 2

VAPOR PRESSURE OF 3 TEST COMPOUNDS
AND RESIDUAL FRACTION OF 31X CRUDE OIL

	ln (P)	1/T (deg K)
Methylcyclopentane	5.14	.0032988
	5.72	.0031413
	6.24	.0030008
	6.57	.0029151
Methylcyclohexane	4.20	.0032987
	4.70	.0031934
	4.94	.0030945
	5.30	.0030017
Heptane	4.13	.0032977
	4.75	.0031413
	5.32	.0030008
Residual fraction	2.27	.0032987
	3.26	.0031422
	3.71	.0029999
	3.93	.0029142

FIGURE 3

TEMPERATURE DEPENDENCE OF VAPOR PRESSURE
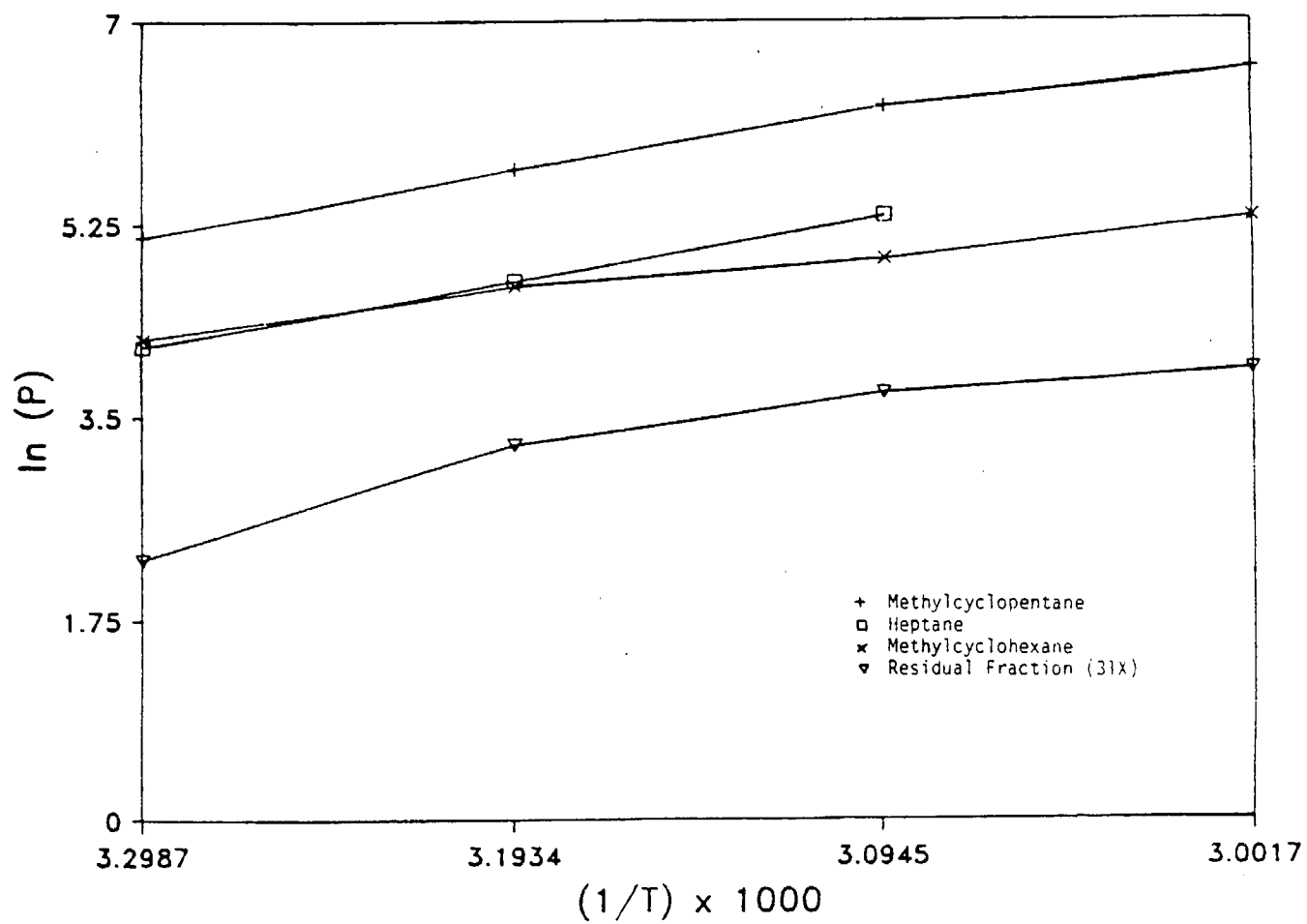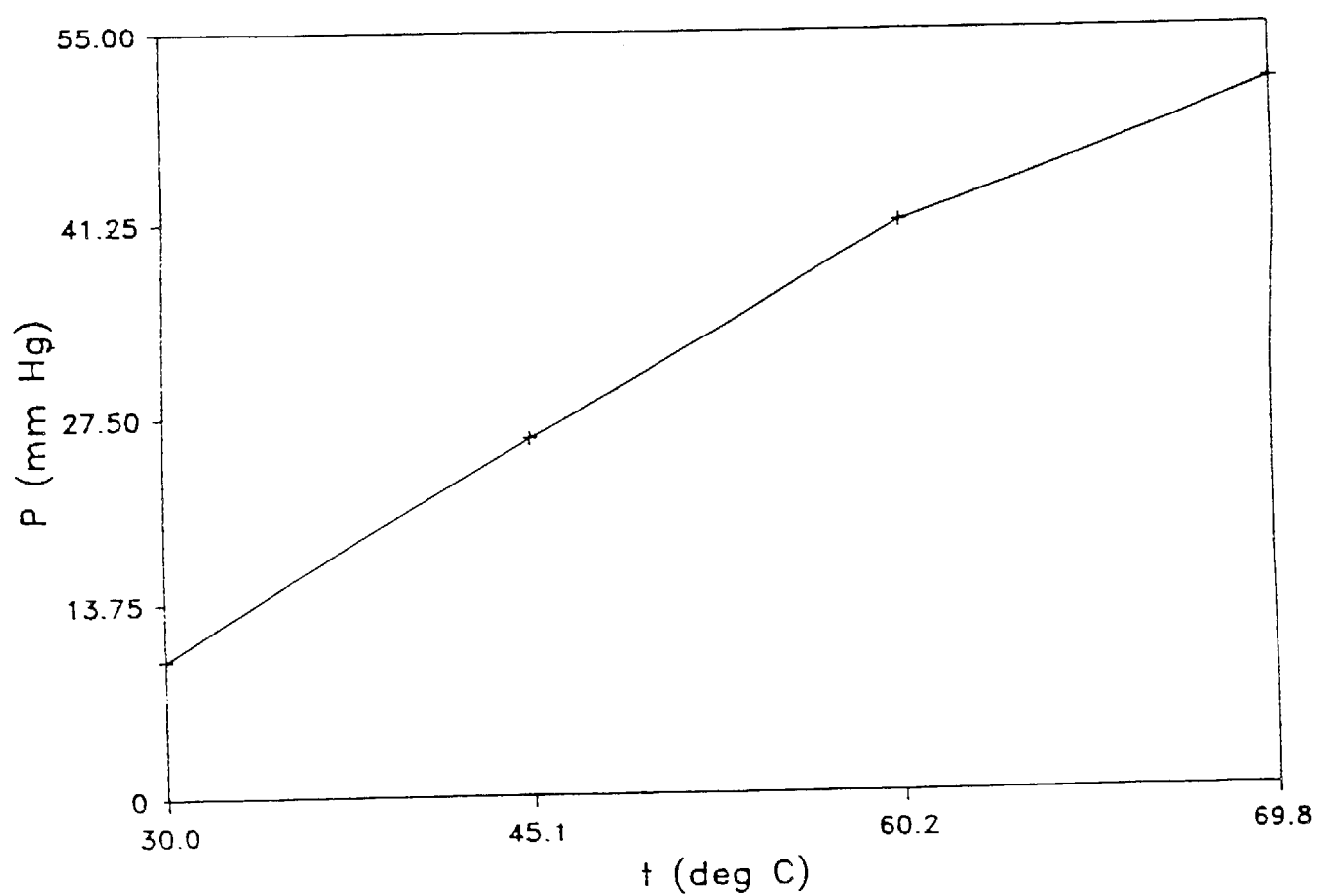Three Test Compounds and 31X Residual Fraction

FIGURE 4

TEMPERATURE DEPENDENCE OF VAPOR PRESSURE
Residual Fraction of 31X Crude Oil

the thermostat will allow agitation of the sample during the period it takes to reach equilibrium at each temperature. It is expected this will reduce the foaming and facilitate the degassing of the residuum.

CONCLUSIONS

The isoteniscope equipment and method has been calibrated by measuring vapor pressure of pure hydrocarbons. The results are generally satisfactory, and suggest that the method is adequate for measuring the vapor pressure of a binary mixture of non-volatile oil residue and a pure volatile hydrocarbon. If the non-volatile component makes a negligible contribution to the total vapor pressure, then a good approximation of the distribution of the volatile component between vapor and liquid phases can be obtained from vapor pressure and liquid composition data only, and the vapor phase composition need not be determined.

NOMENCLATURE

C   molar concentration (gmole/cm^3)

C_L total molar concentration of the liquid phase

C_G total molar concentration of the gas phase

c_i^G molar concentration of solute (i) in the gas phase

c_i^L molar concentration of solute (i) in the liquid phase

f_i fugacity of solute (i) (mm Hg)

f_i^o reference fugacity of solute i

f_i^{liq} fugacity of solute (i) in the liquid phase

f_i^{vap} fugacity of solute (i) in the vapor phase

H_M Henry's Law constant

K_i Distribution coefficient of solute (i) (- yi/xi) (dimensionless)

P   pressure (mm Hg or in Hg)

P_i partial pressure of solute (i)

P_i^{sat} saturation vapor pressure of solute (i) at the system temperature and pressure

x_i mole fraction of solute (i) in the liquid phase

y_i mole fraction of solute (i) in the vapor phase

Greek

γ_i activity coefficient of solute i

ϕ_i fugacity coefficient of solute i

REFERENCES

1. Bryan, R.J. (1981). "Analysis of potential methods to determine volatilities of heavy crude oils," for USEPA contract No. 68-02-3509 by Engineering-Science Inc.

2. Hermsen, R.W. (1962). "Thermodynamic studies in solutions of polysegmented hydrocarbons." PhD dissertation in Chemical engineering, University of California, Berkeley.

3. Mackay, D., and Shiu, W.Y. (1981). "Critical review of Henry's Law constants for chemicals of environmental interest." J. Phys. Chem. Ref. Data. 10 (4):1175-1199.

4. Prausnitz, J.M. (1969). Molecular thermodynamics of fluid-phase equilibria. Prentice-Hall Inc., N.J.

5. Smith, J.M., and Van Ness, H.C. (1975). Introduction to chemical engineering thermodynamics. 3rd edition. McGraw-Hill Inc., N.Y.

APPENDIX

Sample Calculations for a Typical Run

ADDENDUM D

Volume II

SAMPLE CALCULATIONS FOR A TYPICAL RUN

HEPTANE

Bath T = 60.1°C

Room T = 26.0°C

l_1 = 797.60 mm L_1 = 799.55 mm

l_2 = 798.90 mm L_2 = 592.65 mm

Uncorrected pressure = $(L_1 - L_2) - (l_2 - l_1)$

= 799.55 - 592.65 + 797.60 - 798.90

= 205.60 mm

Correction for Hg density

^{7598}σρ at 0.0°C = 13.5951 g/cc

ρ at 26.0°C = 13.5311 g/cc

Correction is: $\dfrac{-(205.60)(13.5951 - 13.5311)}{13.5951}$ = -0.97 mm

Corrected pressure is then:

205.6 - 0.97 = 204.63 mm Hg

TABLE A1

DATA FOR CALCULATION OF VAPOR PRESSURE
OF METHYLCYCLOPENTANE

Bath T =	30.00 deg C		45.20 deg C		60.10 deg C		69.90 deg C
L1 =	365.8 mm Hg	L1 =	858.05 mm Hg	L1 =	962.50 mm Hg	L1 =	720.00 mm Hg
L2 =	190 mm Hg	L2 =	552.45 mm Hg	L2 =	446.20 mm Hg	L2 =	.00 mm Hg
l1 =	776.45 mm Hg	l1 =	777.25 mm Hg	l1 =	777.45 mm Hg	l1 =	775.75 mm Hg
l2 =	781.05 mm Hg	l2 =	777.6 mm Hg	l2 =	778.35 mm Hg	l2 =	782.00 mm Hg

Uncorrected P = (L1 - L2)-(l2 - l1)

	171.2 mm Hg		305.25 mm Hg		515.4 mm Hg		713.75 mm Hg

Correction for Hg density:
Room T = 26.50 deg C
$V = V_o (1+0.0001818*T)$
$V_o = 1/rho (o)$
rho (T) = 1/V
rho (o) = 13.5951 g/cc
V = .0739103
rho = 13.52992
correction = -(13.5951-rho)/13.5951*P

	-.820836 mm Hg	-1.46355 mm Hg	-2.47114 mm Hg	-3.42215

corrected P = correction + uncorrected P

	170.3792 mm Hg	303.7864 mm Hg	512.9289 mm Hg	710.3279 mm Hg

Predicted Vapor pressure

Antoine constants

A =	6.86283			
B =	1186.059			
C =	226.042			
T =	303.14 deg K	318.34 deg K	333.24 deg K	343.04 deg K
	30.00 deg C	45.2 deg C	60.1 deg C	69.9 deg K
log(P) =	2.230547	2.490133	2.717829	2.855089
P(cal) =	170.0384 mm Hg	309.1244 mm Hg	522.1900 mm Hg	716.2896 mm Hg
P(expt) =	170.3792 mm Hg	303.7864 mm Hg	512.9289 mm Hg	710.3279 mm Hg

TEMPERATURE DEPENDENCE OF VAPOUR PRESSURE

ln (P)	1/T (deg K)
5.14	.0032988
5.72	.0031413
6.24	.0030008
6.57	.0029151

t (deg C)	P (mm Hg)		
	Calculated	Experimental	% error
30	170.04	170.38	.20
45.2	309.12	303.79	-1.73
60.1	522.19	512.93	-1.77
69.9	716.29	710.33	-.83

TABLE A2

DATA FOR CALCULATION OF VAPOR PRESSURE
OF METHYLCYCLOHEXANE

Bath T =	30.00 deg C	40.00 deg C	50.00 deg C	60.00 deg C
L1 =	355.00 mm Hg	L1 = 376.00 mm Hg	L1 = 335.20 mm Hg	L1 = 363.00 mm Hg
L2 =	289.00 mm Hg	L2 = 272.00 mm Hg	L2 = 193.50 mm Hg	L2 = 159.00 mm Hg
l1 =	784.50 mm Hg	l1 = 786.90 mm Hg	l1 = 785.10 mm Hg	l1 = 786.25 mm Hg
l2 =	783.30 mm Hg	l2 = 780.90 mm Hg	l2 = 787.00 mm Hg	l2 = 788.55 mm Hg

Uncorrected P = (L1 – L2)–(l2 – l1)

67.2 mm Hg	110 mm Hg	139.8 mm Hg	201.7 mm Hg

Correction for Hg density:
Room T =   26.50 deg C
V = Vo (1+0.0001818*T)
Vo = 1/rho (o)
rho (T) = 1/V
rho (o) = 13.5951 g/cc
V =   .0739103
rho =   13.52992
correction = -(13.5951–rho)/13.5951*P
       -.322197 mm Hg

-.322197 mm Hg	-.527406 mm Hg	-.670285 mm Hg	-.967071 mm Hg

corrected P = correction + uncorrected P

66.87780 mm Hg	109.4726 mm Hg	139.1297 mm Hg	200.7329 mm Hg

Predicted Vapor pressure

Antoine constants
A =   6.823
B =   1270.763
C =   221.416
T =   303.15 deg K

	303.15 deg K	313.15 deg K	323.15 deg K	333.15 deg K
	30.00 deg C	40 deg C	50 deg C	60 deg K
log(P) =	1.768576	1.961924	2.141025	2.307397
P(calc) =	58.69164 mm Hg	91.60605 mm Hg	138.3645 mm Hg	202.9536 mm Hg
P(expt) =	66.87780 mm Hg	109.4726 mm Hg	139.1297 mm Hg	200.7329 mm Hg

TEMPERATURE DEPENDENCE OF VAPOUR PRESSURE

ln (P)	1/T (deg K)
4.20	.0032987
4.70	.0031934
4.94	.0030945
5.30	.0030017

t (deg C)	P (mm Hg)		
	Calculated	Experimental	% error
30	58.69	66.88	13.95
40	91.61	109.47	19.50
50	138.36	139.13	.55
60	202.95	200.73	-1.09

TABLE A3

DATA FOR CALCULATION OF VAPOR PRESSURE
OF HEPTANE

Bath T =   30.10 deg C   45.20 deg C   60.10 deg C

     L1 =   726.1 mm Hg   L1 =   753.8 mm Hg   L1 =   799.55 mm Hg
     L2 =   665.3 mm Hg   L2 =   637.75 mm Hg   L2 =   592.65 mm Hg
     l1 =   798.05 mm Hg   l1 =   799.05 mm Hg   l1 =   797.60 mm Hg
     l2 =   796.2 mm Hg   l2 =   799.3 mm Hg   l2 =   798.90 mm Hg

Uncorrected P = (L1 - L2)-(l2 - l1)
                62.65 mm Hg   115.8 mm Hg   205.6 mm Hg

Correction for Hg density:
Room T =   26.00
V = Vo (1+0.0001818*T)
Vo = 1/rho (o)
rho (T) = 1/V
rho (o) = 13.5951 g/cc
V =   .0739036
rho =   13.53114
correction = -(13.5951-rho)/13.5951*P
              -.294741 mm Hg   -.544788 mm Hg   -.967258 mm Hg

corrected P = correction + uncorrected P
              62.35526 mm Hg   115.2552 mm Hg   204.6327 mm Hg

Predicted Vapor pressure

Antoine constants
    A =   15.8737
    B =   2911.32
    C =   -56.51
    T =   303.24 deg K   318.34 deg K   333.24 deg K

 ln(P) = 4.074081   4.754577   5.353265
 P(calc) = 58.79642 mm Hg   116.1145 mm Hg   211.2970 mm Hg
 P(expt) = 62.35526 mm Hg   115.2552 mm Hg   204.6327 mm Hg

TEMPERATURE DEPENDENCE OF VAPOUR PRESSURE

ln (P)	1/T (deg K)
4.132848	.0032977
4.747149	.0031413
5.321217	.0030008

t (deg C)	P (mm Hg)		
	Calculated	Experimental	% error
30.1	58.79642	62.35526	6.052815
45.2	116.1145	115.2552	-.740048
60.1	211.2970	204.6327	-3.15400

TABLE A4

DATA FOR CALCULATION OF VAPOR PRESSURE
·OF RESIDUAL FRACTION OF 31X CRUDE OIL

Bath T = 30.00 deg C	45.10 deg C	60.20 deg C	69.80 deg C
L1 = 700.25 mm L2 = 693.75 mm 11 = 798.9 mm 12 = 795.65 mm	L1 = 709.05 mm L2 = 685.5 mm 11 = 797.9 mm 12 = ·795.4 mm	L1 = 718.05 mm L2 = 675.25 mm 11 = 795.00 mm 12 = 796.60 mm	L1 = 725.25 mm L2 = 669.70 mm 11 = 795.90 mm 12 = 800.15 mm

Uncorrected P = (L1 - L2)-(12 - 11)

9.75 mm Hg	26.05 mm Hg	41.2 mm Hg	51.3 mm

Correction for Hg density:
Room T = 26.00 deg C
$V = V_o (1+0.0001818*T)$
$V_o = 1/rho (o)$
$rho (T) = 1/V$
rho (o) = 13.5951 g/cc
V = .0739036
rho = 13.53114
correction = -(13.5951-rho)/13.5951*P

-.045869 mm Hg	-.122554 mm Hg	-.193828 mm Hg	-.241344

corrected P = correction + uncorrected P

9.704131 mm Hg	25.92745 mm Hg	41.00617 mm Hg	51.05866 mm Hg

T = 303.15 deg K	319.25 deg K	333.35 deg K	342.95 deg K

ln (P) = 2.272552 P(expt) = 9.704131 mm Hg	3.255302 25.92745 mm Hg	3.713723 41.00617 mm Hg	3.932975 51.05866 mm Hg

TEMPERATURE DEPENDENCE OF VAPOUR PRESSURE

ln (P)	1/T (deg K)
2.27255	.0032987
3.25530	.0031323
3.71372	.0029999
3.93298	.0029159

t (deg C)	vapor pressure (mm Hg)
	Experimental
30	9.70413
45.1	25.92745
60.2	41.00617
69.8	51.05866

ADDENDUM E

Volume II

*MASS SPECTRA AND PHYSICAL PROPERTIES OF
IDENTIFIED COMPONENTS OF THE VOC*

ADDENDUM E

MASS SPECTRA AND PHYSICAL PROPERTIES OF IDENTIFIED COMPONENTS OF THE VOC

INTRODUCTION

As was mentioned in Section 1.0 of the text, GCMS analysis of the distillates of Monte Cristo, 31X, and 36W oil resulted in the identification of 68 components in the light fraction. A booklet of the mass spectra of each identified peak, along with physical data has been compiled. Only four of these components have been included in this addendum in deference to allowable space.

PHYSICAL PROPERTIES:

A sheet of physical properties is available for each component found in the VOC. Specifically, we have concentrated on boiling point, molecular weight, density, Antoine constants, and viscosity.

Antoine constants are the empirical constants, A , B , and C which can be substituted into the Antoine equation,

$$\ln(\text{vapor pressure}) = A - B/(T+C)$$

to calculate the vapor pressure in millimeters mercury (mm Hg) at any temperature, T (degrees Kelvin). TMIN and TMAX represent the temperature range over which the equation is valid for any particular compound (Reid, Prausnitz, and Sherwood, 1977).

The liquid viscosity can be determined using the equation

$$\log(\text{viscosity}) = (\text{VISB}) * (1/T - 1/\text{VISTO})$$

where VISB and VISTO are constants, T is the temperature in degrees Kelvin, and viscosity is given in centipoise (Reid, Prausnitz, and Sherwood, 1977).

MASS SPECTRA

For the purpose of future reference, mass spectra were collected for each component from three types of sources: already-prepared mass spectra, injection and analysis of the distillates of the oils, and injection and analysis of known components. In the first category are three sources of spectra: the National Bureau of Standards (NBS) library and two Hewlett Packard computerized libraries (NBS and PNA). The Hewlett Packard NBS library contains 30,000 compounds selected from the NBS library and the PNA library contains 71 compounds known to occur in petroleum samples. These libraries of spectra were accessed through the GCMS computer system to assist in the identification of each component, and may or may not be present for any given compound. The NBS library spectra were copied from the texts merely for the sake of completion, and should be available for each compound.

The second source of mass spectra is self-explanatory, being from the GCMS analysis of our distillates. The third source, however, contains compounds in the Hewlett Packard PONA calibration mixture and available chemicals in the lab. Mass spectrometers have idiosyncrasies. For this reason, the analysis of known compounds or known mixtures of compounds results in mass spectra closer in nature to those in a mixture of unknowns than those which are fond in the libraries.

For each component, the mass spectra have been arranged in the following order according to their source: 1) NBS library spectra; 2) Hewlett Packard NBS computerized library spectra; 3) Hewlett Packard PNA computerized library spectra; 4) 31X spectra; 7) 36W spectra; 8) pure component spectra. The mass spectra from each category has not been presented for each component, and has been included only when available.

CYCLOPENTANE

B.P. =   49.252 C

M.W. =   70.135

DENSITY (gm/ml) [1]:
          AT 0 C :   0.765
          AT 20 C :   0.7454
          AT 40 C :   0.7258
          AT 50 C :   0.716

ANTOINE CONSTANTS FOR
DETERMINING VAPOR PRESSURE [2]:
          A =   15.8574
          B =   2588.48
          C =   -41.79
       TMAX =   345 K
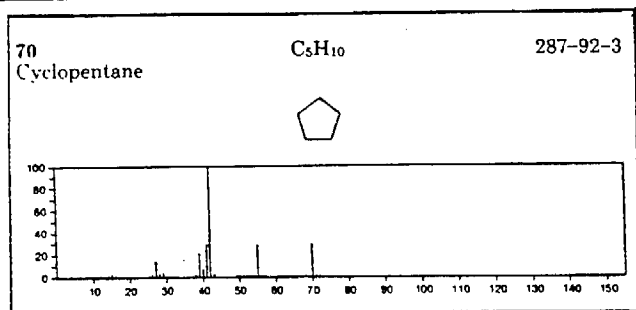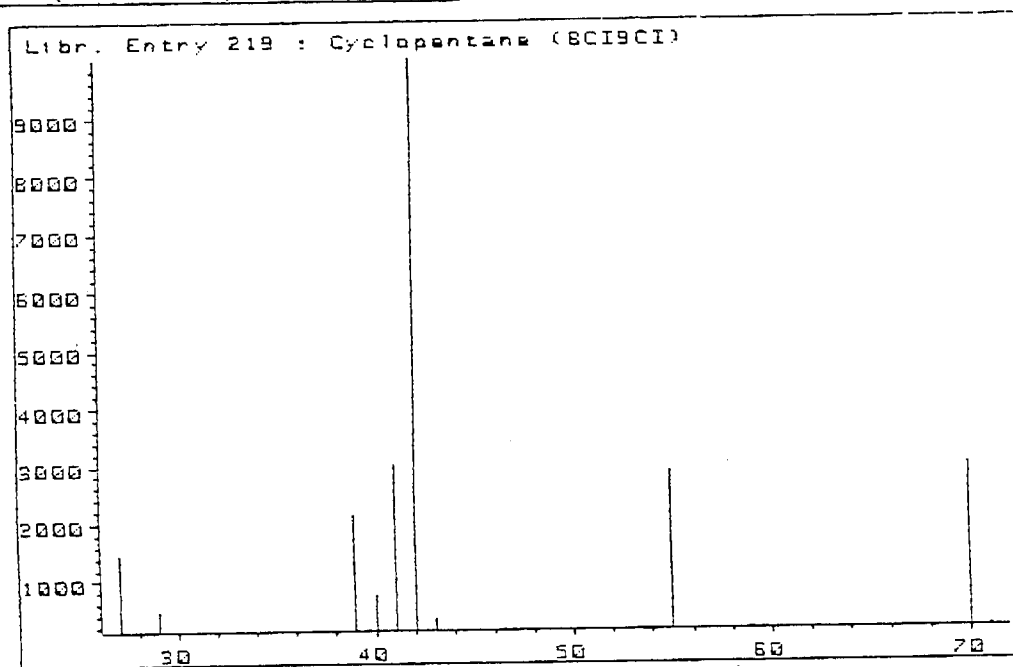   TMIN =   230 K

LIQUID VISCOSITY [3]:
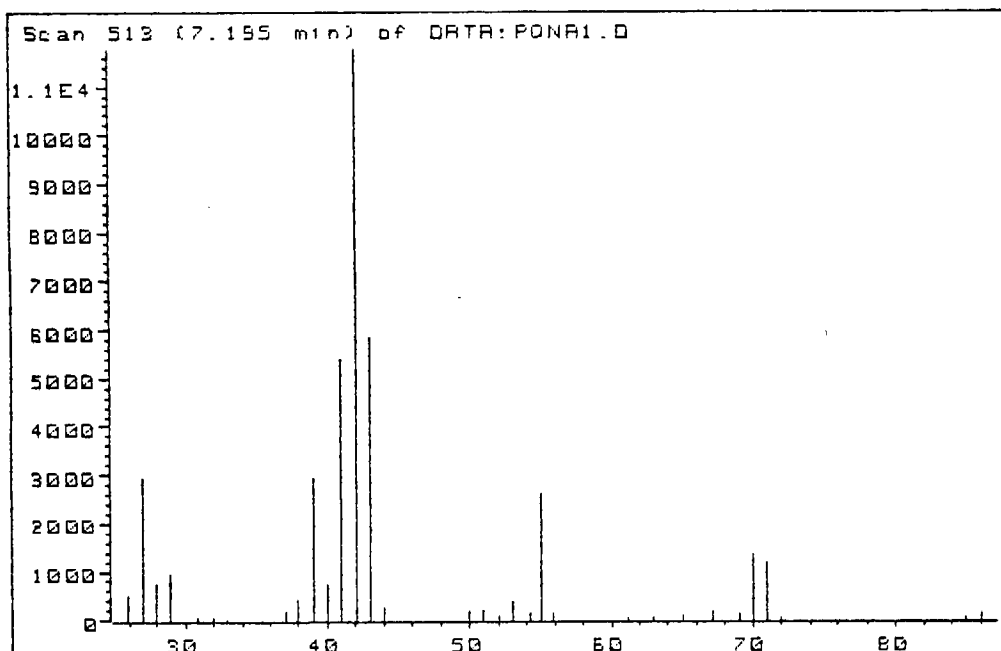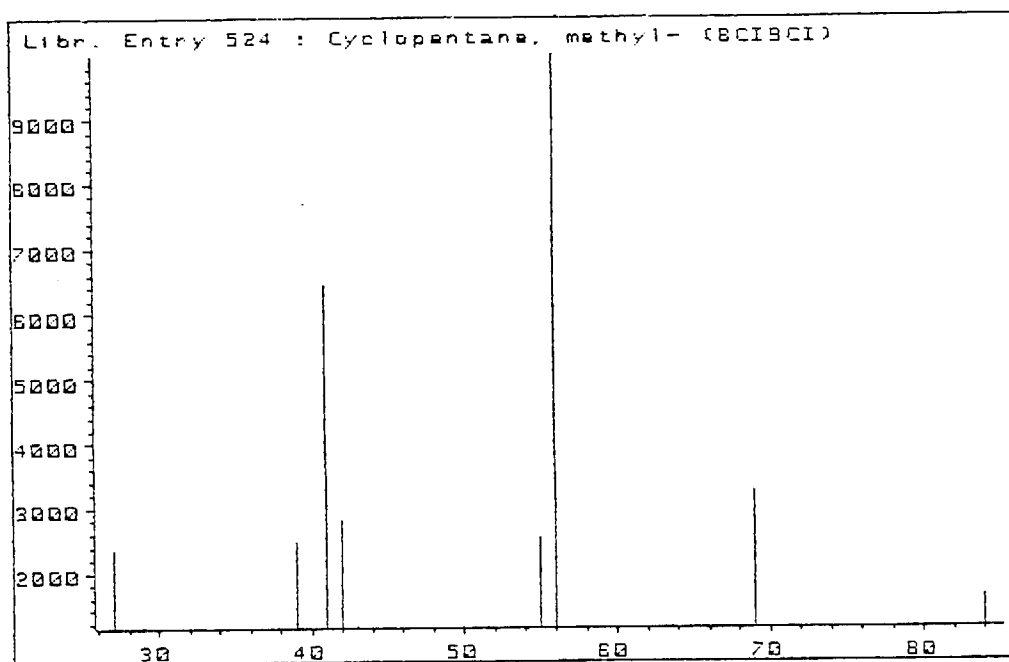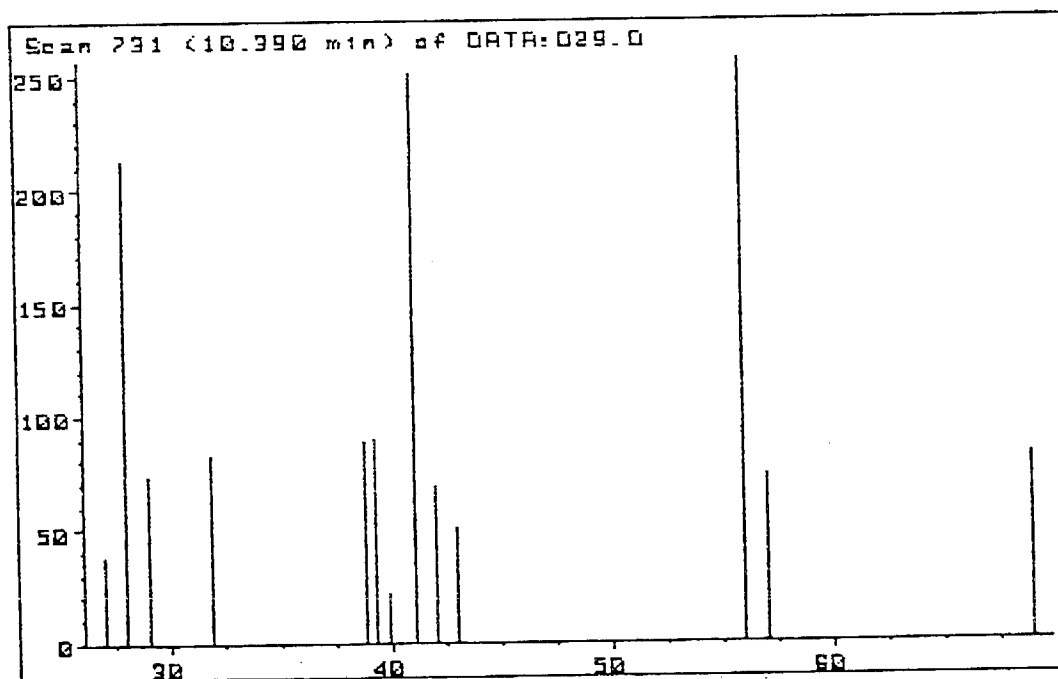   VISB =   406.69
          VISTO =   231.67

ABSOLUTE VISCOSITY (CP)
          AT 0 C :   0.553 cp
          AT 25 C: 0.45 cp
          AT 50 C: 0.322 cp

NBS MASS SPECTRUM

| 70
Cyclopentane | C_5H_{10} | 287-92-3 |

NBS (HP LIBRARY) MASS SPECTRUM

Libr. Entry 219 : Cyclopentane (BCI9CI)

PNA MASS SPECTRUM

N.A.

CYCLOPENTANE

PONA CALIBRATION MIXTURE MASS SPECTRUM

Scan 513 (7.155 min) of DATA:PONA1.D

MONTE CRISTO MASS SPECTRUM

N.A.

METHYLCYCLOPENTANE

B.P. =   71.804 C

M.W. =   84.162

DENSITY (gm/ml) [1]:
        AT 0 C : 0.7672
        AT 20 C : 0.7486
        AT 50 C : 0.7207
        AT 100 C: .

ANTOINE CONSTANTS FOR
DETERMINING VAPOR PRESSURE [2]:
             A = 15.8023
             B =   2731
             C =   -47.11
          TMAX =   375 K
   TMIN =   250 K

LIQUID VISCOSITY [3]:
          VISB =   440.52
          VISTO = 243.24

ABSOLUTE VISCOSITY (CP)
          AT 0 C: cp

NBS MASS SPECTRUM

84
Cyclopentane, methyl-   C6H12   96-37-7

NBS (HP LIBRARY) MASS SPECTRUM

Scan 722 (10.109 min) of DATA:PONA1.D
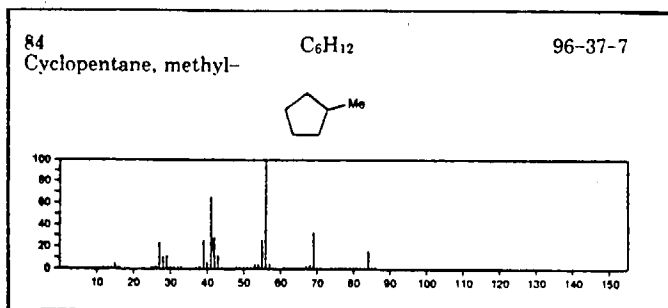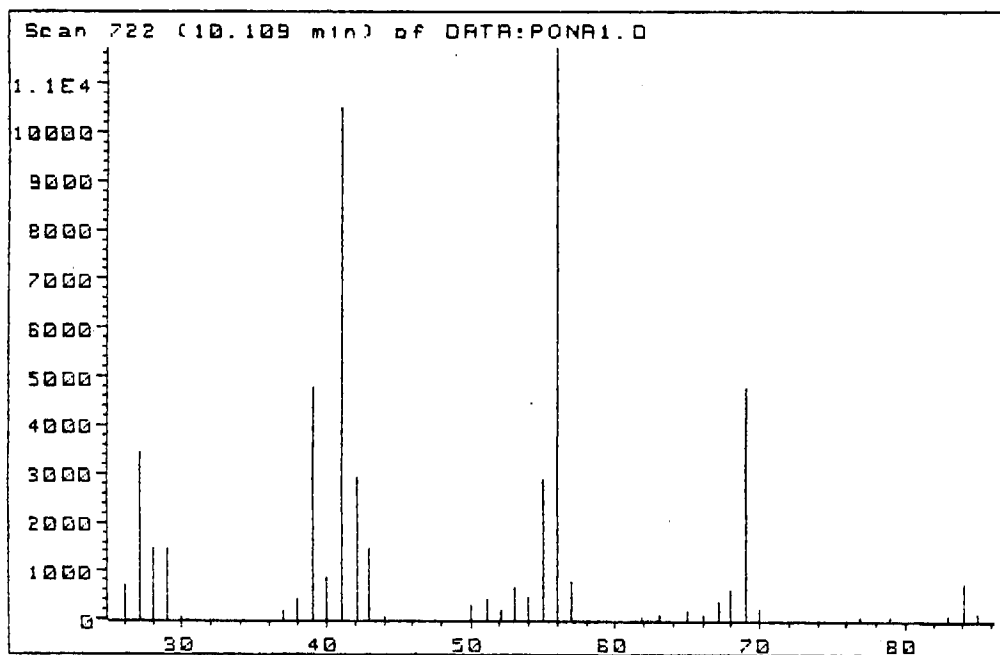
PNA MASS SPECTRUM

N.A.

METHYLCYCLOPENTANE

PONA MIXTURE MASS SPECTRUM

Libr. Entry 524 : Cyclopentane, methyl- (BCIBCI)

MONTE CHRISTO MASS SPECTRUM

Scan 731 (10.390 min) of DATA:029.0

METHYLCYCLOPENTANE

31X MASS SPECTRUM

Scan 730 (10.325 min) of DATA:31XI.D

36W MASS SPECTRUM

Scan 733 (10.382 min) of DATA:D27.D
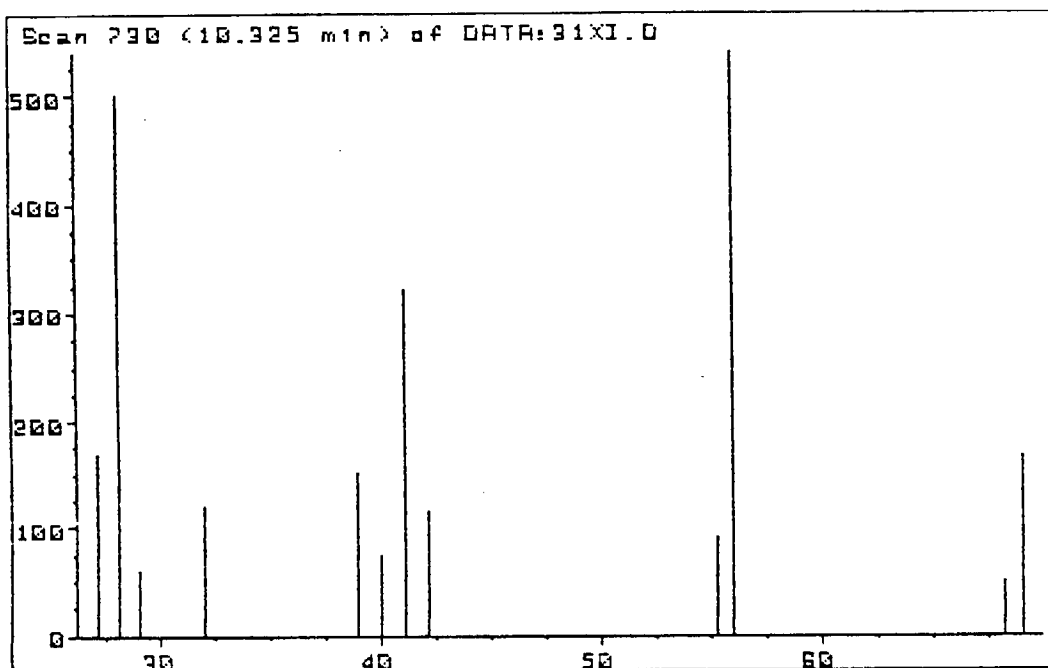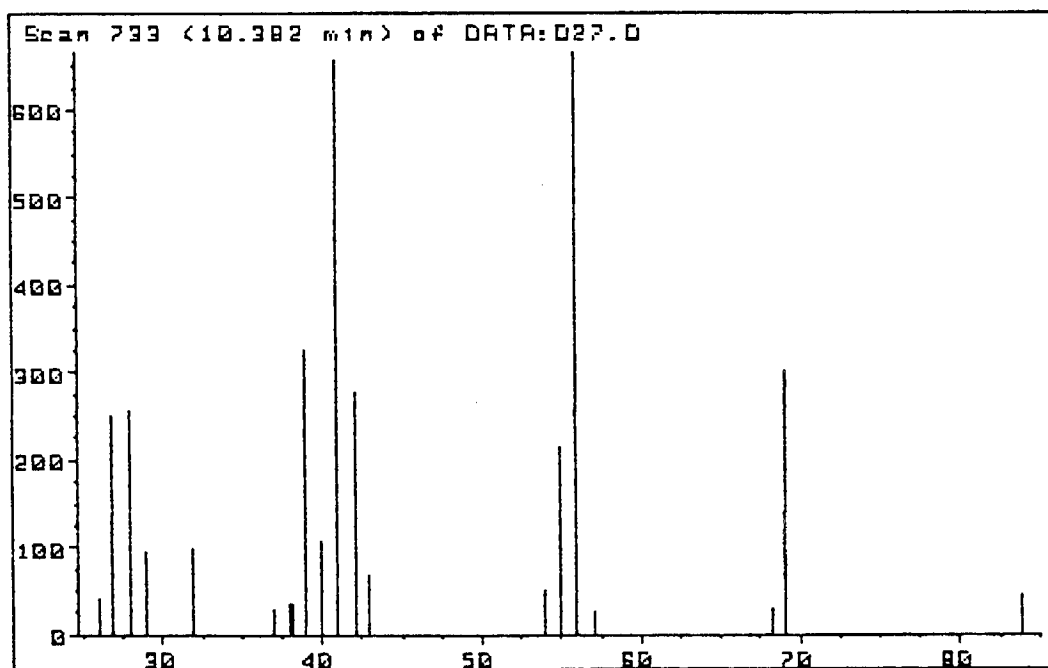
METHYLCYCLOPENTANE

SINGLE-COMPONENT MASS SPECTRUM:

Scan 253 (10.119 min) of MECYPE.D

Scan 253 (10.105 min) of MECYPE.D

Scan 254 (10.133 min) of MECYPE.D
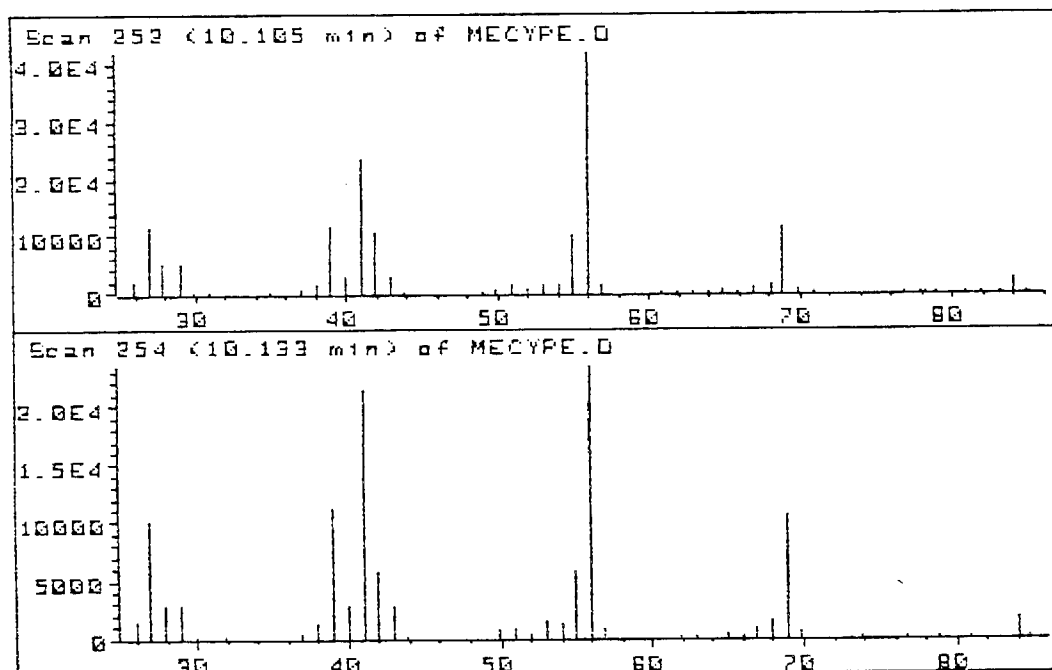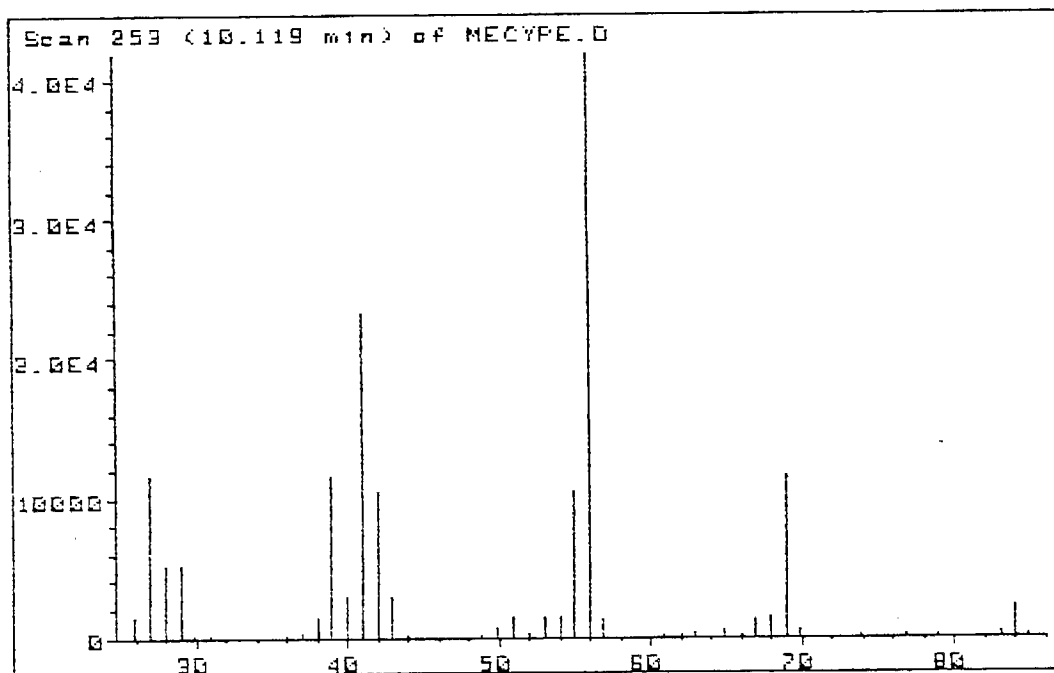
BENZENE

B.P. =   80.094 C

M.W. =   78.114

DENSITY (gm/ml) [1]:
        AT 0 C :
        AT 20 C :   0.879
        AT 50 C :   0.8469
        AT 100 C: 0.301

ANTOINE CONSTANTS FOR
DETERMINING VAPOR PRESSURE [2]:
            A = 15.9008
            B = 2788.51
            C =   -52.36
         TMAX =   377 K
         TMIN =   280 K

LIQUID VISCOSITY [3]:
         VISB =   545.64
         VISTO =   265.34

ABSOLUTE VISCOSITY (CP)
        AT 25 C :   0.601 cp
        AT 50 C :   0.4347 cp
        AT 100 C: 0.301 cp

NBS MASS SPECTRUM

78
Benzene

C_6H_6

71-43-2

NBS (HP LIBRARY) MASS SPECTRUM

Libr. Entry 369 : Benzene (BCI9CI)
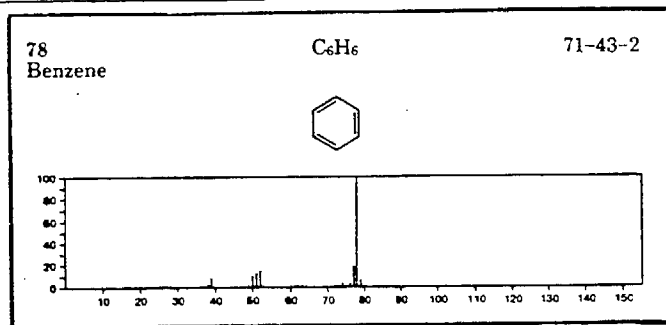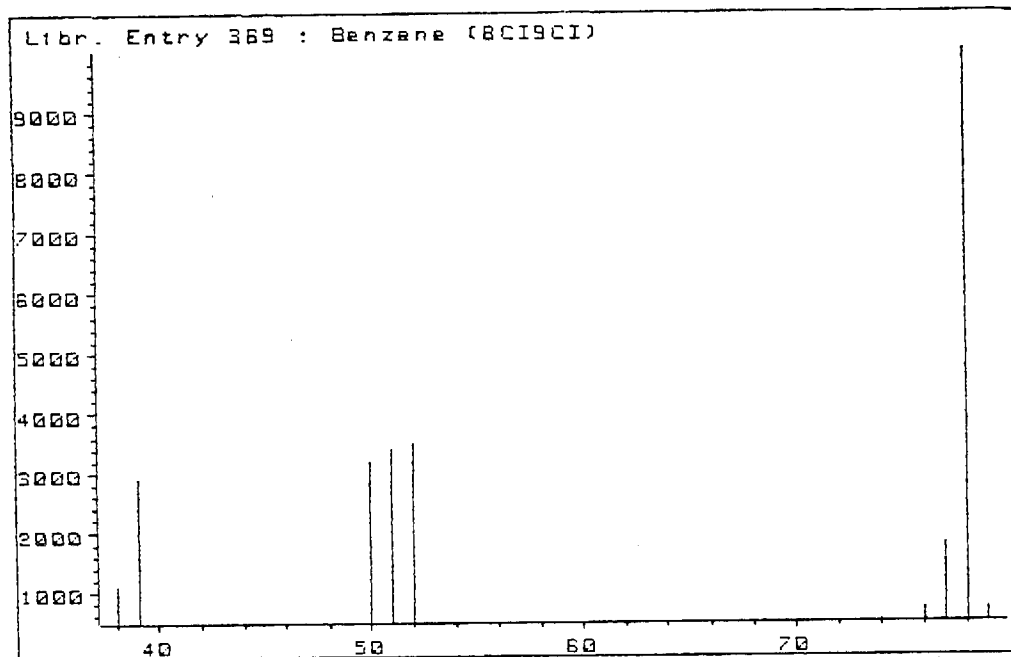
PNA MASS SPECTRUM

N.A.

BENZENE

PONA CALIBRATION MIXTURE MASS SPECTRUM

Scan 831 (11.611 min) of DATA:PONA1.D
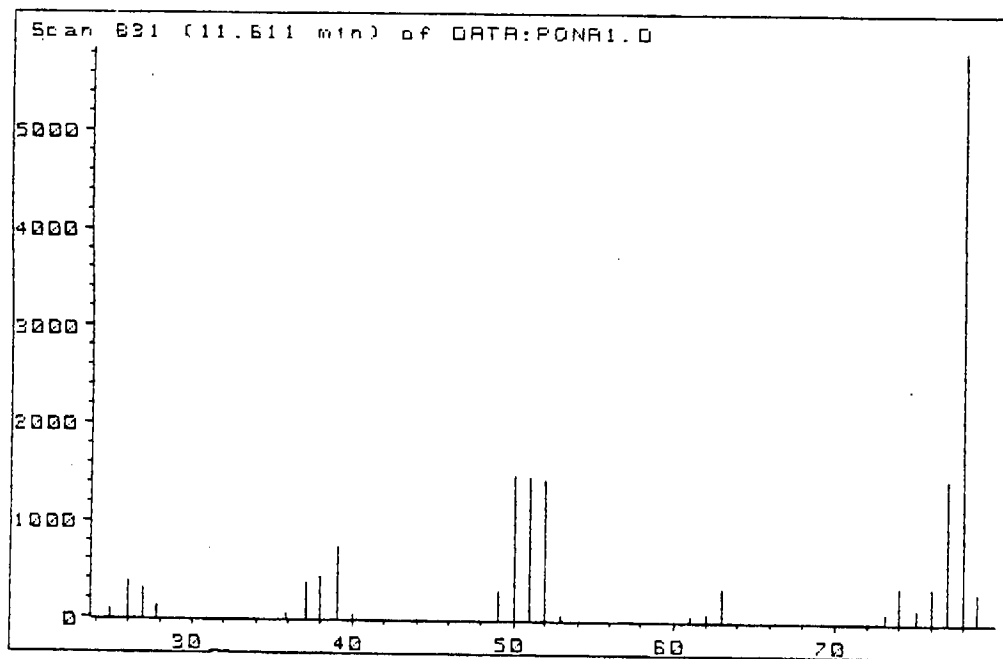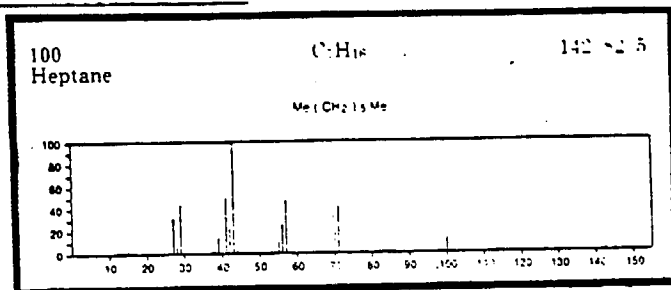

MONTE CRISTO MASS SPECTRUM

N.A.

BENZENE

31X MASS SPECTRUM

N.A.

36W MASS SPECTRUM

Scan 843 (11.919 min) of DATA:027.0

BENZENE

SINGLE-COMPONENT MASS SPECTRUM:

Scan 363 (11.642 min) of DATA:BENZ.D

Scan 362 (11.638 min) of DATA:BENZ.D

Scan 364 (11.656 min) of DATA:BENZ.D
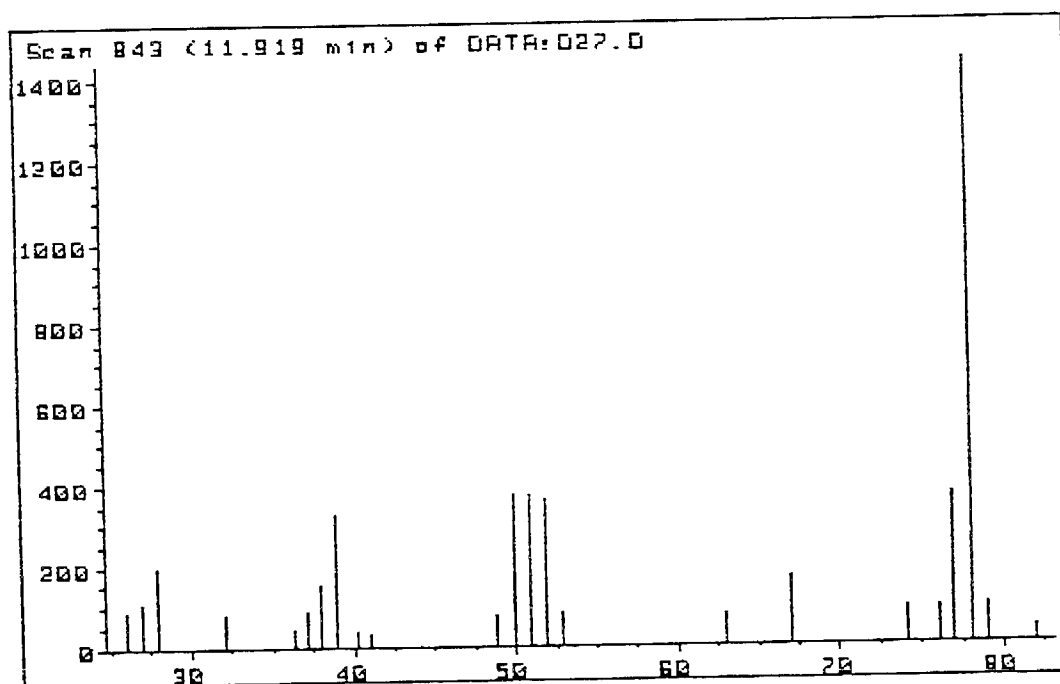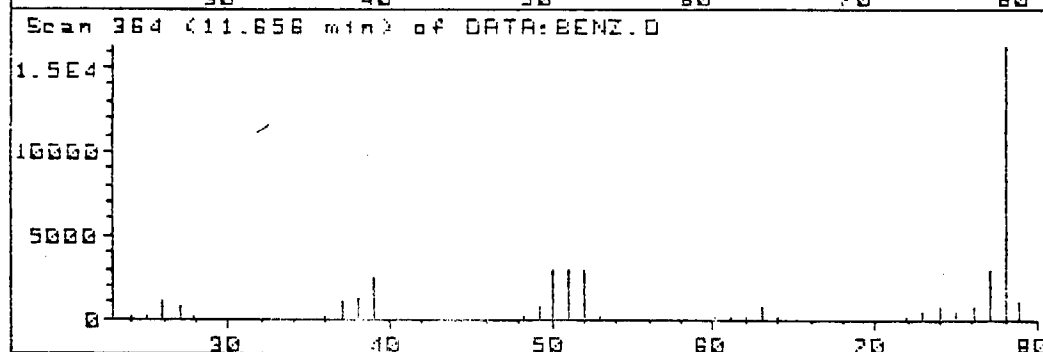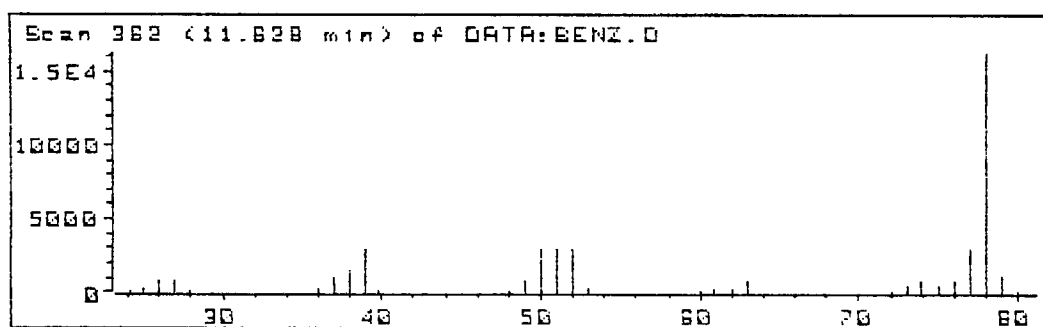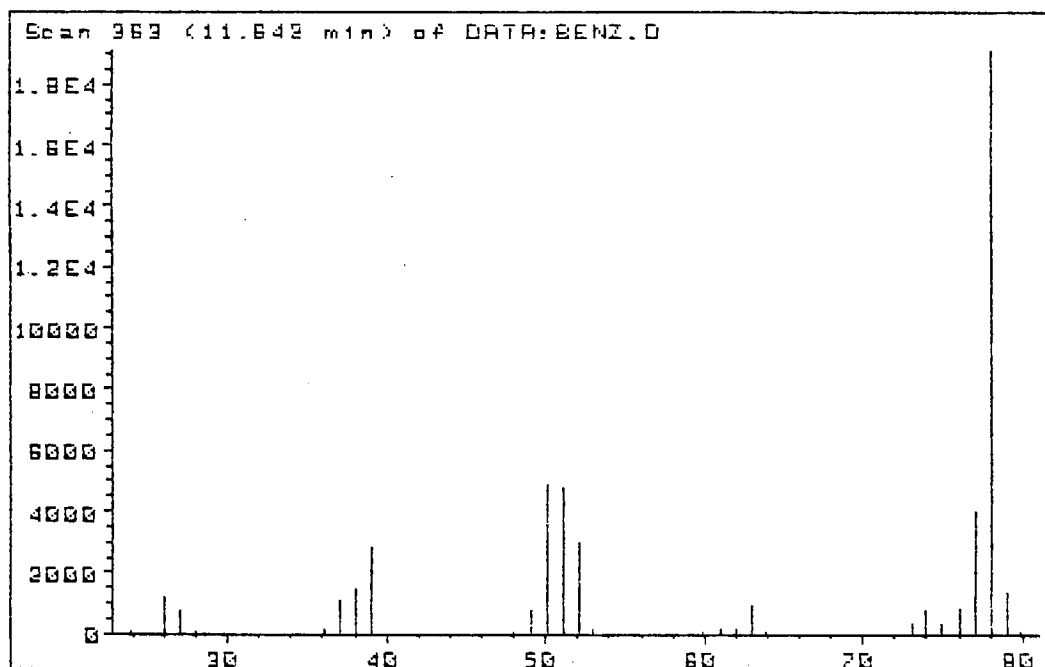
N-HEPTANE

B.P. =   98.4 C

M.W. =   100.205

DENSITY (gm/ml) [1]:
            AT 0 C :   0.7007
            AT 25 C : 0.67946
            AT 50 C :   0.6577
            AT 100 C: 0.612

ANTOINE CONSTANTS FOR
DETERMINING VAPOR PRESSURE [2]:
            A =   15.8737
            B =   2911.32
            C =   -56.51
         TMAX =   400 K
         TMIN =   270 K
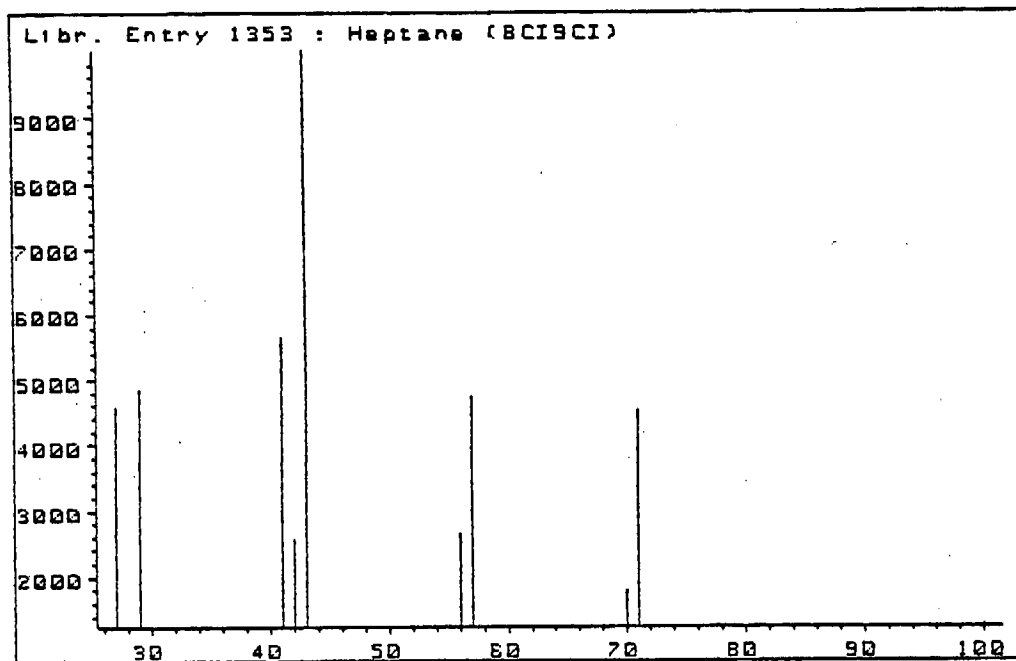
LIQUID VISCOSITY [3]:
         VISB =   436.73
        VISTO =   232.53

ABSOLUTE VISCOSITY (CP)
            AT 0 C :   0.5246 cp
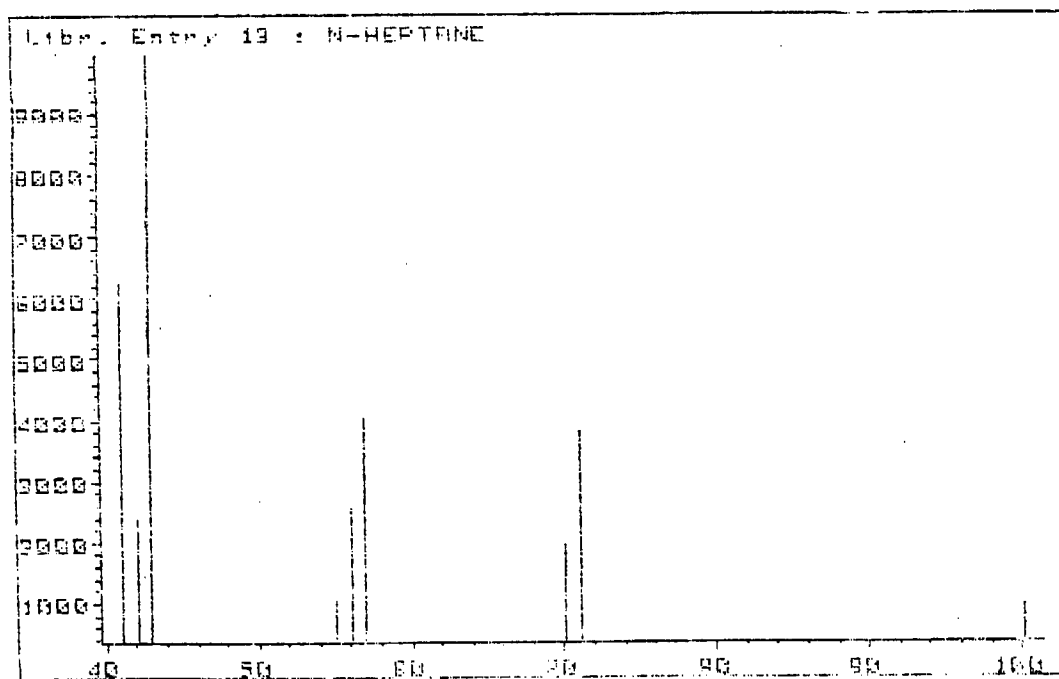   AT 25 C :   0.3955 cp
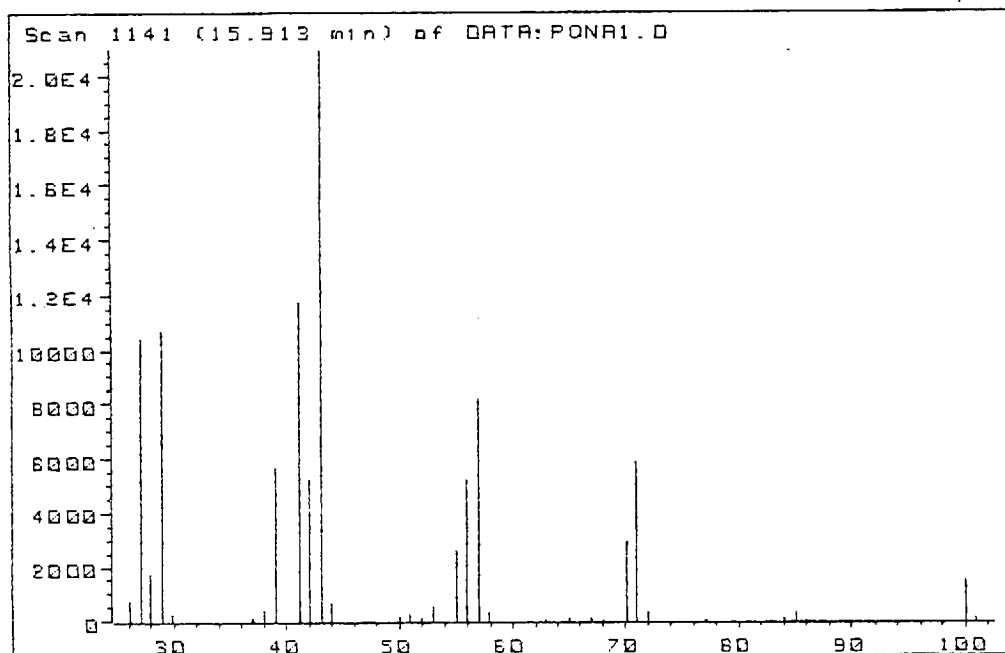   AT 50 C :   0.3119 cp

NBS MASS SPECTRUM

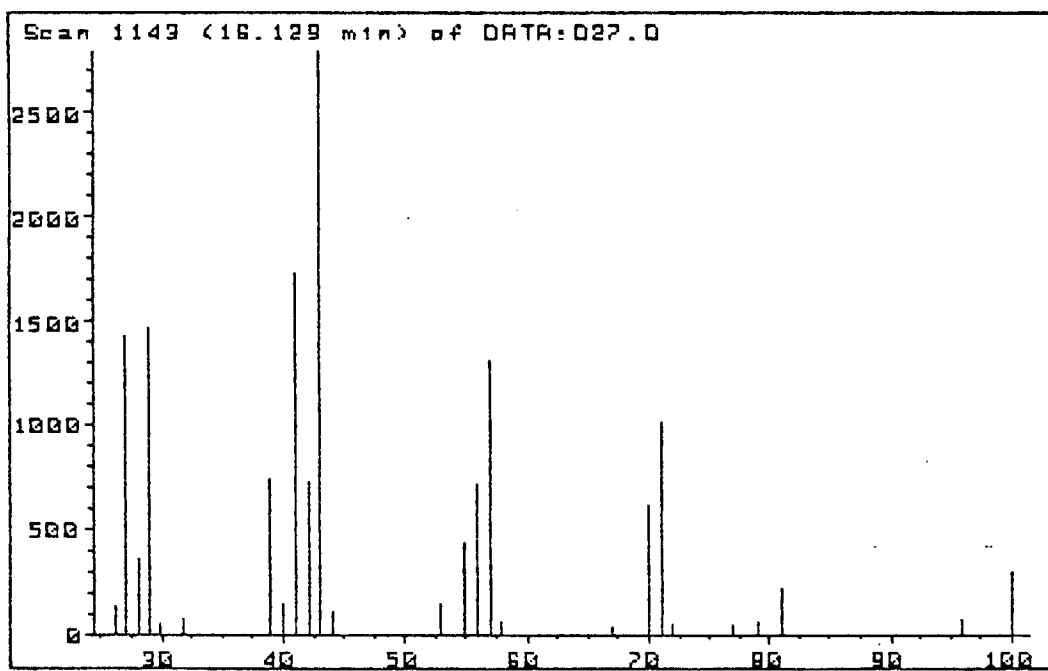

```
100
Heptane                    C7H16                    142 -- 5
                        Me (CH2)5 Me
```

NBS (HP LIBRARY) MASS SPECTRUM

Libr. Entry 1353 : Heptane (BCI9CI)

PNA MASS SPECTRUM

Libr. Entry 13 : N-HEPTANE

N-HEPTANE

PONA CALIBRATION MIXTURE MASS SPECTRUM

Scan 1141 (15.913 min) of DATA:PONA1.D

MONTE CRISTO MASS SPECTRUM

N.A.

N-HEPTANE

31X MASS SPECTRUM

N.A.

36W MASS SPECTRUM

Scan 1143 (16.129 min) of DATA:027.0

N-HEPTANE

SINGLE-COMPONENT MASS SPECTRUM:
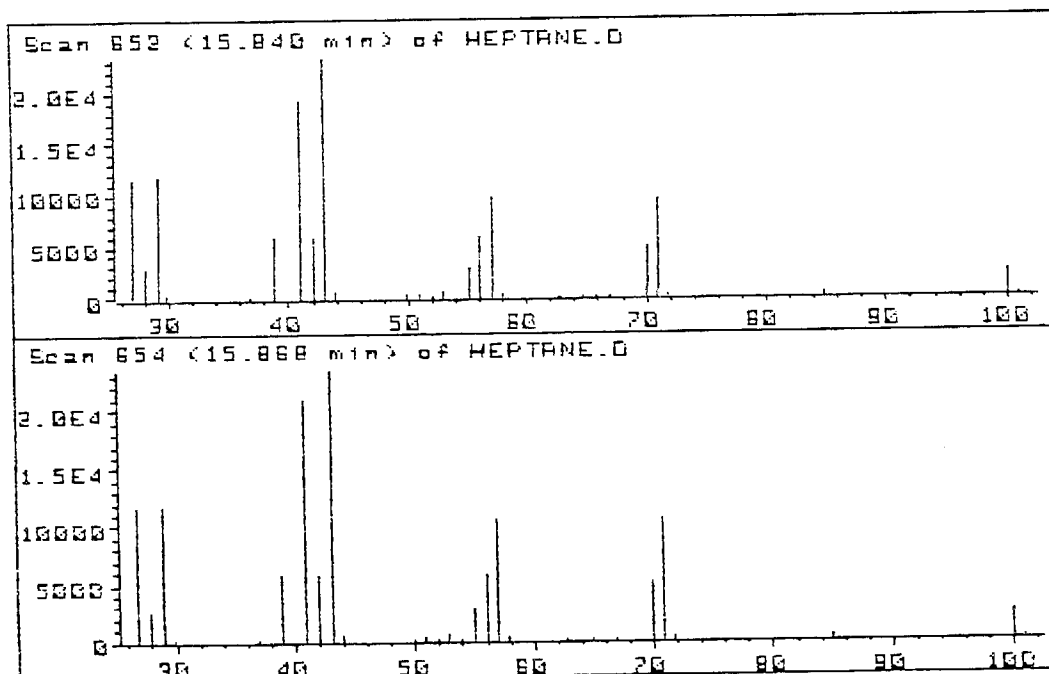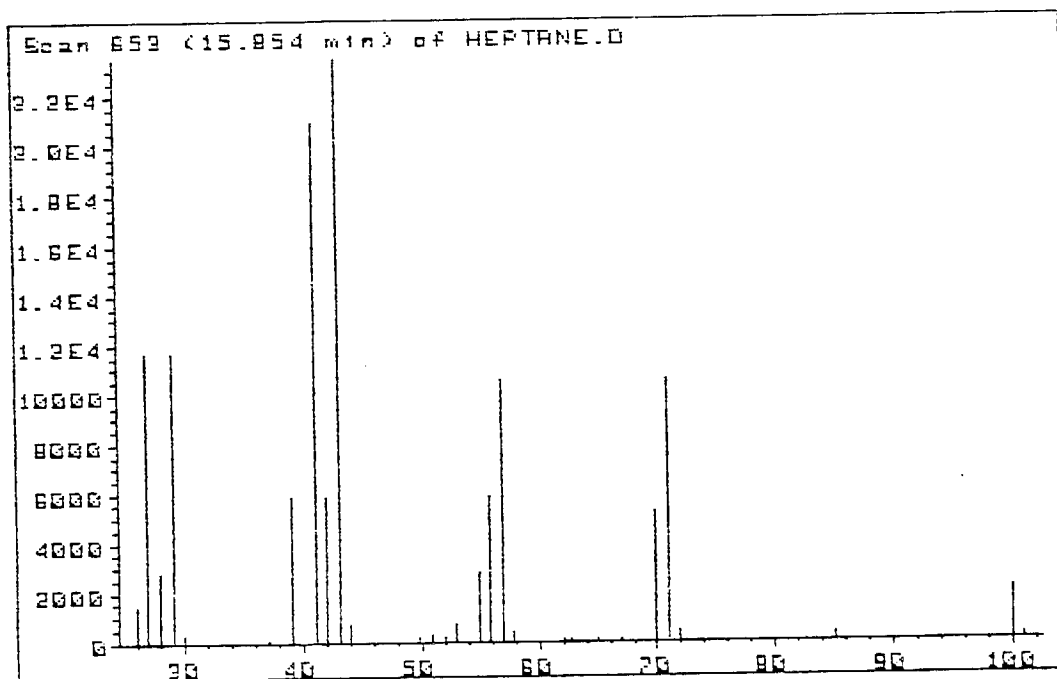
REFERENCES

1. Heller, S.R. and Milne, G.W.A. (1978). EPA/NIH Mass Spectral Data Base. Vol. I. U.S. Dept. of Commerce/National Bureau of Standards.

2. Reid, R.C., Prausnitz, J.M., Sherwood, T.K. (1977). The Properties of Gases and Liquids, 3rd Ed., McGraw-Hill Book Co., N.Y.

3. American Petroleum Industrial Research Project 44 (1984). Selected Values of Properties of Hydrocarbons and Related Compounds. Vol. I. Thermodynamic research Center Hydrocarbon Project.

4. American Petroleum Institute (1977). Technical Data Book -- Petroleum Refining. Vol. I. Washington, D.C.

5. Chemical Rubber Company (1975). Handbook of Chemistry and Physics, 56th Ed.